Design of a Permanent Magnet Synchronous Motor for an Electric Traction Application

by

Hewa Gamage Nandun Senevirathna

Submitted to the Department of Electrical Engineering, Electronics, Computers and Systems
in partial fulfillment of the requirements for the degree of

Erasmus Mundus Master Course in Sustainable Transportation and Electrical Power Systems

at the

UNIVERSIDAD DE OVIEDO

August 2020

Author ....

Nandun Senevirathna

Certified by ....

Dr. Gaurang Vakil
Associate Professor
Thesis Supervisor

Design of a Permanent Magnet Synchronous Motor for an Electric Traction Application

by

Hewa Gamage Nandun Senevirathna

Submitted to the Department of Electrical Engineering, Electronics, Computers and Systems
on August 31, 2020, in partial fulfillment of the
requirements for the degree of
Erasmus Mundus Master Course in Sustainable Transportation and Electrical Power Systems

Abstract

This thesis details a design of an exterior - rotor, fractional - slot, double layer permanent magnet synchronous motor for a two-wheeler application.The cooling method used was natural cooling. The initial design procedure was adopted from previously published works by other authors [1, 2] . ANSYS MotorCAD software was used in design of the machine,optimization and verification of the machine's performance.A review of different electric motor types was carried out to choose a suitable machine type and configuration. Comparative analysis of BLAC and BLDC motors was performed and considering the application requirements Sinusoidally fed permanent magnet synchronous motor was chosen (commonly referred as BLAC motor) . An extensive sensitivity analysis was done using the tools available in MotorCAD simulation platform. Further the optimization of the selected design in terms of electromagnetic performance was carried out using MotorCAD. Finally, the electromagnetic and thermal performance validation was done using the same software.

Keywords : Outer-Rotor, in-wheel motor, Permanent Magnet Synchronous Motor, FEA, Concentrated winding, fractional-slot windings

Thesis Supervisor: Dr. Gaurang Vakil
Title: Associate Professor

Acknowledgments

I bestow my sincere gratitude to the supervisor Dr. Gaurang Vakil for his continuous guidance and support provided for carrying out this work. Erasmus Mundus STEPS (Sustainable Transportation and Electrical Power Systems) master program was a milestone in my career as an engineer.I'm very much thankful to Prof. Pablo Arboleya, Prof. Jorge Garcia and to to all of my professors at the University of Oviedo,Spain, Sapienza University of Rome,Italy and the University of Nottingham,UK for giving me this wonderful opportunity to participate in this excellent academic program. Last but not least I'm very much grateful to my loving parents who supported me from the distance throughout this journey.

Contents

List of Figures

List of Tables

Acronyms

AC - Alternating Current

BLAC - Brushless Alternating Current

BLDC - Brushless Direct Current

DC - Direct Current

EV - Electric Vehicle

EMF - Electro Motive Force

FEA - Finite Element Analysis

FSCW - Fractional-Slot Concentrate Winding

FSM - Flux Switching Machine/Motor

GCD - Greatest Common Divisor

HEV - Hybrid Electric Vehicle

IM - Induction Machine/Motor

IPSM - Interior Permanent Magnet Machine/Motor

LCM - Lowest Common Multiple

MMF - Magneto Motive Force

PMFSM - Permanent Magnet Flux Switching Machine/Motor

PMSM - Permanent Magnet Synchronous Machine/Motor

PMa-SynRelM - Permanent Magnet assisted Synchronous Reluctance Machine/Motor

SPM/SMPM - Surface mounted Permanent Magnet Machine/Motor

SRM - Switched Reluctance Machine/Motor

SynRelM - Synchronous Reluctance Machine/Motor

TFM - Transverse Flux Machine/Motor

WFFSM - Wound Field Flux Switching Machine/Motor

Chapter 1

Introduction

Improvement of the air quality and reducing the environmental impacts is a primary reason for revolutionizing the vehicles through electrification. Introduction of electrified two wheelers such as electric scooters for daily short distance commutations in urban transport systems can help reduce traffic congestion and hence to reduce pollution. Therefore researching on technologies more suitable for low speed low torque applications such applications is important.

1.1 Aim

The aim of this work is to design a permanent magnet synchronous motor for a low-speed,low-power electrical traction application (Two-wheeler) with acceptable performance and size.

1.2 Objectives

The project would focus on developing a solution for an electrified two wheeler and the project objectives include;

1. Understanding the application requirements.

2. Defining the specifications of the machine required for the application.

3. Analysing different typologies used for the electrical machines used in automotive applications.BLDC, BLAC and SynRelM are mainly suggested in literature.

4. Developing initial design approach

5. Modelling the selected designs using MotorCAD software, performing the sensitivity analysis and optimization.

6. Electromagnetic,thermal and mechanical Validation through finite element analysis.

1.3 The Structure of the Thesis

This thesis is organized in the following manner.

Chapter one introduces the project and details the scope of the project and the structure of the thesis. The chapter also includes the equations governing permanent magnet synchronous machines and some background information on permanent magnets.

Chapter two presents the literature review of electrical motors used in traction applications and describes winding options.

Chapter three describes the basic design flow and motivations for the design decisions made.

Chapter four provides the sensitivity analysis results of the selected initial design and the optimization outcomes.

Chapter five describes the validation through finite element analysis. It also includes the conclusion and suggestions for future work.

Chapter six includes the conclusion of the work. Some suggestion for future work are also included at the end.

Appendices and Bibliography are provided at the end of the thesis.

1.4 Direct Drive In-Wheel Motors

The motor can be positioned in different locations of the vehicles using electrical traction. Locating the motor directly inside the wheel is one possibility which reduces the transmission path between the motor and the whee, hence reducing the losses in transmission. The use of direct drives in low-speed electric machines offers benefits attributed to the removal of the gearbox [17] such as:

- Improved efficiency: Removal of the gearbox eliminates losses due to friction in mechanical gears.
- Reduced maintenance: Gearboxes are main sources of mechanical system failures. The necessity of frequent lubrication is also minimized with direct drive systems.
- Improved reliability: Having less number of mechanical components such as gears reduces the probability of failures improving the overall reliability.
- Reduced vibration and noise: Audible noise and vibrations due the gear teeth are eliminated.
- Simpler design: The number of components on the power train is reduced hence simplifying the overall system.

However, there are some drawbacks of in-wheel motors. The unsprung mass (mass components not supported by the suspension system) is increased in in-wheel motor configuration. This results in issues with the suspension and steering and loss of comfort.

1.5 Electrical Machine Classifications

There are various electrical machine topologies and technologies. Therefore several different classifications exist. Some of these classifications are:

Supply for the armature: - AC, DC or Pulsed

Field flux production: - Windings (whether externally supplied or through inductance), Permanent magnets(PM) or no field flux at all in the case of pure reluctance

Position of the stator and rotor: - inner rotor radial, outer rotor radial, axial, transverse, linear or multiple rotors or stators

Rotation speed: Synchronous or asynchronous relative to the armature frequency. A classification of a selection of conventional machines is shown in figure 1-1.A Typical torque speed characteristics of an electrical traction motor is shown in figure 1-2.

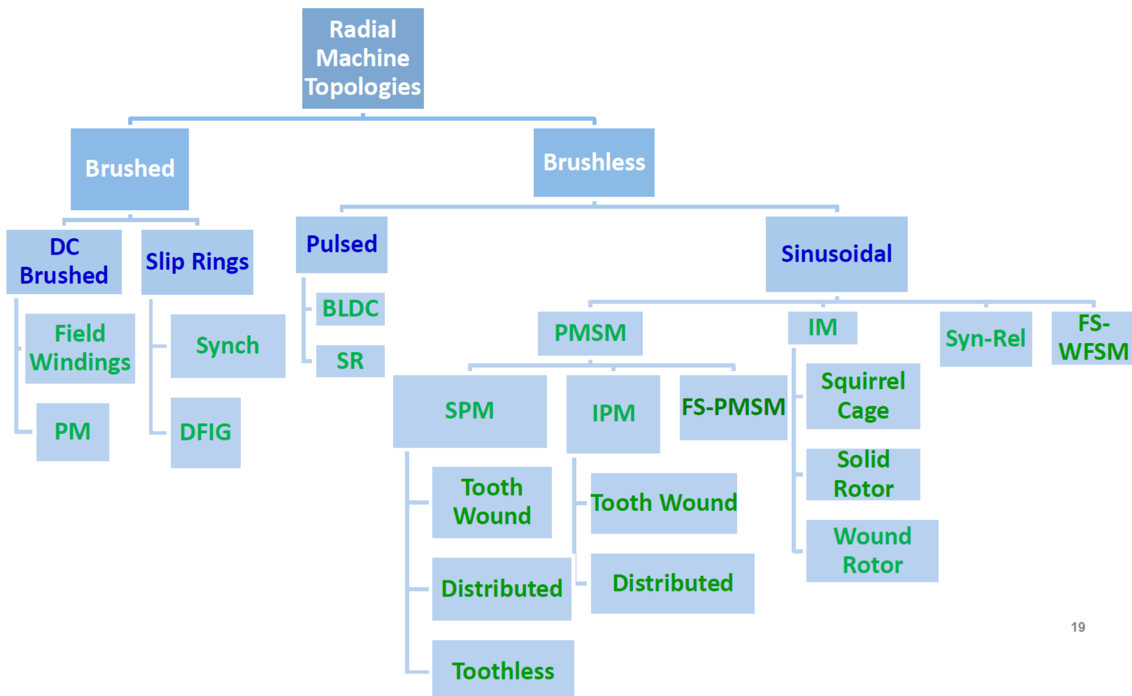

Figure 1-1: Conventional Electrical Machine Classification [3]

1.6 Fundamental Relationships in Permanent Magnet Synchronous Motors

This section presents the basic mathematical equations governing the operation of permanent magnet synchronous motors.

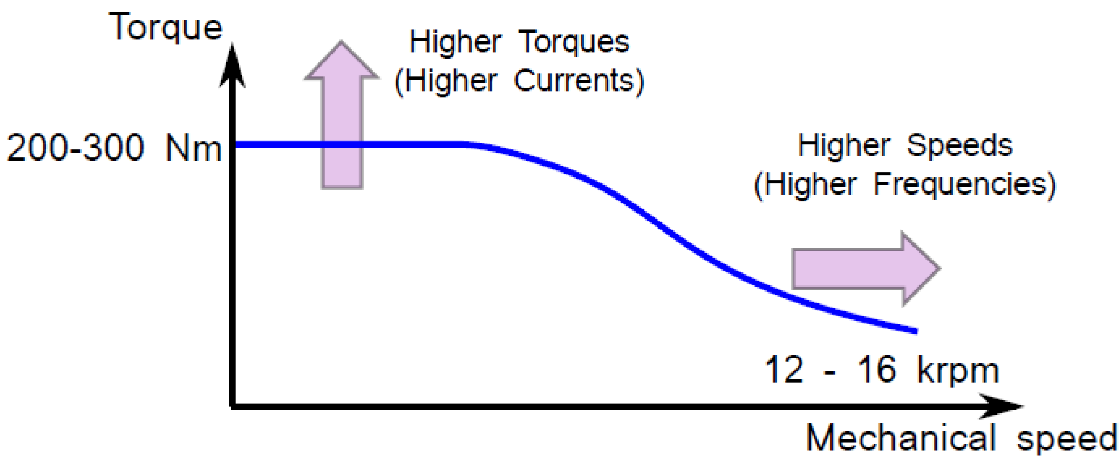

Figure 1-2: Typical torque versus speed characteristic.[4]

1.6.1 Speed

The steady-state rotor speed is given by,

$$n_s = \frac{f}{p} \tag{1.1}$$

where f is the input frequency and p number of pole pairs.n_s is equal to the synchronous speed of the rotating magnetic field produced by the stator.

1.6.2 Air gap magnetic flux density

The fundament air gap magnetic flux density is [15],

$$B_{mg1} = \frac{2}{\pi}\int_{-0.5\alpha_i\pi}^{0.5\alpha_i\pi} B_{mg}\cos\alpha d\alpha = \frac{4}{\pi}\sin\frac{\alpha_i\pi}{2} \tag{1.2}$$

The coefficient α_i is the ratio of the average–to–maximum value of the normal component of the air gap magnetic flux density ($\alpha_i = B_{avg}/B_{mg}$).

1.6.3 Voltage induced (EMF)

The no-load rms voltage induced in one phase of the stator winding (EMF) by the d.c. magnetic excitation flux Φ_f of the rotor is

$$E_f = \pi\sqrt{2} f N_1 k_{w1} \Phi_f \quad (1.3)$$

where N_1 is the number of the stator turns per phase, k_{w1} is the stator winding coefficient, and the fundamental harmonic Φ_{f1} of the excitation magnetic flux density Φ_f without armature reaction is

$$\Phi_{f1} = L_i \int_0^{\tau} B_{mg1} \sin\frac{\pi}{\tau} x dx = \frac{2}{\pi}\tau L_i B_{mg1} \quad (1.4)$$

where τ is the pole pitch.

1.6.4 Armature line current density and current density

The peak value of the stator (armature) line current density (A/m) or specific electric loading is defined as the number of conductors in all phases $2m_1N_1$ times the peak armature current $\sqrt{2}I_a$ divided by the armature circumference πD_{1in},

$$A_m = \frac{2m_1\sqrt{2}N_1I_a}{\pi D_{1in}} = \frac{m_1\sqrt{2}N_1I_a}{p\tau} = \frac{m_1\sqrt{2}N_1J_as_a}{p\tau} \quad (1.5)$$

where J_a is the current density (A/m2) in the stator (armature) conductors and s_a is the cross section of armature conductors including parallel wires. For air cooling systems $J_a \leq 7.5$ A/mm^2 (sometimes up to 10 A/mm2) and for liquid cooling systems $10 \leq J_a \leq 28$ A/mm2. The top value is for very intensive oil spray cooling systems [15].

1.6.5 Electromagnetic Power

Neglecting stator winding resistance, for an m-phase salient pole synchronous motor, the electromagnetic power is given by[15],

$$P_{em} = m\left[\frac{V_1 E_f}{X_{sd}}\sin\delta + \frac{{V_1}^2}{2}\left(\frac{1}{X_{sq}} - \frac{1}{X_{sd}}\right)\sin 2\delta\right] \tag{1.6}$$

where V_1 is the input (terminal) phase voltage, E_f is the EMF induced by the rotor excitation flux (without armature reaction), δ is the power angle which is the angle between V_1 and E_f , X_{sd} is the synchronous reactance in the direct axis (d-axis synchronous reactance), and X_{sq} is the synchronous reactance in the quadrature axis (q-axis synchronous reactance).

Synchronous Reactance

The d-axis and q-axis synchronous reactances of a salient pole synchronous motor are given by,

$$X_{sd} = X_1 + X_{ad} \tag{1.7}$$

$$X_{sq} = X_1 + X_{aq} \tag{1.8}$$

where $X_1 = 2\pi f L_1$ is the stator leakage reactance, X_{ad} is the d-axis armature reaction reactance(d-axis mutual reactance) and X_{aq} is the q-axis armature reaction reactance (q-axis mutual reactance). The reactance X_{ad} is sensitive to the saturation of the magnetic circuit whilst the influence of the magnetic saturation on the reactance X_{aq} depends on the rotor construction [15]. The leakage reactance X_1 consists of the slot, end-connection differential and tooth–top leakage reactances.

1.6.6 Electromagnetic Torque

The electromagnetic torque developed by the synchronous motor is determined by the electromagnetic power P_{em} and synchronous speed $\omega_s = 2\pi\ n_s$ (equal to the mechanical speed of the rotor), and neglecting the stator winding resistance, it is given by,

$$T_d = \frac{m_1}{2\pi n_s}\left[\frac{V_1 E_f}{X_{sd}}\sin\delta + \frac{{V_1}^2}{2}\left(\frac{1}{X_{sq}} - \frac{1}{X_{sd}}\right)\sin 2\delta\right] \tag{1.9}$$

Therefore T_d can be expressed as,

$$T_d = T_{dsyn} + T_{drel} \tag{1.10}$$

where the fundamental synchronous torque

$$T_{dsyn} = \frac{m}{2\pi n_s}\frac{V_1 E_f}{X_{sd}}\sin\delta \tag{1.11}$$

and the reluctance torque,

$$T_{drel} = \frac{m{V_1}^2}{4\pi n_s}\left(\frac{1}{X_{sq}} - \frac{1}{X_{sd}}\right)\sin 2\delta \tag{1.12}$$

For a cylindrical rotor synchronous motor where X_{sd}=X_{sq}, the reluctance component is zero and

$$T_d = T_{dsyn} = \frac{m}{2\pi n_s}\frac{V_1 E_f}{X_{sd}}\sin\delta \tag{1.13}$$

1.7 Magnetic Materials

The excitation field of an electrical machine can be provided either by permanent magnets or by electrically energized windings. However the former method is popular where high efficiency and smaller size of the machines are desirable. Among different magnet grades, Neodymium-Iron-Boron magnets was a main advancement in permanent magnet technology.B-H curves for different types of permanent magnets shown in figure 1-3. The remanent flux density B_r and coercivity H_c of sintered NdFeB magnets are higher than those of other magnet grades shown in the figure 1-3, including those of samarium-cobalt (Sm_2Co_{17}) magnets. Even though NdFeB magnets have attractive performance they have a relatively low Curie temperature compared to other types of magnets, including samarium-cobalt magnets. This is disadvantageous for use in demanding electric machine applications that often push

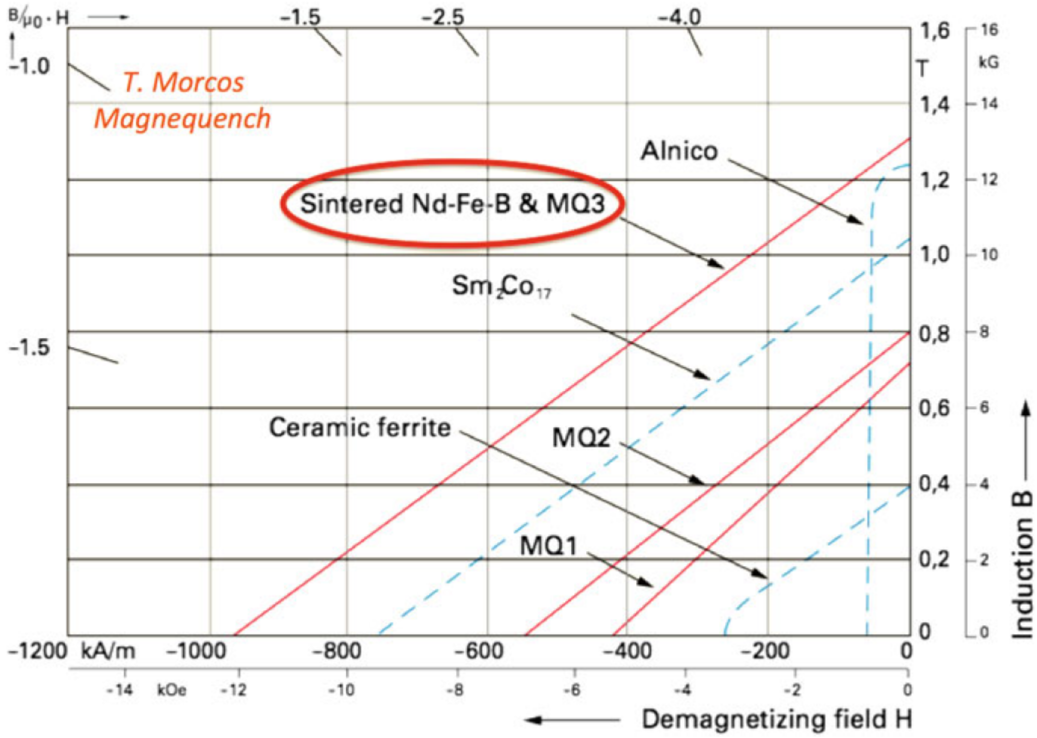

Figure 1-3: Second quadrant normal B-H curves of different types of permanent magnet materials. Source: Magnequench [5]

the thermal limits of their wire insulation systems. Adding small amounts of another rare-earth element, dysprosium (Dy) is one way of increasing the maximum temperature range of NdFeB magnets.This effect is depicted in figure 1-4. Figure 1-4 shows that the maximum operating temperature of NdFeB magnets increases monotonically as the percentage of dysprosium by mass is increased from 0 % to greater than 10 %. This pushes up the maximum operating temperature. However the impact of adding dysprosium on magnet cost is significant as Dy is rarer and more expensive than Nd.

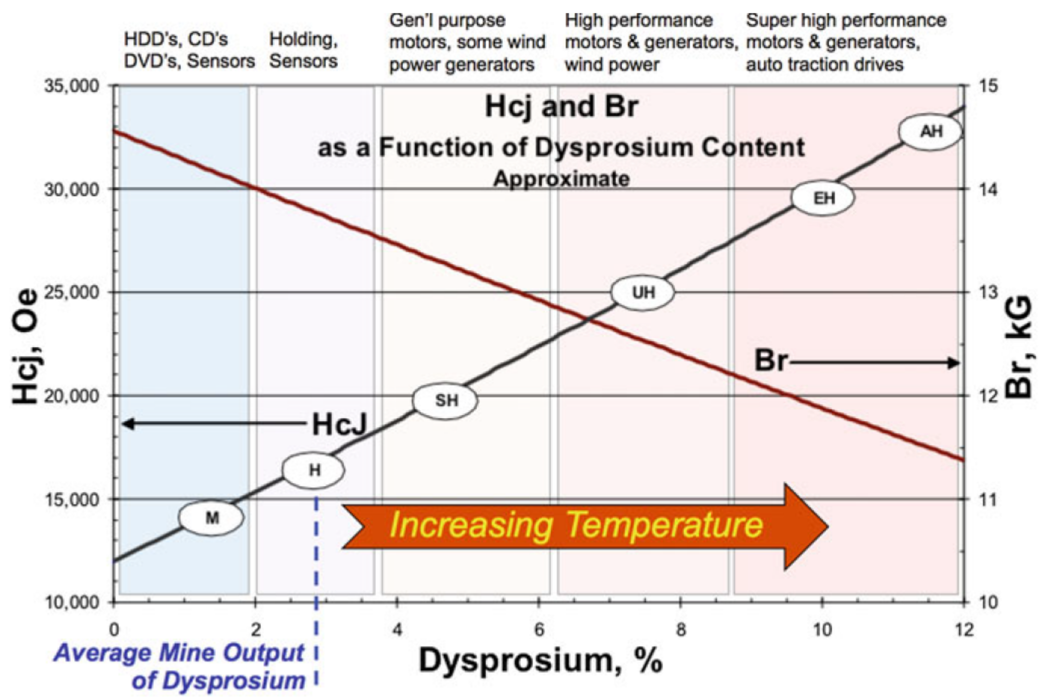

Figure 1-4: Impact of increasing dysprosium content on the coercivity H_{cj} and remanent flux density B_r of NdFeB magnets. Source : Arnold Magnetics [6]

Chapter 2

Study of Machine Topologies and Motor Windings

Various technologies and topologies of machines were considered to achieve the design targets. Each type of machine has its advantages and challenges. The comparison is mainly focused on the ability to meet both the peak torque and speed requirements while offering satisfactory performance in terms of torque ripple,efficiency.

2.1 Conventional Motor Types

Conventional machine technologies have existed for a long time. Most of them have been used in traction applications and those technologies are relatively more mature.

2.1.1 Synchronous Motor (SM)

Wound field synchronous machines have windings on both the stator and the rotor, as shown in Figure 2-1. The flux produced by the stator and rotor current interact to produce a torque that is only present when the machine is running at synchronous speed. A convenient and accurate field flux control is offered by field winding which is useful for both field weakening and strengthening. Supplying the dc field to the rotor poses the main challenge. This will result in additional copper losses, which

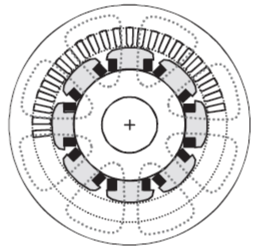

Figure 2-1: Cross Section of a Wound Field SM [7].

are difficult to remove thermally and results in reduction of the overall efficiency. Supplying the current to the rotating conductors is another issue. Usually this is done by implementing brushes or exciters. However, they have significant drawbacks, particularly at high speeds such as sparking, brush wearing etc. PM machines with different rotor magnet configurations are shown in 2-2.

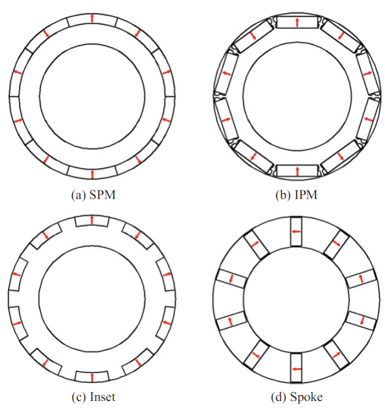

Figure 2-2: PM machines with different rotor configurations [8]

PMSM operational concepts

A PMSM is an electrical machine in which the rotor excitation field is provided by permanent magnets unlike in induction machines where excitation is being induced by feeding current through windings. The stator construction similar to those of in AC induction machines.They require less maintenance since they do not have a system to provide a rotor current.Moreover, PMSM can be designed to operate without a gearbox.The PMSM has a constant magnetic field. Therefore the frequency of induced voltage is equal to the electrical speed of the machine. The stator currents

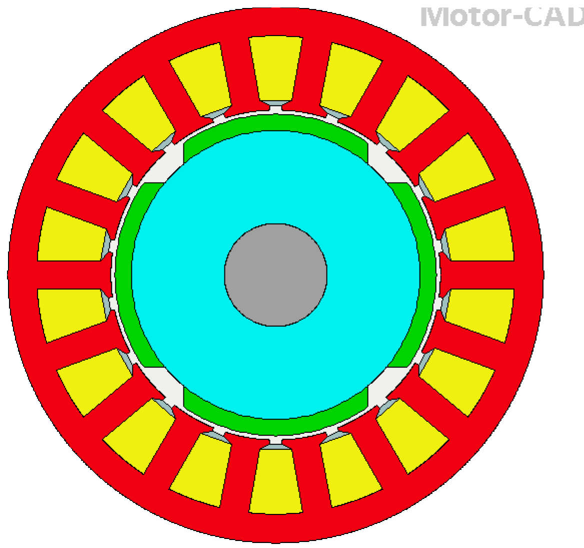

Figure 2-3: Surface Mounted PM motor

must also have the same frequency as the electrical speed of the machine to produce torque. Elimination of gear box means the gearing has to be done electrically. This is done by selecting an appropriate number of poles that the machine is equipped with allowing it to operate at its optimum for a certain speed ranges.

Surface mount permanent magnet synchronous machine (SMPMSM)

SMPMSM machines have PMs on the rotor surface (shown in 2-3). They provide the field flux. When the PMs as close to the air gap as possible ,the maximum magnet utilisation factor resulting in higher torque densities is achieved . However, there are some drawbacks of this. The absence of rotor saliency and so no reluctance torque is produced, this means that obtaining torque in the field weakening region, while maintaining the VA limits is difficult [[18],[19]]. Also, the PMs need a retaining sleeve to withstand the high centrifugal forces present at high speeds [[20]].This type of machine gives the high power and torque density required.But it is unlikely to meet the high speed voltage and efficiency requirements [[20]]. However, the application considered in this thesis does not require high speed operation or operating in the field weakening region.Also high-performance PMs add considerable cost to machines. SMPMSMs are commonly used for low speed high torque traction applications.

2.1.2 Interior permanent magnet synchronous machine (IPMSM)

The IPMSM machine operates on the same principle as the SMPMSM but the PMs are buried under the surface of the rotor, shown in Figure 2-4. This gives an almost as good power density and magnet alignment torque density as the SPM [18].This also improves rotor robustness, even at higher speeds, because the PMs are buried under the rotor surface. The interior magnets also add reluctance torque. It helps improve torque density and high speed performance.However this reluctance value is small compared to some of the topologies mentioned later [21]. The drawbacks are the need

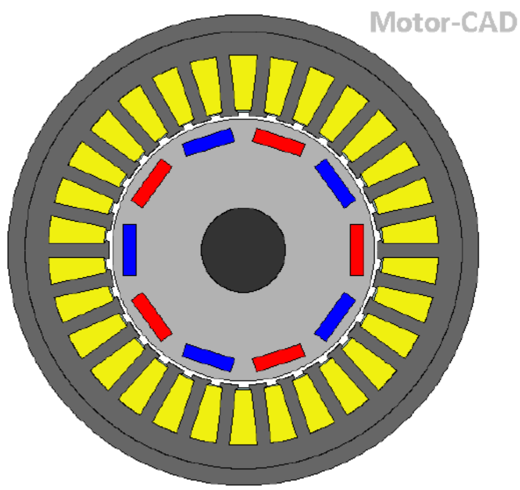

Figure 2-4: Interior Permanent Magnet Synchronous Motor

for expensive PMs and while it can reach higher speeds than the SMPMSM machine, the performance (in terms of efficiency and torque per amp) is not optimal at these higher speeds.IPSM has high torque density and acceptable high speed capabilities. They are used in many current hybrid vehicle applications [22] [23]. They have been heavily investigated for these targets because of the torque density and moderate speed range of the IPMSM design.Major example of this is the General Electric (GE) machine [24].It uses radial spoke PMs inset in the rotor. Another example is the V-shape IPMSMs in [25], performances of these designs are little worse than the radial spoke machine. However the V-shape design used smaller magnets.

2.1.3 Brushless direct current machines (BLDCM)

BLDCMs have a polyphase stator and a rotor with PMs, similar to PM synchronous machines. But in a BLDCM the PMs are designed to produce a square wave flux density, which results in a trapezoidal back EMF and requires a square wave armature current, in contrast to the sinusoidal counterparts found in the PMSM. This machine has similar advantages to the synchronous machines, in that it provides high torque with high efficiency [26]. The control of this BLDC is simpler and easy. In general BLDC produces slightly higher torque than the PM synchronous machines.However this simpler control and increased torque come at a cost which is the much higher torque ripple in the machine than that of a synchronous machine.

2.1.4 Induction machine (IM)

IMs (shown in Figure 2-5) have existed for over a century and have been used regularly in electric vehicles, especially larger vehicles. IMs exploits electromagnetic induction

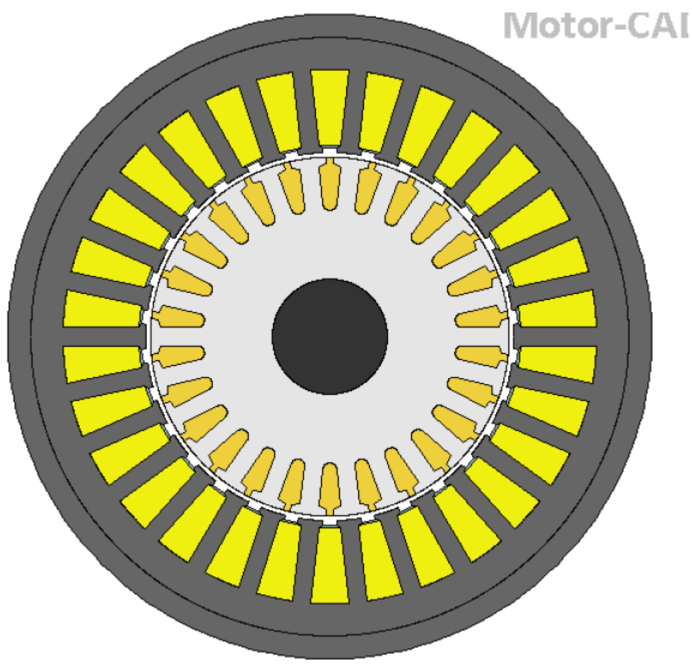

Figure 2-5: Induction Motor

to generate a field flux from electrically conductive rotor bars, shown in Figure 2-5. Therefore only the stator needs to be supplied with current.They are cheap, reliable and rugged and can produce traction adequately [27]. A key benefit of IMs is that the rotor flux can be controlled through field orientated control [28] making them very competitive over PM machines in the high speed region. Current flowing in the rotor causes some drawbacks, such as high losses and rotor cooling complexity [29]. While IMs are comparable to PM motors at high speed, it is unlikely the same design would be able to meet the peak torque requirement with the current and temperature limits.

2.1.5 Switched reluctance machine (SRM)

SRMs produce torque solely based on the reluctance of the rotor. SRMs have a simple, robust, low cost rotor structure and capability for high-speed rotation [30],[31].This is a consequence of the rotor being purely made out of laminated steel (with a toothed shape to produce the reluctance) as shown in Figure 2-6. Compared to other machines

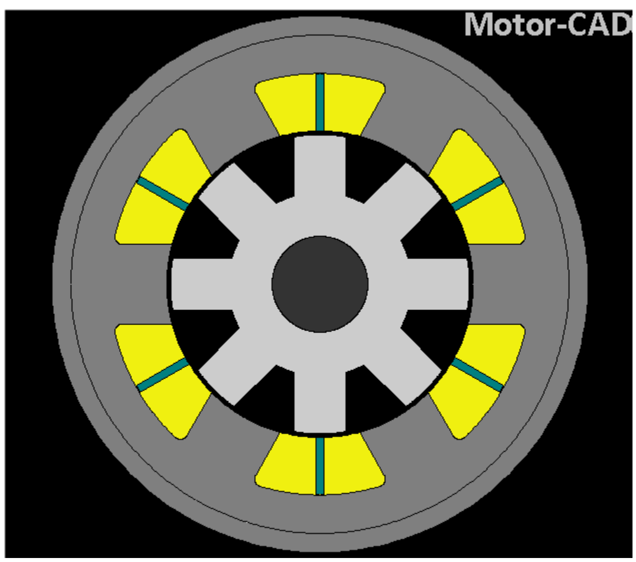

Figure 2-6: Switched Reluctance Motor

the motion of SRM is more discretised and it results in higher vibrations causing acoustic noise and torque ripple [20, 32]. The simple rotor also means lower power and torque density.So high torque SRMs need to be very large.

SRMs do not use a standard 3 phase AC stator winding as many of the other machines do. So they require dedicated power electronics which increases cost and reduces flexibility [32, 33].High torque low speed machines for full electric vehicles are shown in [34] , though the only machines with high enough torque density for the targets have low efficiency. A similar machine with high torque density but with a lower efficiency SRM for EVs is mentioned in [32].The SRMs are optimal for high speed applications, they are also candidates for applications where robustness is important and the vibrations they produce is acceptable such as in off-highway vehicles mentioned in [22].

2.2 Unconventional flux direction machines

These machines use conventional methods of producing the flux fields in the machine. But unlike in conventional machines ,the flux of these machines travels in directions other than radial direction.

2.2.1 Axial flux machines

Axial flux machines have flux travelling in the axial direction. Both the rotor and the stator are annular shaped. Conventional machine types could be made axially, but in generall a surface mount or interior PM rotor is implemented, with a synchronous wound stator.

Axial machines generally have a smaller volume for the same power than their radial counterparts. The extremely high torque density values achievable in axial flux machines is the main benefit. However, this is quite dependent on the dimensions and the power node being investigated. If the specifications favour the size of the axial flux machine it would be very difficult for a different topology to outperform it. However, the range of dimensions and power nodes where this superiority would occur is very narrow [35]. The shape of axial machines makes them very suited to applications where the radial space is limited, such as the in-wheel motor shown in [36] . Because of the shape of axial machines,they can easily have double stator or double rotor machines. This is very common with axial machines [35, 37] [9] , as shown in Figure 2-7. These machines are difficult to scale than radial machines

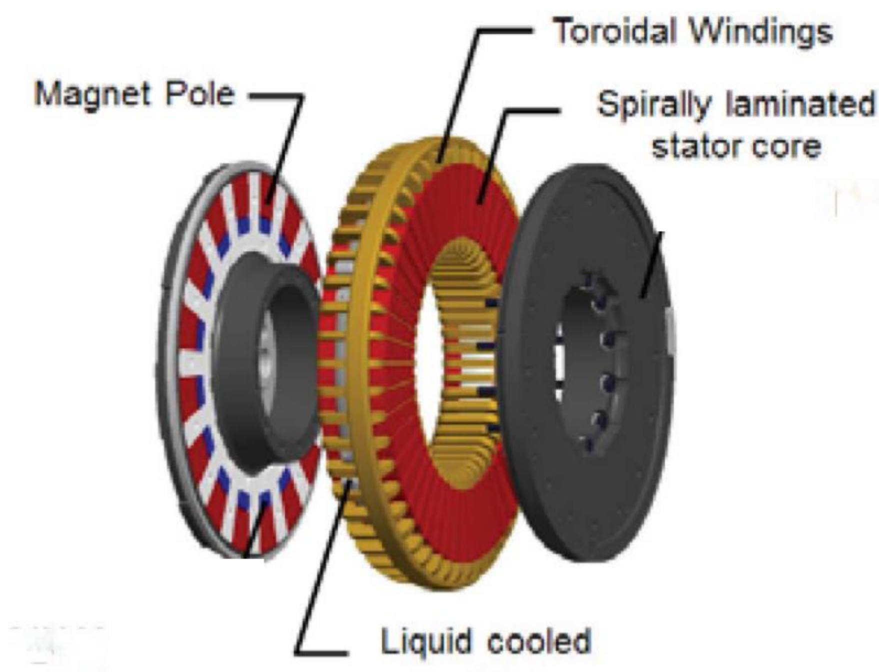

Figure 2-7: Double Rotor Axial Flux IPMSM [9]

because the torque is proportional to the cube of the diameter and independent of the stack length, so to increase the torque produced, the diameter must be increased and so different size laminations must be manufactured. This lack of easy scalability is a big issue when considering traction machines, if they are to be produced for a range of different vehicles which is usually the case.

2.2.2 Transverse flux machines (TFM)

Flux in TFMs travels the transverse direction. This machine uses a homopolar phase winding, a stator core formed by laminated C-cores and a rotor provided with heteropolar PMs[38]. The flux path associated with TFM is shown in the cross-section in figure 2-8(a). Each TFM is single phased, so for multiple phases, multiple machines are needed, a TFM with two phases is shown in Figure 2-8(b).The main advantages of TFM are the potential high torque density and high electric loading [28]. Increasing the pole number increases the power and reduces the speed of the machine for a fixed electrical frequency. This means the torque increases significantly [38]. Each phase is an independent system, giving modularity and improving fault tolerance capability

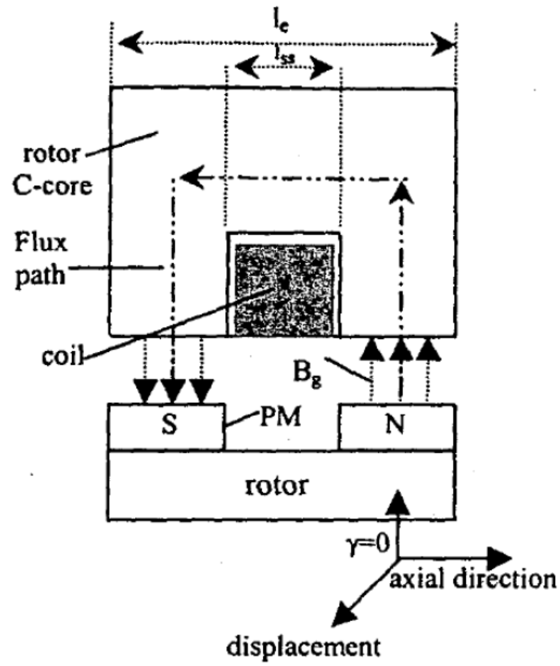

(a) Cross section of a transverse flux machine [38]

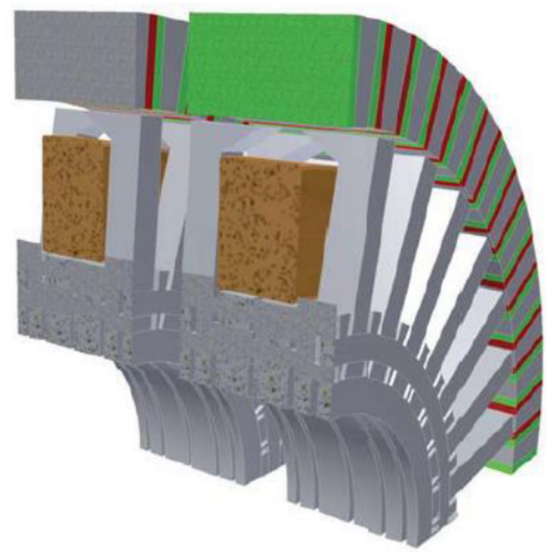

(b) Two phase outer rotor transverse flux machine [39]

Figure 2-8: Transverse Flux Machine

[40].

2.3 Unconventional machine Topologies

These machines have the conventional radial shape of a machine but their methods of producing or using the flux are different. Many of them are a variation of or a hybrid between two of the conventional technologies.

2.3.1 Flux switching machine (FSM)

FSMs can be developed to produce the flux purely in the stator. The stator consists of both the armature windings and the field producing arrangement. The field production arrangement can either be PMs (PMFSM) or with a wound field (WFFSM) to produce the field flux or combination of both methods. The rotor usually have a similar design to an SRM rotor. So It has the same benefits of robustness and

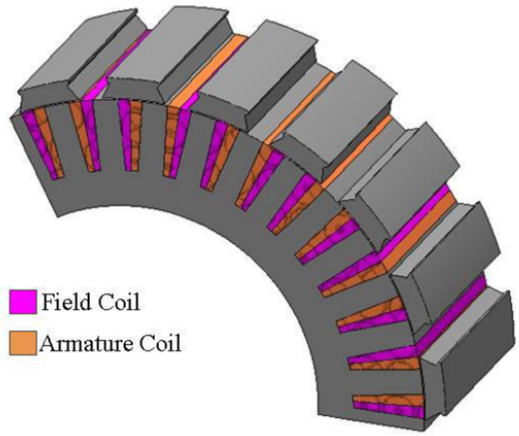

Figure 2-9: Outer Rotor Flux Switching SM

low cost [41]. More Control of the field flux is possible by using field-winding, but it requires a DC current excitation .An exterior rotor machine using this is shown in Figure 2-9.No field current input is required if PMs are used and so losses produced are lower.Though, field weakening is required at higher speeds to reduce the field flux to permissible levels. When both PMs and field windings are present in combination the PMs can produce the most of the field flux and the windings can control this allowing to strengthen or weaken the field.

The PMFSM has high air gap flux density similar to a conventional PM machine[42]. The benefit of this is that the design is less dependent on a small air gap, as SRM are, making the construction simpler.The power density of PMFS machines is comparable to that of a PM synchronous machine while the PM utilisation ratio is lower than that of IPMSM machine [43]. Therefore larger PM mass is needed to get a similar power density to an IPMSM design. However since PMs would be in the stator, they would be closer to the cooling system.Hence less dysprosium (needed to improve the maximum operating temperature of NdFeB) would be required. This can possibly reduce the overall cost of PM material[44].Having fewer issues with magnet retention is another advantage of the PMs in the stator.

2.3.2 Synchronous Reluctance Machine (SynRelM)

A section of synchronous reluctance motor (without PMs) is shown in figure 2-10(a). The stators of SynRelMs is simlilar to those of synchronous machines but only produce

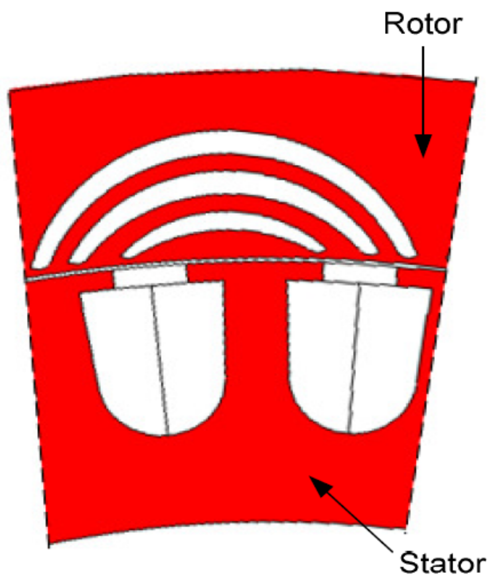

(a) An Outer Rotor SynRel Motor [45]

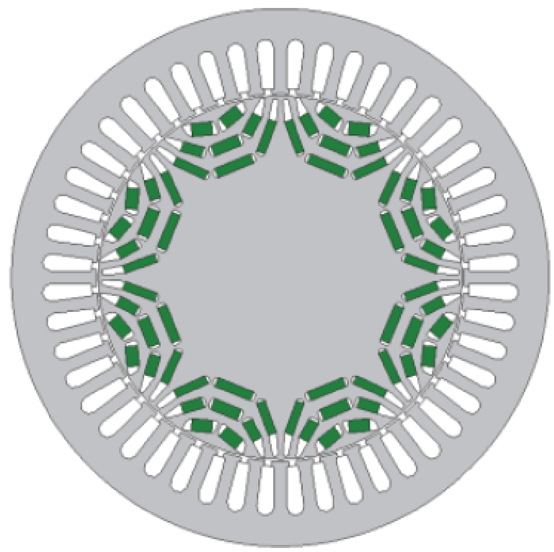

(b) Permanent Magnet Assisted SynRel Motor [46]

Figure 2-10: Synchronous Reluctance Motors

reluctance torque Production of reluctance torque is based on the saliency of the machine. The rotor which has flux barriers placed within it and it is made of laminated steel,depicted in Figure 2-10(a), these flux barriers create different reluctances along the d and q axis.As there's no PMs or windings, the rotor of a SynRelM offers the benefits of the SRM rotor, i.e it is cheap and robust and can be designed to operate at high speeds [47].An acceptable level of torque density can be achieved [47, 48] (having no PMs) with SynRelMs. But its performance cannot be compared to that of a PM machine and thus it is unlikely to reach the requirements of the peak and rated torque of the application being considered while respecting the size restrictions and torque ripple.The required small air-gap to maintain the required performance is an additional complexity of SynRelMs, making constructing and maintaining this air gap more difficult than PM machines.The torque ripple and the power factor are other challenges with SynRelMs. These can be minimized but are still worse than an

IPMSM machine in general [21].

2.3.3 Permanent magnet assisted synchronous reluctance machine (PMa-SynRelM)

PM-assisted synchronous reluctance machine (PMa-SynRelM) has PMs to improve the torque density of the machine. However PMs increase the cost and mechanical issues at high speeds [49] .These machines have an increased reluctance torque compared to an IPMSM, which can be used to reduce supply current or magnet mass requirements for a given torque requirement [50]. Figure 2-10(b) shows a PMa-SynRelM machine where the rotor barriers are filled with ferrite PMs. This design has high saliency while producing a moderate amount of magnet alignment torque.When cheaper PMs or less NdFeB can be used than in an IPMSM the costs can be lowered whilst achieving a high torque density.

The SynRel motor in particular with PM assistance, has been suggested for HEV and EV applications. Using the space within the barriers, by implementing ferrite PMs instead of rare earth is a common approach. In [46],it shows that this machine can have high efficiencies at high speeds. However if large quantities of ferrite PMs are used the mechanical issues caused by the centrifugal forces at high speeds of these machines become even more critical[21].

2.4 Brief comparison of the motor type chosen for the application

Considering the application requirements,the opportunities and limitations posed by each motor type studies in the literature review it was decided to choose BLDC/BLAC surface mounted synchronous motor for the application. Table 2.1 briefly summarizes the comparison among different motor types discussed before.

Machine Type	Permanent Magnet Mass	Torque Density	Field Weakening Range
SMPMSM	High	High	Very Poor
IPMSM	High	High	Poor
IM	None	Medium	Medium
SRM	None	Poor	Very Wide
SynRelM	None	Medium	Wide
FS	Medium	Medium	Wide

Table 2.1: Performance comparison of Motor Topologies

2.4.1 BLDC/SMPM - Strengths

- High torque/power density
- High efficiency
- Torque linearly proportional to I_q, simplifying control
- High compatibility with FSCW stators
- Good candidates for achieving high CPSR using FSCW stators

2.4.2 BLDC/SMPM - Limitations

- Requires magnet containment means for high-speed operation.
- Vulnerable to high rotor losses at high speeds with FSCW stators.
- Magnets may need to be segmented to avoid high losses at high speeds.
- Short-circuit fault currents cannot be extinguished for any non-zero speed.
- Complete dependence on magnet torque requires high magnet content and cost.

2.5 Rotor Configurations

The motor type choice is the most basic design decision,this is due to relatively high cost of magnets and issues related to packaging, magnet retention, and winding [10]. Various configurations of brushless motors which use rotating permanent magnets and stationary phase coils exist. The utilization of different magnet grades in addition to the wide range of applications are the main reasons for having many different variations. For example, for an application needing rapid acceleration and deceleration of the load the torque/inertia ratio should be as high as possible. This call for the use of an interior-rotor motor with high-energy magnets.However,for an application requires constant speed at medium to high speed ,using an exterior-rotor configuration (where rotor is outside of the wound stator) may be the preferred choice.Due to its high inertia an exterior-rotor motor may be a good candidate for applications where a very uniform and constant speed is required.

2.5.1 Interior Rotor Configuration

The interior-rotor motor (shown in figure 2-11) has a similar configuration to that of the traditional SM or the IM.The stator is similar to that of the three-phase induction motor. This design has a high torque/inertia ratio.But considering the manufacturing

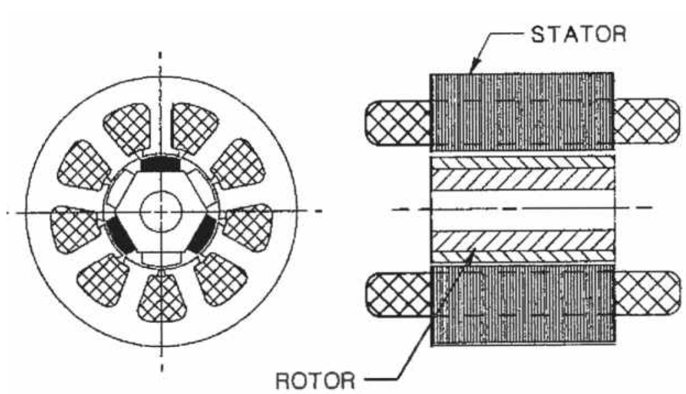

Figure 2-11: Interior-rotor brushless permanent-magnet motor [10]

concerns ,it has the following two shortcomings :

1. Magnet retention must be carefully implemented so that the rotor does not fly apart.

2. Exterior stators are expensive to wind without automatic equipment even though cooling is easier.Examples of interior rotor brushless permanent magnet motors are shown in figure 2-12.

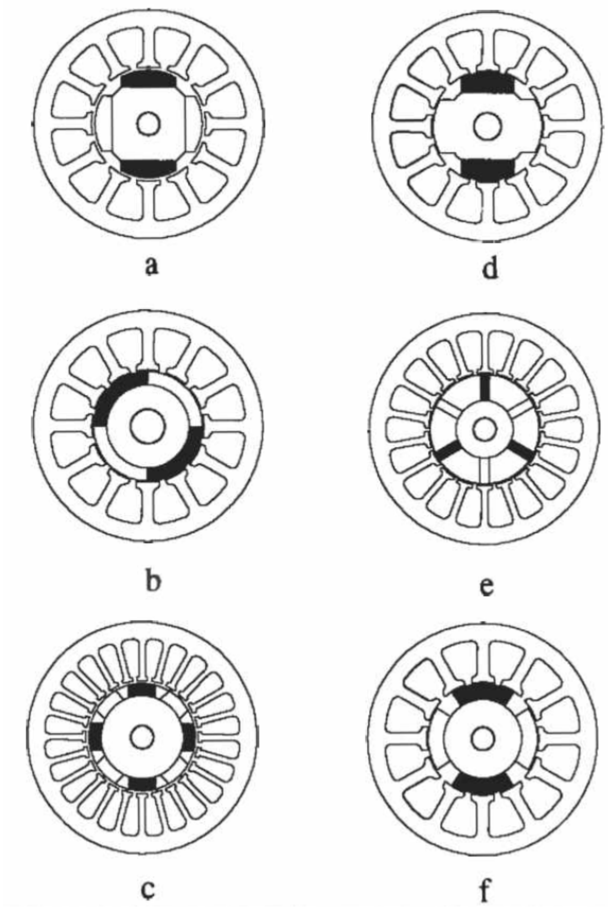

Figure 2-12: Examples of interior-rotor brushless permanent-magnet rotors [10].

2.5.2 Exterior Rotor Configuration

Exterior rotor configuration (shown in figure 2-13) can result in the most cost effective use of ferrite magnets in brushless DC motors [10]. This type of stator is simple to wind using DC-motor fly-winding machines. Some designs are produced on winding machines that wind all three phases simultaneously. The rotor comprises a cup made of soft iron mounted on the shaft with magnet arcs or a molded or bonded ring magnet fixed inside the steel rotor cup with epoxy or Loctite[10]. The balancing is crucial due to the large rotating mass.Magnet retention can be achieved by the rotor cup on the outside of the magnets.The use of a single bearing support of aluminum or die-cast zinc is an advantage of this configuration. Most interior-rotor motors need a bearing at each end,hence requiring two bearing end-bells and higher cost [10]. In general ,exterior-rotor brushless motors are used for continuous- speed applications.

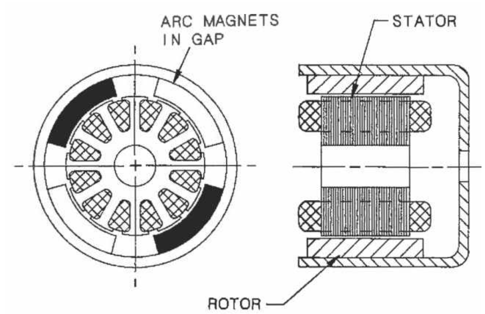

Figure 2-13: Exterior Rotor Configuration [10].

The magnet grades are usually the lower-cost versions of bonded rare-earth, bonded or sintered ferrite grades.Outer rotor motor is popular due to low cost and ease of manufacture.

2.5.3 Exterior Rotor Vs Interior Rotor

The external rotor design has some performance advantages.Outer rotor motor has higher inertia as it has a rotor larger than that of a conventional DC motor. Higher inertia helps to mitigate the torque ripple and hence provides smooth, stable operation even at low speeds.

Generally,external rotor motors can produce higher torque than their similar sized internal rotor counterparts. Torque is proportional to product of the magnetic force and the air gap radius. Outer rotor motors have a larger air gap area than inner rotor counterparts for a fixed motor diameter. The larger air gap permits a higher force to build. They also have a larger air gap radius, which increases the lever arm for torque production. The larger diameter (and, therefore, circumference 2-14) of the rotor in external rotor designs allows the rotor to accommodate more poles further increasing the magnetic flux. In [11], it presents a general comparison of permanent magnet machines of interior and exterior rotor type based on scaling laws. Even though the exterior rotor machine could theoretically produce a much higher torque than achievable with the optimal interior rotor setup. But in real conditions the torque is reduced due to the lowered air gap field in case of magnetic saturation [11].

Outer-rotor motors are shorter in axial direction than inner rotor motors with sim-

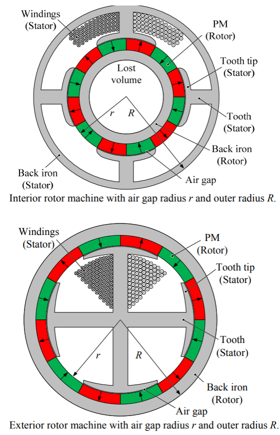

Figure 2-14: Exterior and Interior Rotor Configurations [11]

ilar performance.They have compact size and high torque production. The external rotor can serve as the hub of the fan or blower impeller providing a compact package and allows the impeller to act as a large, rotating heat sink and assist with motor cooling [51]. In [52] a comparison of Outer-Rotor-Type BLDC Motor and BLAC Motor based on numerical analysis is presented where they concluded the BLAC motor to have a reduced of torque ripple and motor size,under identical current density conditions, considering the driving method. In [53] design and optimization of an outer rotor BLDC machine is presented.

2.6 Winding options

Ubiquitously used Winding configurations in three-phase radial-field permanent magnet (PM) brushless machines, can be categorized as [12]:

1) overlapping, either distributed 2-15(a) (two slots/ pole/phase) or concentrated 2-15(b) (one slot/pole/ phase);

2) non-overlapping, that is , concentrated, with either all teeth wound 2-15(c) or alternate teeth wound 2-15(d). Distributed overlapping winding usually results in a more sinusoidal magnetomotive force (MMF) distribution and EMF waveform, and therefore it is ubiquitously used in PM brushless ac (BLAC) machines [54].

Fractional-slot concentrated-windings (FSCW) provide several benefits in synchronous permanent magnet (PM) machines including high-power density, high efficiency, short end turns, high slot fill factor particularly when coupled with segmented stator structures, low cogging torque, flux-weakening capability, and fault tolerance [55][56],[57]. In [58] method for directly calculating the winding factor, without doing a winding layout first has been proposed. Fractional-slot winding machines are good candidates for applications with certain requirements.For example they perform well for low speed applications and the machine can be designed to have a higher number of poles [59]. Fractional -slot winding can minimize the manufacturing costs [60] while reducing end-winding lengths [61]. Further these fractional slot windings can be designed to have a low torque ripple and to reduce the periodicity between Q(the number of slots) and p (the number of pole pairs) [62]. These motors with fractional-slot windings can be used in direct-drive applications.More over they can be candidates to use design machines with fault-tolerance capability [63, 64].

2.6.1 Concentrated Winding Versus Distributed Windings

Concentrated and distributed windings are two common winding configurations.A coil is wound around each tooth in the case of Concentrated windings. In a distributed winding a coil can span multiple teeth.Concentrated windings usually have shorter end windings and it's possible to use segmented stators allowing to achieve better slot fill factors. This can result in reduced copper losses and reduced machine sizes [65].

Distributed windings can produce higher reluctance torque as they can have higher saliency between the d and q axis. This is a consequence of both the d and q axis reluctances being proportional to both the winding factor and ratio of number of coils and square of pole number [10]. Each of these can be equal for concentrated and distributed designs. As distributed winding machines usually have higher number of slots and integral slots per pole per phase typically these values are larger for distributed designs [65, 66]. These distributed sinusoidal windings can result in lower leakage flux and hence lower losses [10, 67].Concentrated winding designs are usually more suitable to achieve a higher torque density as they permits higher slot fill factors [68]. However, since distributed winding machines have a higher reluctance torque they can perform better in field weakening region.

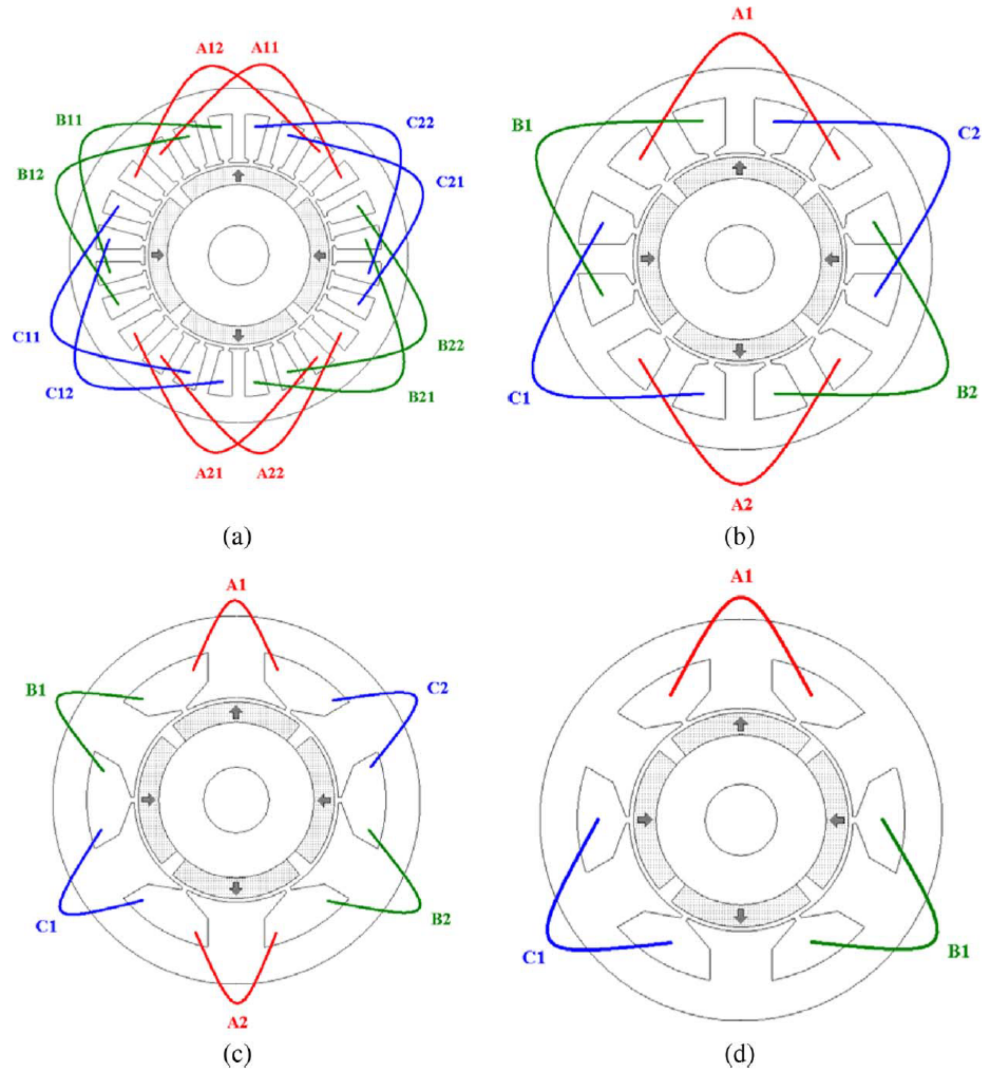

Figure 2-15: Typical stator winding configurations (four pole) [12]. (a) 24-slot, overlapping (distributed). (b) Twelve slot, overlapping (concentrated). (c)6-slot, nonoverlapping, all teeth wound. (d) 6-slot, non-overlapping, alternate teeth wound.

Chapter 3

Developing Initial Design Approach

This chapter details the design approach (mainly adopted from [1]) and the calculations related to basic sizing used in the initial design. Two main initial motor designs viz one with fractional-slot winding fed by a sinusoidal drive and the other one with integer- slot winding fed by a square wave drive are presented for the comparison purpose. The BLDC motor fed by a square-wave drive allows to use a simpler control strategy while offering slightly higher torque per volume. However, BLAC motor fed by sinusoidal drive has much superior performance in terms of torque ripple providing a smooth torque.Therefore eventually BLAC motor fed by sinusoidally drive was chosen for the application and further optimization.

3.1 Understanding the Application requirements

The specifications for the motor are tabulated in 3.1. The motor is an in-wheel motor whose radial and axial dimensions are restricted by the available space which depends on the dimensions of the rim. The maximum speed is as low as 400 RPM and the speed range is narrow which does not require to operate the motor in flux weakening region. The peak torque requirement is approximately 19-20 Nm and the motor peak output power is 800 W($\pm$10%). The transmission is direct drive where there's no gear box. The cooling method is natural air cooling therefore it's required to ensure temperature levela are maintained within the desired limits.

Parameter	value
Voltage Rating	72V/48V
Motor Speed	400/250 RPM
Wheel Radius	0.3 m
Peak Power Rating	800 W/ 500 W ±10%
Torque	20 Nm/ 10 Nm ±10%
Continuous Power	500 W/ 250 W
Max Frequency	400 Hz
Transmission	Direct drive
Winding Type	Double layer concentrated
Temperature limits	100 C/ 150 C

Table 3.1: Basic Specifications of the Motor.

3.2 Preliminary Design Considerations

The aim was to design a permanent magnet motor for an electrical traction application which is able to able to satisfy the following features:

high efficiency;

smaller size and light weight

suitable for direct-drive;

variable speed;

low noise and vibration;

easy to manufacture and assemble;

moderate cost.

3.3 Generalized Design procedure

The basic design algorithm and motor sizing procedure was adopted from previously published works and textbooks by other authors [69, 1, 2]. The general design flow is shown in figure 3-1

- Determination of application requirements
- Interior-rotor, exterior rotor, or axial-gap configuration

- Select magnet grade
- Select number of poles
- Select number of stator slots and phases

- Perform rough sizing estimate
- Select air gap length and determine
- magnetic Loading

- Design rotor and determine flux/pole
- Layout stator lamination dimensions
- Calculate wire size, resistance and inductance/phase

- Calculate Performance
- Check temperature rise, current density, flux densities, demagnetization of magnet

- Optimization, Modify design and reiterate until objectives are met

Figure 3-1: Generalized Design Procedure.

3.3.1 Exterior Rotor Configuration

Exterior-rotor configuration was selected to achieve a higher torque while keeping the motor dimensions sufficiently smaller. The torque is produced at a radius that is quite large relative to the outside diameter of the machine.This implies the same torque can be obtained with lower electric and magnetic loading than would be required in a traditional interior rotor motor [13].Permanent magnets are retained inside rotor cup. It also provides a return flux path. It offers simplicity in manufacturing. This solution does not require to apply any banding for the magnet retention. Further it permits reducing the air-gap length compared the interior rotor counterpart. Cross section of a typical exterior rotor is shows in figure 3-2.

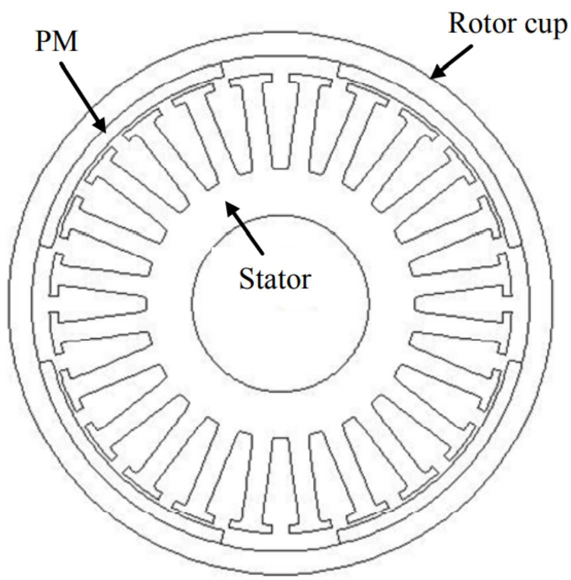

Figure 3-2: Typical cross section of the exterior-rotor surface PM motor. courtesy:[13]

3.4 Determination of Motor Dimensions

The determination of the main dimensions of the motor (outer stator diameter D_e and the stack length L_{stk}) are chosen based on the available space and other physical restrictions imposed by the application itself. Being the rated torque T_n of the machine related to the active volume, the adopted procedure is based on the ratio between the torque and the outer volume of the machine itself. For this purpose factor k_{TV} is defined, which corresponds to this ratio. Typical k_{TV} (TRV) values are given in following table 3.2.

Cooling Type	Typical values of TRV (kN/m^3)	Sigma lbf/in^2	K lbf-in/in^3
Small totally enclosed motors (Ferrite)	7- 14	0.5 -1	0.8-1.6
Totally enclosed motors (sintered rare earth or NdFeB)	14-42	1-3	1.6 -4.7
Totally enclosed motors (Bonded NdFeB)	21 typ.	1.5 typ.	2.4 typ.
Integral-hp industrial motors	7-30	0.5 -2	0.8-3
High-performance servo motors	15 -50	1-3	1.5 -5
Aerospace machines	30-75	2-5	3-7.5
large liquid-cooled machines	100 -250	10-15	15 -200

Table 3.2: Typical values of TRV, K and Sigma. Reference:[10]

The air gap volume is typically related to the rated motor torque, since the tangential (shear) stress due to the interaction between the electric and magnetic fields occurs at the air gap surface. However, the volume considered here refers to the outer diameter. The outer volume has a more direct relation with the machine size.Since the ratio between outer and inner stator diameters, D_e and D_i respectively, changes with the machine dimensions (small size machines have a D_e-to-D_i ratio larger than large size machines).This means the factor k_{TV} also depends on the rated torque. For example rated torque in the range between 5 and 50 Nm, a proper value (expressed in Nm/litre) is, [70],

$$k_{TV} \simeq 10Nm/l \tag{3.1}$$

It is noted that the value of k_{TV} is within the range between 8 and 12 N m/l. This range depends on the cooling effectiveness.Once the outer volume is fixed, D_e and L_{stk} are segregated on the basis of further practical needs, such as maximum outer space, maximum available length, existing stator lamination, and so on [70]. The geometrical parameters of the outer-rotor designs are defined in 3-3.

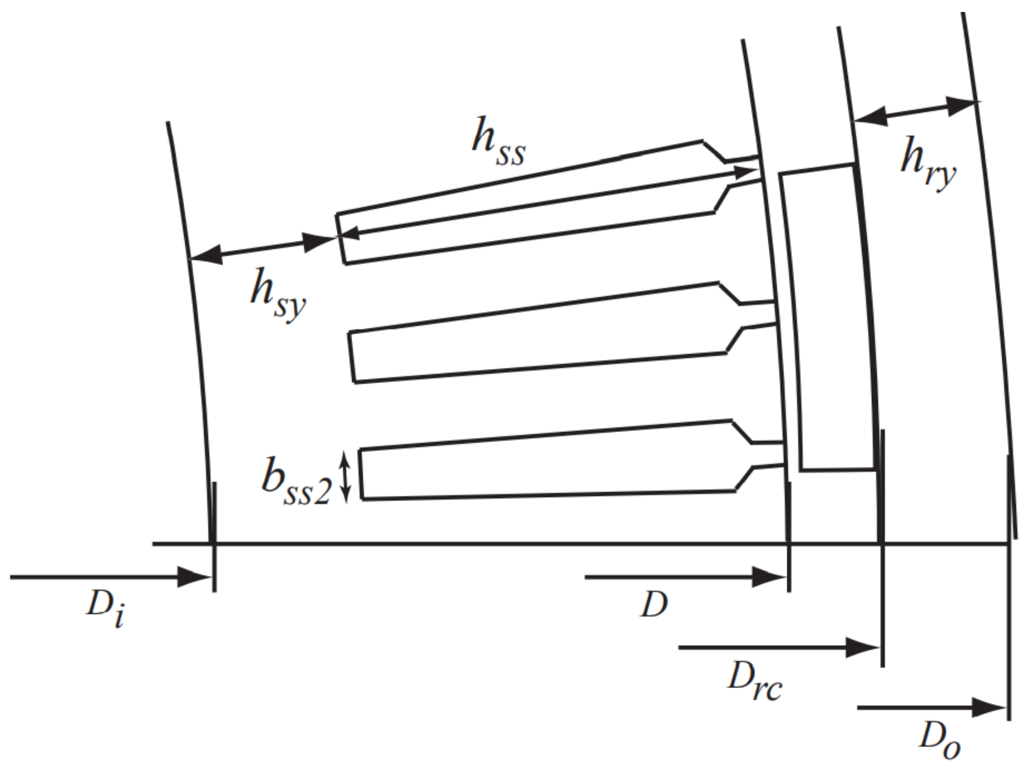

Figure 3-3: Definition of the geometrical parameters for the outer-rotor SMPM motors [14]

3.5 Magnet Selection

A comparison of different magnet grades are tabulated in 3.3.

Material of Magnet	BHmax	Br T	Hc kA/m
NdFeB	200-500	0.97-1.45	740-1000
SmCo	120-400	0.85-1.10	620-840
Ferrite	7-42	0.20-0.48	120-360
AlNiCo	10-35	0.60-1.16	40-120

Table 3.3: Comparison of Magnets. [16]

Ferrite magnets have lower electrical conductivity than rare-earth magnets, so the eddy current losses are much lower, hence the temperature rise due to eddy current losses are lower. Ferrite magnets have a lower remanent magnetic flux density compared to neodymium magnets, however ferrite magnets have a higher Curie temperature, So ferrite magnets are suitable to use in high-temperature environments, such as electric vehicles, thus offering improved reliability compared to the use of rare-earth permanent magnets [71]. The figure 3-4 depicts the demagnetization curves for NdFeB magnets.

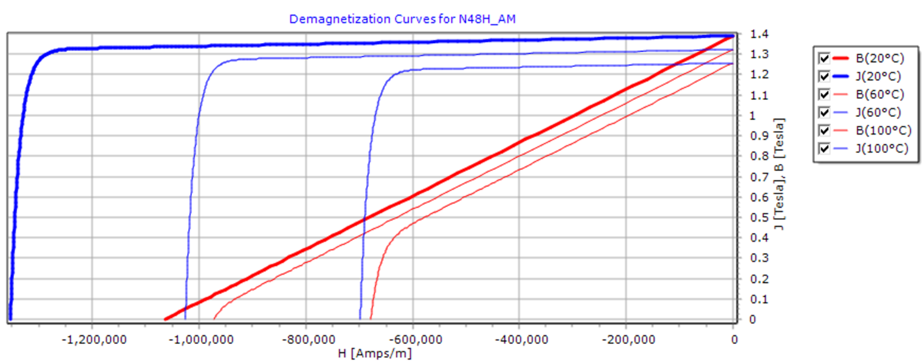

Figure 3-4: Demagnetization Curves for NdFeB magnets.

3.6 Selection of the Number of Poles and Slots

The selection of pole and slot combinations is based on some rules when designing an electrical machine. These are also applicable to concentrated windings.

The pole number is an even number.

the number of pole pairs, P_p, in a section of the machine can not be a multiple of the phase number. This would lead to unbalanced windings [72, 73].

The number of poles can not be equal to the number of slots. This could results in an undesired cogging torque in the machine in addition to the machine being a single phase machine. The number of slots must be a multiple of N_{ph}.

3.7 Concentrated Windings

Concentrated windings are usually preferred in industry especially due to the low cost production technology.The motor length is main constraint for in-wheel motors,and therefore concentrated winding is preferred. Moreover, the reduction of copper loss and weight , higher fill factor and the lowered production cost are other advantages. The main drawback is higher torque ripple of concentrated winding compared to distributed winding . So modifying the geometrical parameters such as the stator teeth to reduce the torque ripple is crucial and the most important method is the combination between number of poles and slots [74, 75].

Fractional slot Windings

The chart in figure 3-5 shows the winding factors corresponding to different slot-pole combinations.

A multipole PM motor can be a good solution for low-speed high-torque applications.Low iron mass per rated torque due to rather low flux per pole is the benefit here. A high pole number in conventional distributed winding motors result a high slot number increasing costs and, in the worst cases it can result in a low copper fill factor. The fractional-slot concentrated-winding solution does not require many slots although the pole number is high. This reduces both the iron and copper mass in the motor. The fractional-slot winding allows a longer stator stack in the same frame length than conventional windings as the axial length of end winding is typically shorter. It is possible to have a larger airgap diameter in a certain limited

Q_s		Poles 4	6	8	10	12	14	16	20	22	24	26
6	ξ_1	**0.866**	**	0.866	0.5	**	0.5	0.866	0.866	0.5	**	0.5
	q	0.5		0.25	0.2		0.143	0.125	0.1	0.091		0.077
9	ξ_1		**0.866**	**0.945***	**0.945***	**0.866**	0.617	0.328	0.328	0.617	0.866	0.945
	q		0.5	0.375	0.3	0.25	0.214	0.188	0.15	0.136	0.125	0.115
12	ξ_1			0.866	0.933	**	0.933	0.866	0.5	0.25	**	0.25
	q			0.5	0.4		0.286	0.25	0.2	0.182		0.154
15	ξ_1				0.866	**	**0.951***	**0.951***	0.866	0.711	**	0.39
	q				0.5		0.357	0.313	0.25	0.227		0.192
18	ξ_1					**0.866**	0.902	0.945	0.945	0.902	0.866	0.74
	q	$q > 0.5$				0.5	0.429	0.375	0.3	0.273	0.25	0.231
21	ξ_1						0.866	0.89	**0.953***	**0.953***	**	0.89
	q						0.5	0.438	0.35	0.318		0.269
24	ξ_1							0.866	0.933	0.949	**	**0.949**
	q							0.5	0.4	0.364		0.308

* not recommended because of the unbalanced magnetic pull

** not recommended because denominator n ($q = z/n$) is a multiple of the number of phases m.

Figure 3-5: Fundamental winding factors ξ_1 for concentrated two-layer windings ($q \leq 0.5$). [2]

stator outer diameter as the stator yoke can be manufactured very thin. This offers a great potential to increase the torque density. Thus ,the multipole PM motor with fractional-slot concentrated windings is selected as the direct-drive motor.In a fractional-slot winding motor, various possible slot and pole number combinations exist. It is crucial to select the slot and pole number combinations that can achieve the best machine performance. The selection criteria for fractional-slot winding motors under study are as follows [75].

The fundamental winding factor should be as high as possible. This alllows to produce the highest possible torque.

The lowest common multiple (LCM) between the number of poles and slots should be as high as possible. The LCM order value increases the cogging torque frequency and lowers its magnitude.

An unbalanced magnetic pull should be avoided. The slot/pole combinations (Q_s/2p) giving winding layouts without any symmetry such as combinations with Q_s = 9+6m, where m = 0, 1, 2,..., and 2p = $Q_s \pm 1$ should be avoided [76].

In addition to these criteria, a two-layer winding is used in order to achieve the shortest possible end windings.

3.7.1 Winding Factors and Winding Feasibility

The machine periodicity t, the greatest common divisor (GCD) between Q and p is,

$$t = GCD(Q, p) \tag{3.2}$$

A winding is feasible when the number of spokes per phase are equal,that is the ratio q_{ph} = Q/mt should be an integer [77].

Distribution Factor

The ratio between the geometrical and the arithmetic sum of the phasors of the same phase is defined as the distribution factor. The fundamental winding factor can be calculated by [77],if q_{ph} is even,

$$k_d = \frac{\sin \frac{q_{ph}}{2} \frac{\alpha_{ph}}{2}}{\frac{q_{ph}}{2} \sin \frac{\alpha_{ph}}{2}} \tag{3.3}$$

and if q_{ph} is odd k_d i,s given by

$$k_d = \frac{\sin q_{ph} \frac{\alpha_{ph}}{4}}{q_{ph} \sin \frac{\alpha_{ph}}{4}} \tag{3.4}$$

where

$$\alpha_{ph} = \frac{2\pi}{(\frac{Q}{t})} \tag{3.5}$$

Pitch Factor

The pitch factor is computed from the coil throw. The slot pitch y_q is approximated by,

$$y_q = round \frac{Q}{2p}$$

The lowest possible value for y_q is unity. The coil span angle is ,

$$\sigma_w = \frac{(2\pi p y_q)}{Q}$$

The fundamental pitch factor is given by [77],

$$k_p = \sin\frac{\sigma_w}{2} \tag{3.6}$$

The winding factor for an motor (without skewing) can be expressed by

$$k_w = k_d.k_p \tag{3.7}$$

3.8 Design Approach with Analytical Formulae

The elementary block of a SMPM illustrating geometrical parameters is shown in figure 3-6.

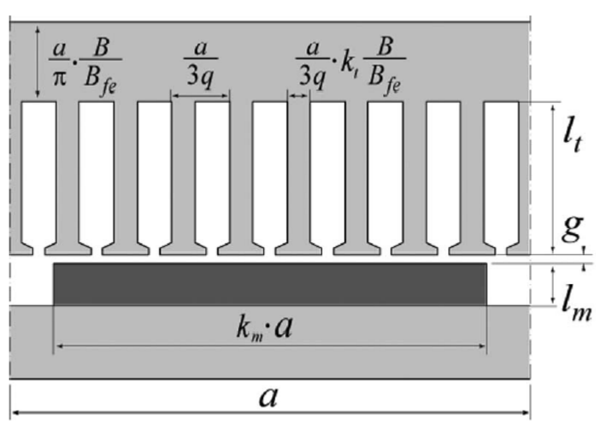

Figure 3-6: Elementary block of an SPM machine [1]

Main design parameters including shear stress (related to torque density), power factor (PF), and Joule loss per exterior surface unit is expressed as a function of q and the geometric quantities. The PF can be maximized by design, given the shear stress, or vice versa. It's beneficial to maximize PF specially for fractional slot machines due to the following facts[1].

• A low PF negatively affects the size of the power converter.

• A low PF indicates that the machine can be prone to load dependent core saturation, leading to a torque reduction.

• The machine inductance is the key design parameter of fractional slot SPM machines. [1]

3.8.1 Per-Unit Machine Model

Magnetic Loading

Magnetic loading B (peak fundamental flux density) at no load

$$B = \hat{B}_{gap,fund} = k_b . \frac{B_r}{1 + k_c . \frac{g}{l_m}} \tag{3.8}$$

Where B_r is the remanence flux of permanent magnets, k_c is carter coefficient and k_b is a shape factor accounting for quantifying fundamental and is given by [78]

$$k_b = \frac{4}{\pi} . \sin k_m \frac{\pi}{2} \tag{3.9}$$

where k_m is magnet's pole arc

For a fixed air-gap length, the no-load magnetic loading B depends on rotor parameters and k_c only. It does not depend on rotor pole pitch a.

The magnetic loading and the resistance to demagnetization of the machine is eventually determined by the normalized PM thickness l_m/g. In [1] , It says that Over certain values, such as l_m/g = 6, it is not convenient to further increase l_m/g to improve B,unless it is required by special overload needs and related demagnetization issues.

Electric Loading and Shear Stress

The electrical loading is given by

$$A = \frac{3}{2}.\frac{N}{a}.k_w.I_q \tag{3.10}$$

where k_w is the winding factor, N is the number of conductors in series per pole per phase, and I_q is the phase current amplitude.To satisfy the maximum torque per ampere scenario the current vector is aligned with the quadrature axis. The average shear stress is given by,

$$\sigma = BA[N/m^2] \tag{3.11}$$

For a cylindrical machine σ is proportional to its torque per rotor volume density. The electromagnet torque is given by,

$$T_{em} = \frac{\pi}{2}D^2L\sigma = 2V_r\sigma \tag{3.12}$$

Once B is determined then the shear stress will depend on the electric loading only.The upper limit of electrical loading related to thermal limit or efficiency target or to demagnetization.

Specific Joule Loss

Joule loss factor k_j is given by [1],

$$k_j = \frac{2\rho_{Cu}k_{end}}{k_Cu(1 - k_t.\frac{B}{B_{fe}})}.(\frac{A}{k_w})^2.\frac{l}{l_t} \tag{3.13}$$

where ρ_{Cu} is the electric resistivity of copper, k_{Cu} is the slot filling factor and k_{end} is the length of the conductors, including end connections, divided by their active length. B_{fe} is the peak flux density in the stator back iron. B_{fe} is inversely proportional to the cross section of the stator yoke, as defined in figure 3-6. k_t is the tooth scaling factor which is proportional to the tooth width.k_j (in W/m^2) can be calculated by dividing the copper loss of the elementary block by its outer surface area.k_j does not

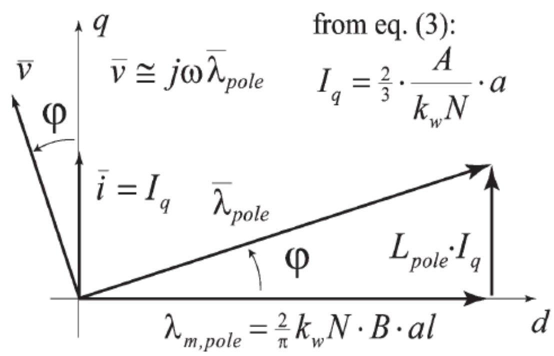

Figure 3-7: Definition of Power Factor [2]

depend on pole pitch and air-gap length. It mainly depends on tooth length hence at continuous conditions k_j determines tooth length value.

Power factor

The current vector is in time quadrature with the PM flux linkage $\lambda_{m,pole}$, and the stator resistance voltage drop is neglected. The PF angle Φ can be calculated in normalized quantities by,

$$\tan\Phi \cong \frac{4\mu_0}{3\pi}.\text{Ł}_{pole,pu} \cdot \frac{A}{B} \tag{3.14}$$

where $L_{pole,pu}$ is base inductance and the base inductance is given by,

$$L_{base} = \frac{\mu_0.l}{2}(\frac{2}{\pi}.k_w.N)^2$$

Here l is the stack length. If rare earth magnets are used then factor B has very little variations when changing from one machine to another,and then the per-unit inductance directly relates the PF to the shear stress (torque density)[1].

3.8.2 Analysis of Inductance

In this section , the minimization of the pole per-unit inductance is described. The criteria for a best compromise between shear stress and PF is presented.The inductance of the elementary block in Figure 3-6 is the sum of the slot leakage and the air-gap inductances

$$L_{pole,pu} = L_{g,pu} + L_{slot,pu} \tag{3.15}$$

In per unit values, components of $L_{pole,pu}$ depend on the geometric variables defined in Figure 3-6, with distinct expressions for distributed (integer q) and concentrated (fractional q) windings.

Distributed Winding Machines

The magnetization inductance is given by[1],

$$L_{g,pu} \simeq \frac{\pi^2}{6.{k_w}^2}.(\frac{1}{k_c + \frac{l_m}{g}}).\frac{a}{g} \tag{3.16}$$

The slot inductance is,

$$L_{slot,pu} = \frac{\pi^2}{2{k_w}^2}.\frac{\frac{l_t}{g}}{1 - \frac{B}{B_{fe}}k_t}.(\frac{a}{g})^{-1} \tag{3.17}$$

Equations 3.16 and 3.17 are valid for q = 1.

It can be shown that the minimum inductance condition is when $L_g = L_{slot}$ [1].Setting $L_g = L_{slot}$, the polepitch- to-air-gap ratio that minimizes the inductance can be calculated by,

$$(\frac{a}{g})_{L_{min}} = \sqrt{\frac{3.\frac{l_t}{g}.(1 + \frac{l_m}{g})}{1 - \frac{B}{B_{fe}}k_t}}$$

(3.18)

The minimum inductance, corresponding to 3.8.2 is [1]

$$(L_{pole,pu})_{min} = \frac{\pi^2}{\sqrt{3}{k_w}^2}.\sqrt{\frac{\frac{l_t}{g}}{(1 + \frac{l_m}{g}).(1 - \frac{B}{B_f e}K_t)}} \tag{3.19}$$

Typical values of kt are 0.8–0.9 for distributed windings [1].

Fractional Slot Machines

The slot inductance for n_l number of layers is,

$$L_{slot,p} = \frac{\pi^2}{2{k_w}^2}.\frac{\frac{l_t}{g}}{\left(1-\frac{B}{B_{fe}}k_t\right)}.\left(1-\frac{3.(n_l-1)}{4.Q_0}\right).(\frac{a}{g})^{-1} \tag{3.20}$$

Q_0 is the number of slots corresponding to half the electrical periodicity of the machine [77], for those q where antiperiodic symmetry conditions apply, or corresponding to the full electrical period, when they do not. $L_{g,pu}$ is given by [1],

$$L_{g,pu} = \frac{1}{n_l}.\frac{\pi^2}{12(qk_w)}.\left(\frac{1}{k_c+\frac{l_m}{g}}\right).\frac{a}{g} \tag{3.21}$$

the minimum inductance condition and the minimum inductance value are given by[1],

$$\left(\frac{a}{g}\right)_{Lmin} = q\sqrt{\frac{6n_l\left(1-\frac{3(n_l-1)}{4.Q_0}\right)\frac{l_t}{g}\left(1+\frac{l_m}{g}\right)}{\left(1-\frac{B}{B_{fe}}k_t\right)}} \tag{3.22}$$

$$(L_{pole,pu})_{min} = \frac{1}{q}.\frac{\pi^2}{\sqrt{6}{k_w}^2}\sqrt{\frac{\frac{l_t}{g}\left(1-\frac{3(n_l-1)}{4Q_0}\right)}{n_l\left(1+\frac{l_m}{g}\right).\left(1-\frac{B}{B_{fe}}k_t\right)}}$$

(3.23)

The minimum inductance pole pitch in equation (3.28) is proportional to the fractional q, while it was independent of integer q.

3.8.3 Power factor Maximization

The following conclusions about machines having minimized inductance have been made in [1]

- Fractional slot machines tend to have a smaller $(a/g)_{Lmin}$ and then a higher number of poles when the minimum inductance criterion is satisfied.

• In such conditions, double-layer machines can be close to integral slot ones for values such as q = 1/2 or 2/5.

• Low-q machines and single-layer machines tend to have a high number of poles (low a/g) for keeping the inductance low.

• Integral slot machines are insensitive to q, whereas fractional slot ones are very sensitive to q.

• The minimum inductance is inversely proportional to the fractional q and becomes very large for little values of q such as 1/8 or 1/10.

3.8.4 Design Algorithm

Machine's torque T and number of pole pairs are given by,

$$T = \sigma.2\pi.r^2.l \tag{3.24}$$

$$p = \frac{\pi.r}{a} \tag{3.25}$$

where σ is shear stress, r is rotor radius, l is stack length and a is pole pitch. Initial designing of the elementary block , the reference value for Power factor is set and designs that do not satisfy the requirements are rejected and the model is to be redesigned with new input parameter values.An spread sheet was prepared for the calculation and the results are provided in Appendix A.

Preliminary Input data

• Air-gap length g.

• q and type of winding.

• PM grade B_r and thickness l_m/g.

• Steel exploitation B_{fe} (peak).

• Cooling and thermal constraint, represented by target specific loss k_{j0}.

• Target shear stress σ_0, with reference to typical figures of machines having the same type of cooling and the same size.

Design of the Elementary Block

1) Magnetic loading B is calculated via 3.8.

2) The electric loading is calculated from B and the σ_0 target shear stress, according to the equation 3.11.

3) The tooth length is chosen appropriately according to the loss target k_{j0}, according to the equation 3.13. The end connection factor k_{end} is also an approximate value. So it would be recalculated once the active length and the pole pitch are determined. This step might require iterative calculations.

4) Reference pole pitch $(a/g)_{Lmin}$ is calculated according to the minimum inductance condition (3.8.2 or 3.19) respectively.

5) The minimized PF is evaluated and compared with the threshold.

i)If the PF is satisfactory, then the block is completely defined.

ii) If the PF is lower than the satisfactory threshold , then l_t is reduced and the flowchart is restarted from point 3. One of the two targets σ_0 and k_{j0} must be relaxed.

iii). If there is a PF margin much greater than the reference PF , then the pole pitch is reduced with respect to $(a/g)_{Lmin}$ for increasing the number of poles. The outputs of this stage are:

• pole pitch a/g and tooth length l_t/g;

• the shear stress, the PF, and the Joule loss factor.

Sizing of the Motor

The additional input data are,

• target torque T_0 and the rated speed

• maximum outer radius R_0 and stack length l_0. The following six conditions are met when the shear stress is provided.

1) The product r^2l is evaluated by 3.24, according to the target torque.

2) The rotor radius and stack length can be determined from r^2l within the allowable length limit.

3) The number of pole pairs 3.25 is calculated and approximated to the closest feasible number. Because only certain integers are feasible with fractional slots.

4) The end connection length and the specific loss are re-calculated accordingly.

5) Additionally the machine inductance and the PF are recomputed once the pole-pair number is determined.

6) The stator outer radius is determined. If dimensions are within the permissible limits then the flowchart is completed, the final design is modelled in MotorCAD and FEA evaluated.

Preliminary data for the elementary block are tabulated in table 3.4.

Parameter	value
Air-gap length	1 mm
q	4/11, 1
Winding Type	Concentrated , Double layer
Br	1.45T
lm/g	10
B_{fe}(peak)	1.7T
Target k_{j0}	600 W/m2
L_{stack}	5cm
σ_0	7kN/m2
Target Torque	19.1 ±10% N at 400 RPM
maximum outer radius R_0	10 cm

Table 3.4: Preliminary Design Data of Elementary Block

3.8.5 Summary of Equations Applicable to Radial Flux Permanent Magnet Motors

Back emf and Torque Equations: Sinusoidal Excitation

It is assumed the phase currents sinusoidal and all three phases are conducting during the commutation period. Considering only fundamental back emf component , the electromagnetic torque is given by,

$$T_e m = \frac{3e_{rms}I_{rms}}{\omega_m} \tag{3.26}$$

Peak back emf is given by,

$$e_{peak} = -\omega_{electrical}\frac{d\lambda}{d\theta} \tag{3.27}$$

$$\frac{d\lambda}{d\theta} = N_{ph}A_g B_{av} \tag{3.28}$$

$$e_{peak} = \frac{\pi}{2}\omega_m N_{ph} B_{gav} D_i L \tag{3.29}$$

$$e_r ms = \frac{e_{peak}}{2} \tag{3.30}$$

Torque expressed in geometrical parameters,

$$T_e m = \frac{3\pi}{2\sqrt{2}} N_{ph} B_{gav} D_i L I_{rms} \tag{3.31}$$

Electrical loading A is defined by,

$$A = \frac{2mN_{ph}I_{rms}}{\pi D_i} \tag{3.32}$$

For a 3-phase motor where m = 3,

$$A = \frac{6N_{ph}I_{rms}}{\pi D_i} \tag{3.33}$$

Therefore finally the torque under sine-wave excitation $T_{em,sine}$ becomes,

$$T_{em,sine} = \frac{\pi^2}{4\sqrt{2}} B_{gav} A {D_i}^2 L \tag{3.34}$$

Back emf and Torque Equations : Square-wave Excitation

In this case, it is assumed that two phases are conducting simultaneously in commutation period. The peak value of trapezoidal current is the dc link current I_{DC}. For a flattop value of the phase back emf E_{ph}, the electromagnetic power is given by,

$$P_{em} = 2E_{ph}I_{DC} = T_{em}\omega_{mech} \tag{3.35}$$

The rms value of a DC trapezoidal current with 120^0 electrical angle is given by,

$$I_{rms} = \sqrt{\frac{3}{2}}I_{DC} \tag{3.36}$$

The following set of equations are used to calculate flattop value of back emf E_{ph}.

$$\lambda = N_{ph}\Phi_g \tag{3.37}$$

$$e = -\frac{d\lambda}{dt} = -\frac{d\lambda}{d\theta_{elec}}\frac{d\theta_{elec}}{dt} = -\omega_{elec}\frac{d\lambda}{d\theta_{elec}} \tag{3.38}$$

$$\phi_g = B_g A_g = B_g \theta_{mech} R_i L = B_g \frac{2}{p}\theta_{mech} \tag{3.39}$$

$$E_{ph} = \frac{P}{2}\omega_{mech}\frac{2N_{ph}\Phi_g}{\theta elec} = N_{ph}B_g L D_i \omega_{mech} \tag{3.40}$$

The torque equation under square-wave excitation becomes,

$$T_{em,square} = \frac{\pi}{\sqrt{6}}B_g A {D_i}^2 L \tag{3.41}$$

3.9 Simulation Results of Sinusoidally fed PMSM

For comparison purposes ,two initial designs viz one with fractional slot winding with sinusoidal excitation and another one with integer slot (q=1) with square-wave excitation were considered. An excel spread sheet was used for the initial calculations done by using analytical equations mentioned in previous sections. The resulting values are provided as tables in appendix A. Using those calculated parameter values the initial design was simulated in MotorCAD software.

A wide range of slot-pole combinations and q values were considered and slot number Q = 18 and pole number 2p = 20 was chosen for the fractional slot machine with sinusoidal excitation.For the integer slot machine (q =1) , 12 poles and 36 slots were chosen accordingly.The former machine and the latter machine will be referred as 20P18Q motor and 12P36Q motor for the rest of this document.The radial cross section of initial design of 20P18Q machine (with sinusoidal excitation) is shown in 3-8(a).The magnetic flux density distribution of the radial cross section is shown in figure 3-8(b). The preliminary design data of the sinusoidal excited machine are

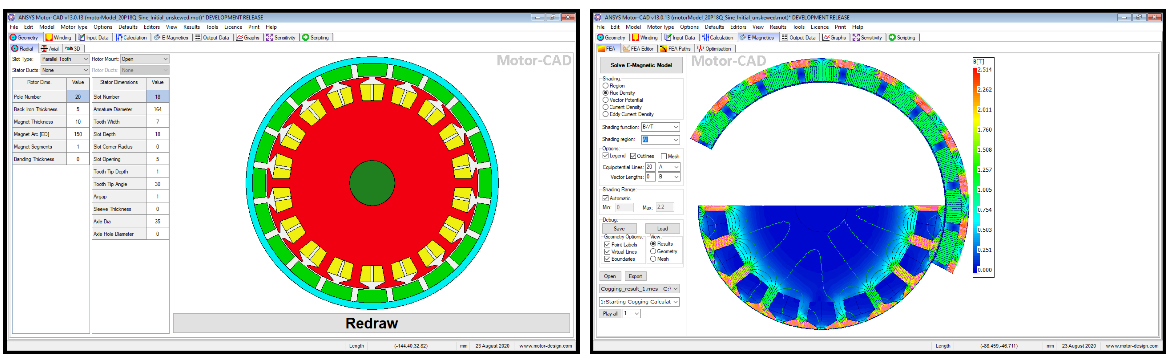

(a) Initial Design -Radial cross section (Sinusoidal) (b) Electromagnetics Window

Figure 3-8: Motor CAD model of Initial Design -Radial cross section 20P18Q Machine.

tabulated in table 3.5. The winding layout of 20P18Q machine is shown in figure 3-9. The torque-speed characteristic of the 20P18Q machine's initial design is shown in figure 3-10. The output waveforms fractional Slot 20P18Q motor initial Design are shown in figure 3-11. The drive output data of initial 20P18Q machine are tabulated in the table 3.6. Electromagnetic output data of the initial 20P18Q machine are tabulated the table 3.7. The flux densities of preliminary design 20P18Q Motor are tabulated in table 3.8. The winding data of initial 20P18Q motor are shown in tabel 3.9.

Stack length mm	5
Outer rotor diameter mm	164
Outer stator diameter mm	147
PM thickness mm	10
N.turns per phase	20
Wire size mm	2.28
Copper Slot Fill	0.4
Phase current A_{max}	14.98
Average torque @ 400 rpm Nm	19.1±10%
Output power W	800
Temperature: Winding C^0	140
PM C^0	120
Magnetization	Radial
Peak Current	15.2A
RMS Current	10.75A
RMS Current Density	2.8A/mm^2

Table 3.5: PMSM Preliminary Design Data Fractional Slot 20P18Q Machine

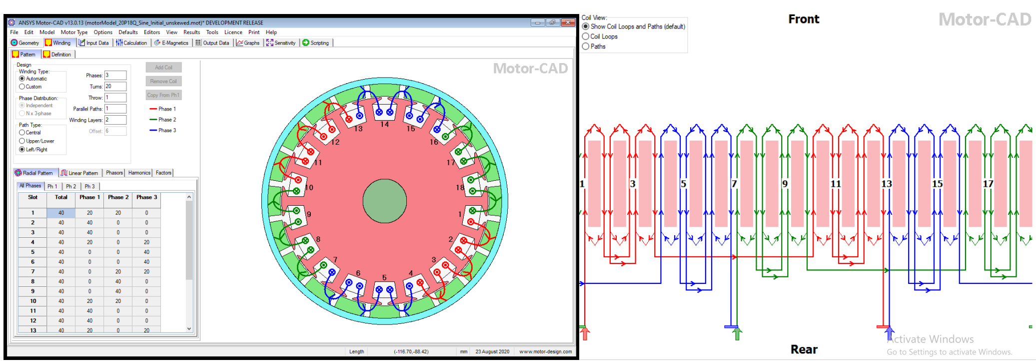

(a) Winding Layout Radial view (b) Linear Coil Pattern.

Figure 3-9: Winding Layout of 20P18Q Machine.

3.9.1 Simulation Results of the initial Design BLDC Motor fed with Square-wave Drive

Preliminary design data for the integer slot motor are tabulated in table 3.10. The radial cross section of initial design of integer motor is shown in 3-12(a).The magnetic flux distribution of 12P36Q motor is shown in figure 3-12(b). The winding layout (radial view) of the 12P36Q motor is shown in figure 3-13(a).The linear winding pattern of 12P36Q motor is shown in figure 3-13(b). The torque- speed characteristics of 12P36Q integer slot motor is shown in figure 3-14. The output waveforms of 12P36Q motor is shown in figure 3-15. The output data of integer slot motor fed by

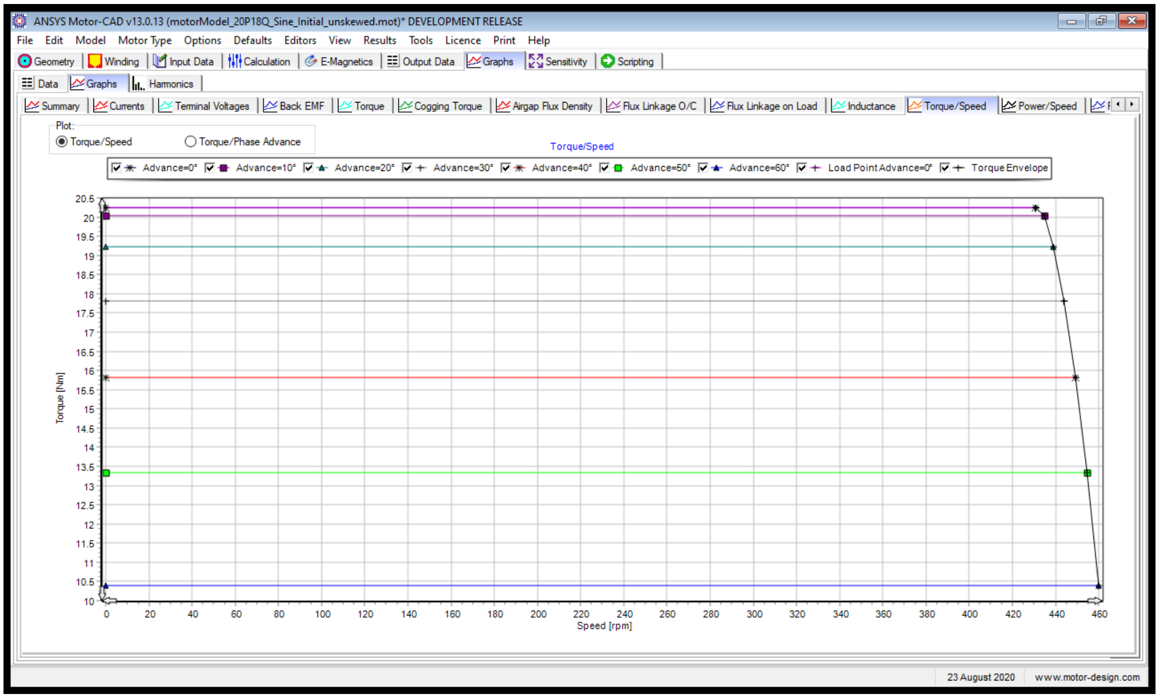

Figure 3-10: Torque-Speed Curve Initial Design Fractional Slot 20P18Q Motor

square-wave drive is tabulated in table 3.11.

3.10 Choice between 20P18Q motor and 12P36Q Motor

According to the simulation results 12P36Q motor with square-wave excitation has a higher torque for the same peak drive current than that of 20P18Q motor with sinusoidal excitation. This is mainly due to higher the RMS current in 12P36Q machine, hence 12P36Q machine has a higher torque per rotor volume compared to 20P18Q machine. 12P36Q machine can have a simpler control strategy compared to the complicated control scheme to be used in 20P18Q machine with sinusoidal drive. However the efficiency of 20P18Q motor is little higher than that of 12P36Q machine. Most importantly the torque ripple in 12P36Q machine with square-wave excitation exhibits a extremely high torque ripple due to higher harmonic content which is at an acceptable level. In contrast 20P18Q machine with sinusoidall excitation has a very little torque ripple as low as 6%. The torque ripple of both of the machines can

Variable	Value	Units	Variable	Value	Units
DC Bus Voltage	72	Volts	D Axis Inductance	0.3024	mH
Line-Line Supply Voltage (rms)	50.91	Volts	Q Axis Inductance	0.488	mH
Phase Supply Voltage (rms)	29.39	Volts	Line-Line Inductance (DQ)	0.7904	mH
Line-Line Terminal Voltage (peak)	67.32	Volts	Self Inductance	1.059	mH
Line-Line Terminal Voltage (rms)	47.18	Volts	Mutual Inductance	-0.07318	mH
Phase Terminal Voltage (rms)	27.3	Volts	Line-Line Inductance	2.265	mH
Harmonic Distortion Line-Line Terminal Voltage	1.585	%	"Armature End Winding Inductance		
Harmonic Distortion Phase Terminal Voltage	6.557	%	(Rosa and Grover)"	0.02921	mH
Back EMF Line-Line Voltage (peak)	64.91	Volts	D Axis Current (rms)	0	Amps
Back EMF Line-Line Voltage (peak) (fundamental)	64.2	Volts	Q Axis Current (rms)	10.75	Amps
Back EMF Phase Voltage (peak)	38.65	Volts	Torque Constant (Kt)	1.317	Nm/A
Back EMF Line-Line Voltage (rms)	45.4	Volts	Motor Constant (Km)	3.548	Nm/(Watts^0.5)
Back EMF Phase Voltage (rms)	26.26	Volts	Back EMF Constant (Ke)	1.55	Vs/Rad
Harmonic Distortion Back EMF Line-Line Voltage	1.682	%	Back EMF Constant (Ke) (fundamental)	1.533	Vs/Rad
Harmonic Distortion Back EMF Phase Voltage	6.374	%	Electrical Constant	4.299	msec
Max Line-Line / Phase Voltage Ratio	1.732		Mechanical Constant	0.8813	msec
DC Supply Current (mean)	12.09	Amps	Electrical Loading	1.502E004	Amps/m
Line Current (peak)	15.2	Amps	Stall Current	391.6	Amps
Line Current (rms)	10.75	Amps	Stall Torque	515.9	Nm
Phase Current (peak)	15.2	Amps	Short Circuit Line Current (peak)	242.7	Amps
Phase Current (rms)	10.75	Amps	Short Circuit Current Density (peak)	63.58	Amps/mm
Phase Advance	0	EDeg	Short Circuit Current Density (rms)	44.96	Amps/mm
Drive Offset Angle (Open Circuit)	130	EDeg	Short Circuit Braking Torque	-193.9	Nm
Drive Offset Angle (On load)	130	EDeg	Short Circuit Max Braking Torque	-206.3	Nm
Phase Advance to give maximum torque	1.818	EDeg	Short Circuit Max Braking Torque Speed	283.9	rpm
Phasor Offset Angle	30	EDeg	Short Circuit Max Demagnetizing Current	-587.6	Amps
Phasor Angle (Ph1)	0	EDeg	Fundamental Frequency	66.67	Hz
Phasor Angle (Ph2)	120	EDeg	Current Shaft Speed RPM	400	rpm
Phasor Angle (Ph3)	240	EDeg	Max Angle Between Phasors	120	EDeg

Table 3.6: Preliminary Design Drive Output Data of Fractional-Slot Machine

be reduced by skewing the rotor or the stator. However this would complicate the manufacturing of the machine and on the other hand skewing would cause reduction in winding factor hence reducing the torque. Therefore considering all these facts 20P18Q machine with sinusoidal excitation was chosen for the application and for further optimization.

Variable	Value	Unit	Variable	Value	Unit
Maximum torque possible (DQ)	72	Volts	Flux Linkage D (Q axis current)	88.7622	mVs
(For Phase Advance of 1.818 EDeg)	20.248	Nm	Flux Linkage Q (Q axis current)	7.37758	mVs
Average torque (virtual work)	20.099	Nm	Flux linkage D (On load)	88.518	mVs
Average torque (loop torque)	20.035	Nm	Flux linkage Q (On load)	7.26165	mVs
Torque Ripple (MsVw)	1.3636	Nm	—		
Torque Ripple (MsVw) [%]	6.8094	%	Torque Constant (Kt)	1.31741	Nm/A
Cogging Torque Ripple (Ce)	21.634	Nm	Motor Constant (Km)	3.54777	Nm/(Watts^0.5)
Cogging Torque Ripple (Vw)	0.075363	Nm	Back EMF Constant (Ke)	1.54969	Vs/Rad
Speed limit for constant torque	64.91	Volts	Back EMF Constant (Ke) (fundamental)	1.53256	Vs/Rad
(For Phase Advance of 0 EDeg)	430.73	rpm	—		
No load speed	443.67	rpm	Stall Current	391.617	Amps
Speed limit for zero current	1E009	rpm	Stall Torque	515.921	Nm
Electromagnetic Power	838.79	Watts	—		
Input Power	870.65	Watts	Cogging Period	2	MDeg
Output Power	807.92	Watts	Cogging Frequency	1200	Hz
Total Losses (on load)	62.728	Watts	Fundamental Frequency	66.6667	Hz
System Efficiency	92.795	%	Mechanical Frequency	6.66667	Hz
Shaft Torque	19.288	Nm	Optimum Skewing Angle	2	MDeg
Power Factor [Waveform] (leading)	0.99689	Amps	—		
Power Factor Angle [Waveform]	4.5208	EDeg	Magnetic symmetry factor	2	
Power Factor [Phasor] (leading)	0.99619	EDeg	Magnetic Axial Length (Slice1)	50	mm
Power Factor Angle [Phasor]	5	EDeg	Magnetic Axial Length Multiplier	1	
Load Angle [Phasor]	4.6096	EDeg	Number of Force Points	180	
Phase Terminal Voltage (rms) [Phasor]	27.337	Volts	X Force (On Load)	0	kN
Rotor Inertia	0.019573	kg.m^2	Y Force (On Load)	0	kN
Shaft Inertia	0	kg.m^2	Unbalanced Magnetic Pull (Open Circuit)	0	kN
Total Inertia	0.019573	kg.m^2	Unbalanced Magnetic Pull Angle (Open Circuit)	0	MDeg
Torque per rotor volume	44.264	kNm/m	Tangential Force (Open Circuit)	-0.0135626	kN
Rotor peripheral velocity (on load)	3.4348	m/s	Radial Force (Open Circuit)	-8.07932	kN
Unbalanced Magnetic Pull (On Load)	0	kN	X Force (Open Circuit)	0	kN
Unbalanced Magnetic Pull Angle (On Load)	0	MDeg	Y Force (Open Circuit)	0	kN
Tangential Force (On Load)	0.225589	kN	Radial Force Ripple (Open Circuit) (Rotor)	0.0393789	kN
Radial Force (On Load)	-8.06805	kN	Radial Force Ripple (On Load) (Rotor)	0.0416875	kN

Table 3.7: Preliminary Design ElectroMagnetic Output Data of Fractional-Slot Machine

Variable	Value	Units
Airgap flux density (mean)	0.9017	Tesla
Airgap Flux Density (peak)	1.182	Tesla
Stator Tooth Flux Density (peak)	2.022	Tesla
Stator Tooth Tip Flux Density (peak)	2.243	Tesla
Stator Back Iron Flux Density (peak)	0.04306	Tesla
Rotor Back Iron Flux Density (peak)	2.374	Tesla

Table 3.8: Flux Densities PMSM Preliminary Design Fractional Slot Motor

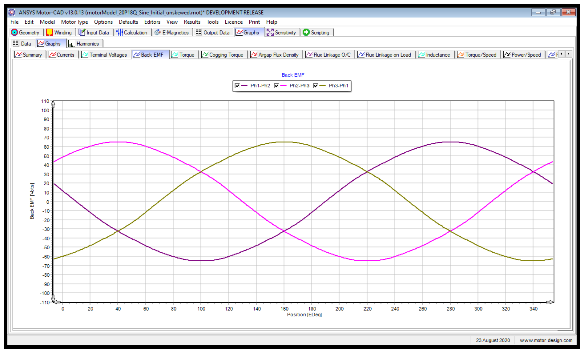

(a) Back EMF

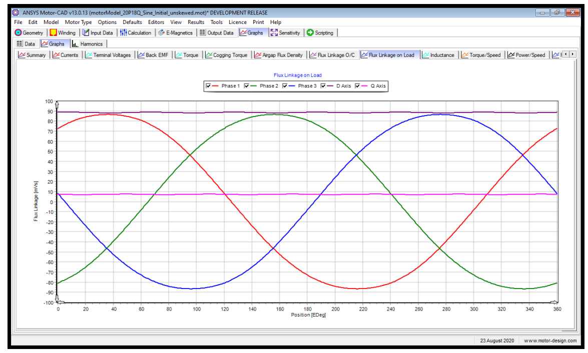

(b) On-Load Flux Linkage

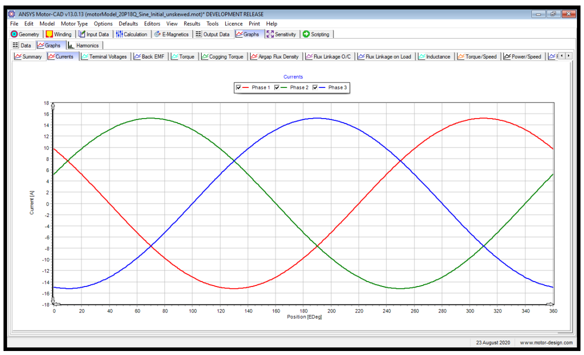

(c) Drive Currents

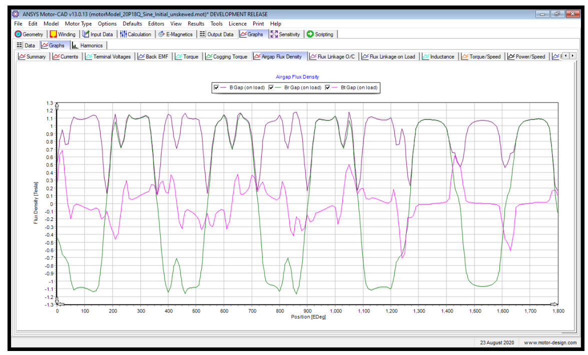

(d) Air Gap Flux Density

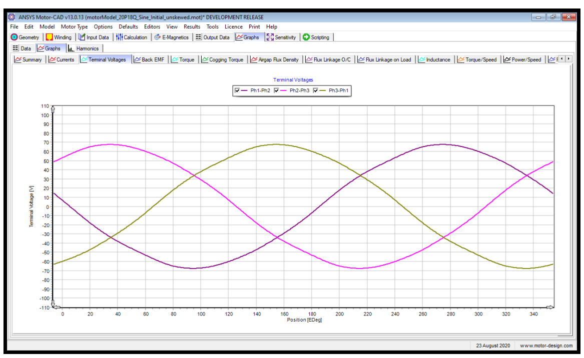

(e) Terminal Voltages

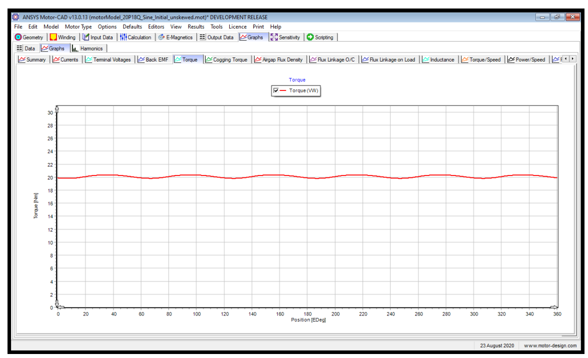

(f) Torque

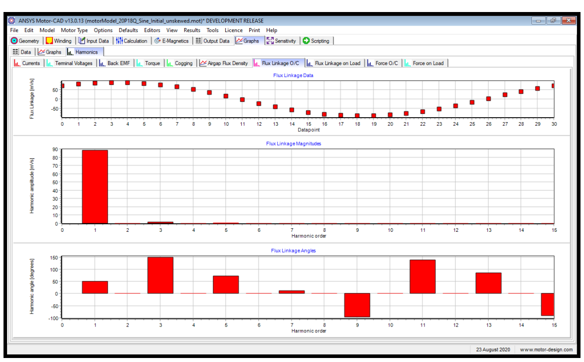

(g) Harmonics: currents

(h) Harmonics:BackEMF

Figure 3-11: Output waveforms Fractional Slot Motor Initial Design

Variable	Value	Units	Variable	Value	Units
Armature Conductor CSA	3.817	mm_2	Wire Slot Fill (Wdg Area)	0.8699	
Armature Conductor Current Density	2.816	Amps/mm_2	Copper Slot Fill (Wdg Area)	0.8082	
Armature Conductor MLT	169.6	mm	Wire Slot Fill (Slot Area)	0.592	
Armature Turns per Phase	120		Copper Slot Fill (Slot Area)	0.55	
Armature Turns per Coil	20		Heavy Build Slot Fill	1.108	
Length of phase	2.035E004	mm	Slot Area	277.6	mm_2
Phase Resistance	0.09193	Ohms	Winding Area (+Liner)	199.1	mm_2
Line-Line Resistance	0.1839	Ohms	Slot Area (FEA)	223.9	mm_2
Armature Conductor Temperature	20	C	Wedge Area	53.69	mm_2
Mean Coil Pitch (Calculated)	15.78	mm	Slot Opening Area	5.127	mm_2
Mean Coil Pitch (Used)	15.78	mm	Liner-Lam Imp Area	0	mm_2
Fundamental Winding Factor	0.9452		Impreg Area	24.57	mm_2
Winding Factor Sum	0.009002		Liner Area	10.17	mm_2
Armature End Winding MLT (Calculated)	69.59	mm	Coil Divider Area	24.81	mm_2
Armature End Winding MLT (User adjustment)	1		Volume Copper EWdg Front	4.351E004	mm_3
Armature End Winding MLT (Used)	69.59	mm	Volume Copper Active	1.374E005	mm_3
Wire Ins Thickness	0.04134	mm	Volume Copper EWdg Rear	4.351E004	mm_3
Copper Diameter	2.204	mm	Conductors/Slot	40	

Table 3.9: Winding Data Initial Design 20P18Q Motor

Stack length mm	5
Outer rotor diameter mm	164
Outer stator diameter mm	147
PM thickness mm	10
N.turns per phase	20
Wire size mm	1.48
Copper Slot Fill	0.55
Peak Phase current A_{max}	10.91
Average torque @ 400 rpm Nm	19.1
Output power W	800
Temperature: Winding C^0	140
PM C^0	60
Magnetization	Radial
Peak drive Current	15.2A
RMS drive Current	12.41A
RMA Current Density	4.6A/mm^2

Table 3.10: PMSM Preliminary Design Data Integer Slot Machine

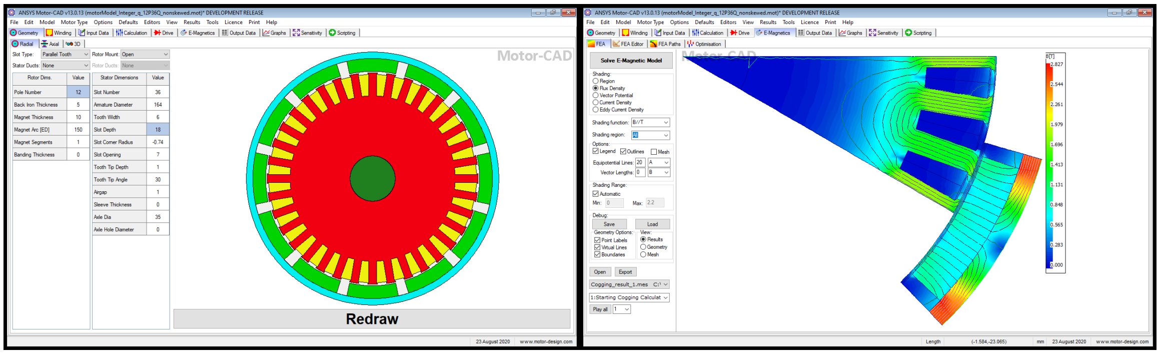

(a) Motor CAD model of Initial Design Integer slot 12P36Q Motor -Radial cross section

(b) Electromagnetics Window Integer Slot Machine

Figure 3-12: Motor CAD model of Initial Design Integer slot Motor -Radial cross section (Square-Wave drive).

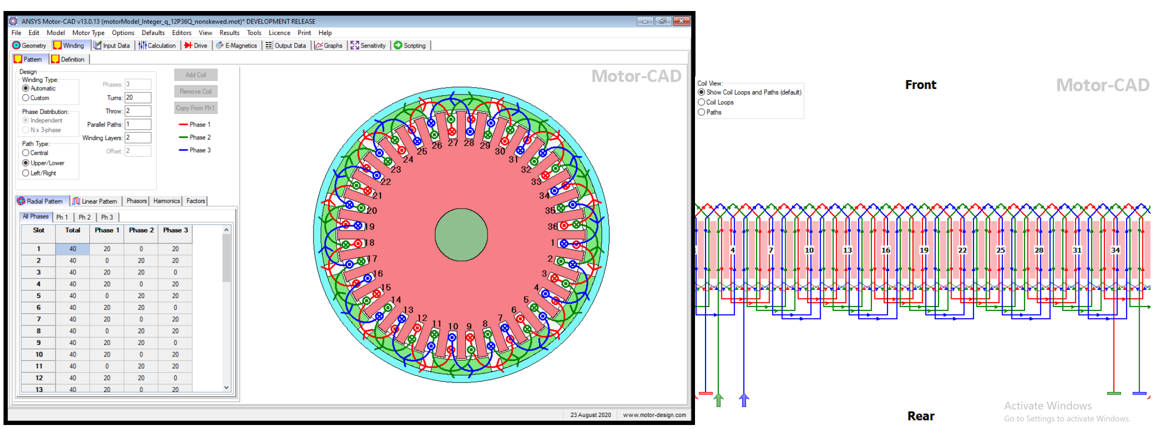

(a) Winding Layout of Integer Slot 12P36Q Machine Radial view

(b) Linear Coil Pattern

Figure 3-13: Winding Layout of Integer Slot 12P36Q Machine.

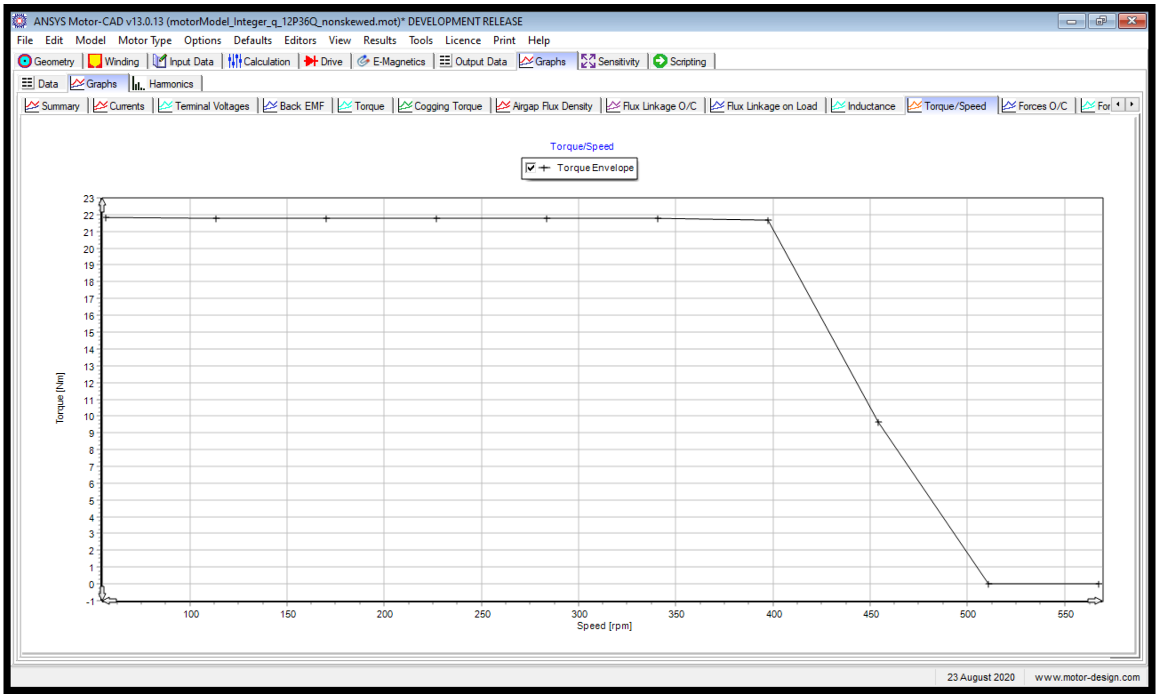

Figure 3-14: Torque-Speed Curve Initial Design Integer Slot Motor

Parameter	value	Units	Parameter	Value	Units
Average torque (virtual work)	22.121	Nm	Torque Constant (Kt)	1.44971	Nm/A
Average torque (loop torque)	21.789	Nm	Motor Constant (Km)	2.41449	Nm/(Watts^0.5)
Torque Ripple (MsVw)	59.492	Nm	Back EMF Constant (Ke)	1.58832	Vs/Rad
Torque Ripple (MsVw) [%]	269.55	%	Back EMF Constant (Ke) (fundamental)	1.62977	Vs/Rad
Electromagnetic Power	924.48	Watts	Stall Current	198.515	Amps
Input Power	1006.1	Watts	Stall Torque	287.789	Nm
Output Power	905.56	Watts	Cogging Period	10	MDeg
Total Losses (on load)	100.58	Watts	Cogging Frequency	240	Hz
System Efficiency	90.004	%	Fundamental Frequency	40	Hz
Shaft Torque	21.619	Nm	Mechanical Frequency	6.66667	Hz
Power Factor [Waveform] (leading)	0.94436		Optimum Skewing Angle	10	MDeg
Power Factor Angle [Waveform]	-19.203	EDeg	DC Bus Voltage	72	Volts
Rotor Inertia	0.030365	kg.m^2	Line-Line Supply Voltage (rms)	50.91	Volts
Armature Conductor Current Density	4.619	Amps/mm^2	Phase Supply Voltage (rms)	50.91	Volts
Total Inertia	0.030365	kg.m^2	Line-Line Terminal Voltage (peak)	71.74	Volts
Torque per rotor volume	48.786	kNm/m^3	Line-Line Terminal Voltage (rms)	51.74	Volts
Rotor peripheral velocity (on load)	3.4348	m/s	Phase Terminal Voltage (rms)	51.74	Volts
Airgap flux density (mean)	0.6951	Tesla	Harmonic Distortion Line-Line Terminal Voltage	16.51	%
Airgap Flux Density (peak)	1.078	Tesla	DC Supply Current (mean)	13.98	Amps
Stator Tooth Flux Density (peak)	1.788	Tesla	Drive Current Limit	15.2	Amps
Stator Tooth Tip Flux Density (peak)	1.831	Tesla	Drive Current (peak)	15.2	Amps
Stator Back Iron Flux Density (peak)	0.1565	Tesla	Line Current (rms)	12.32	Amps
Rotor Back Iron Flux Density (peak)	2.682	Tesla	Phase Current (peak)	10.89	Amps
Electrical Constant	2.784	msec	Phase Current (rms)	7.144	Amps
Mechanical Constant	7.174	msec	Harmonic Distortion Line Current	30.48	%
Electrical Loading	3.444E004	Amps/m	Harmonic Distortion Phase Current	31.96	%

Table 3.11: Output Data of Integer-Slot Motor :Square-Wave Drive

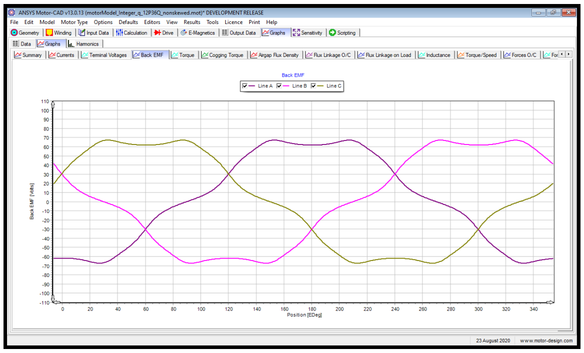

(a) Back EMF

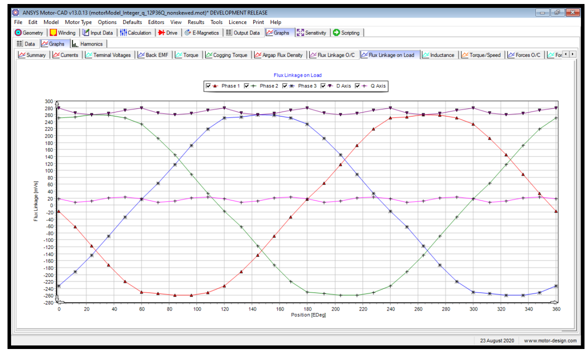

(b) On-Load Flux Linkage

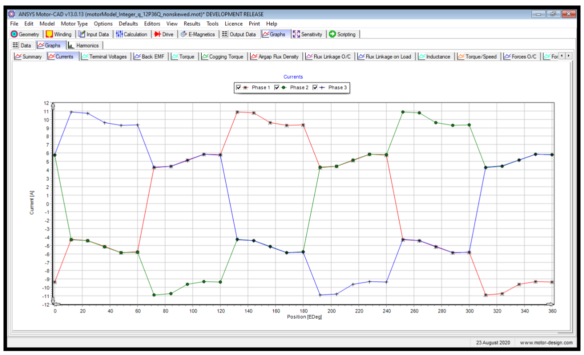

(c) Drive Currents

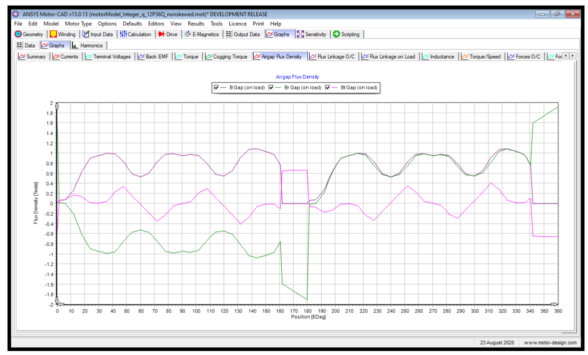

(d) Air Gap Flux Density

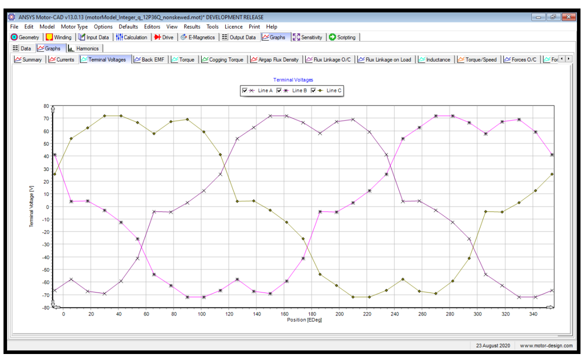

(e) Terminal Voltages

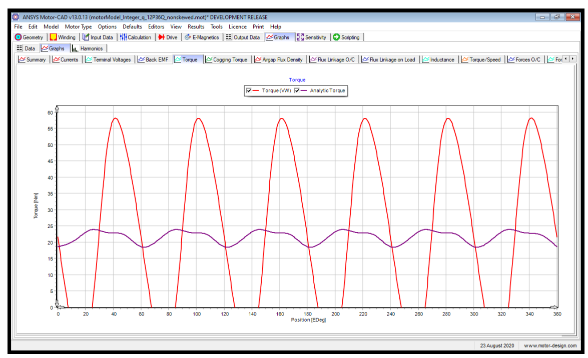

(f) Torque

(g) Harmonics: currents

(h) Harmonics:BackEMF

Figure 3-15: Output Waveforms Integer Slot Motor Initial Design : Square-wave drive

Chapter 4

Sensitivity Analysis and Design Optimization

4.1 Sensitivity Analysis

This section presents the results obtained from MotorCAD sensitivity analysis tool.

4.1.1 Electromagnetic Model Sensitivity Analysis

The parameters affecting the electromagnetic performance of the motor were analyzed using Motor-CAD's built-in sensitivity analysis tool.

Sensitivity analysis was performed by varying number of different design parameters including geometrical parameters, winding parameters and other parameters such as peak current, magnet temperatures. Some of these parameters mainly affects the electromagnetic performance of the machine while some others mainly affects the thermal performance of the machine.The resulting graphs illustrating the variation motor important output variables according to the variation of design parameters are depicted in the following sections.

Magnet Thickness

Resulting graphs from sensitivity analysis with respect to magnet thickness are depicted in figure 4-1.

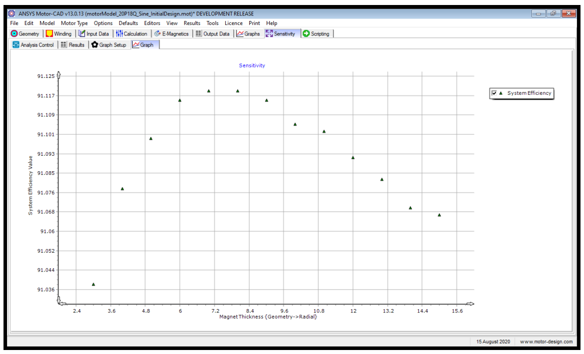

(a) efficiency

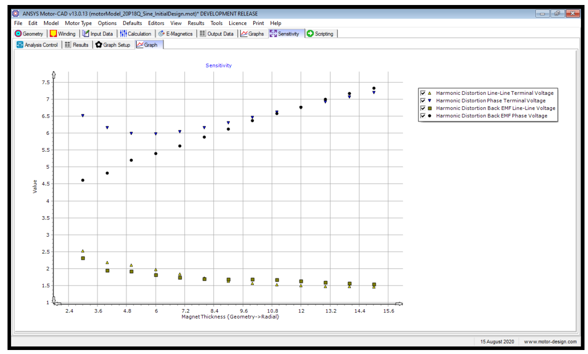

(b) Harmonic Distortion

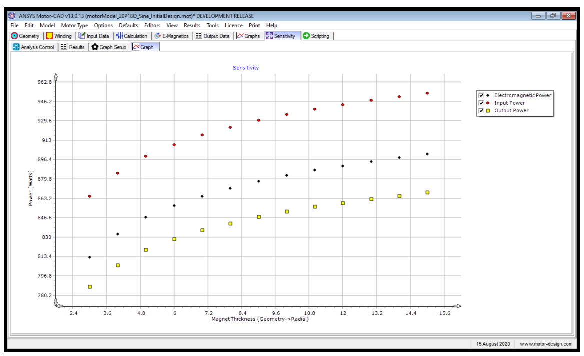

(c) Power

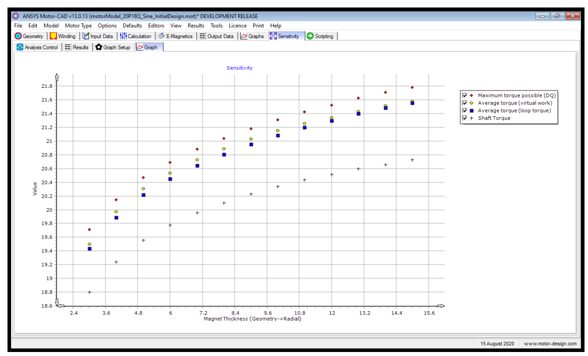

(d) Torque

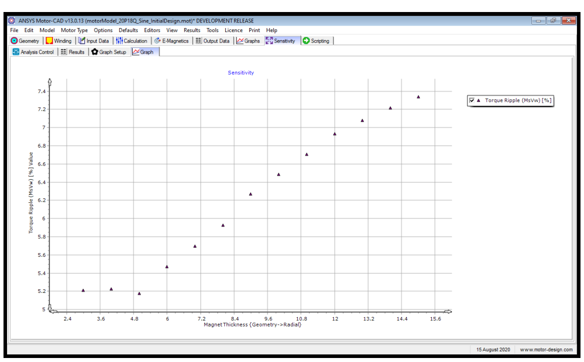

(e) Torque Ripple Percentage

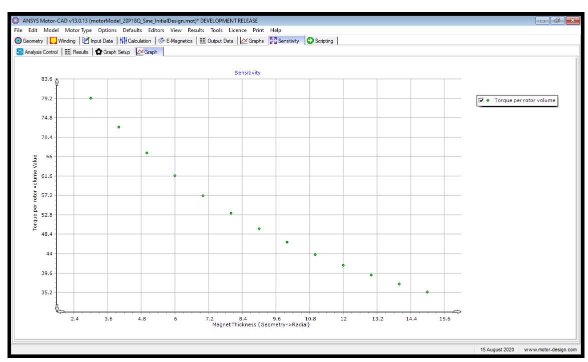

(f) torque per Rotor Volume

Figure 4-1: Effect of Magnet Thickness

Air Gap Length

Resulting graphs from sensitivity analysis with respect to air-gap length are depicted in figure 4-2.

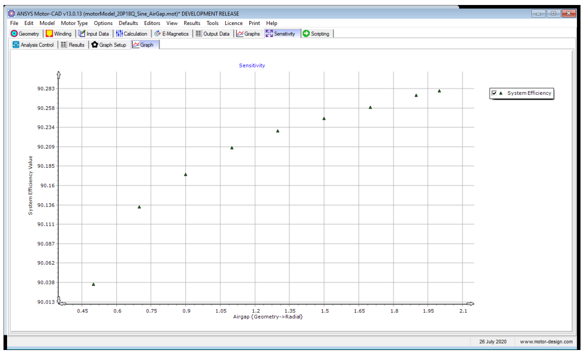

(a) Efficiency

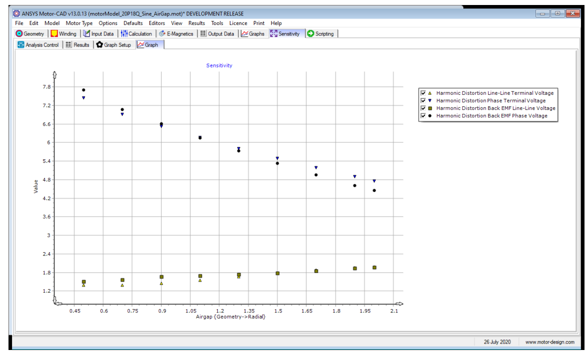

(b) Harmonic Distortion

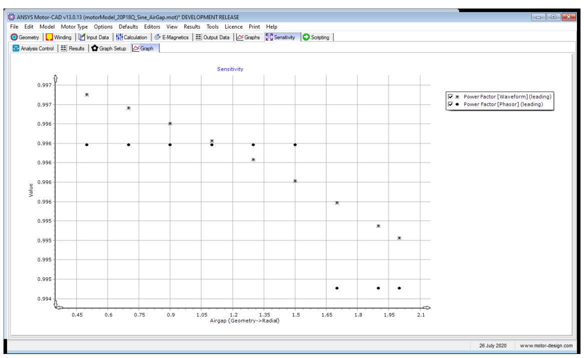

(c) Power Factor

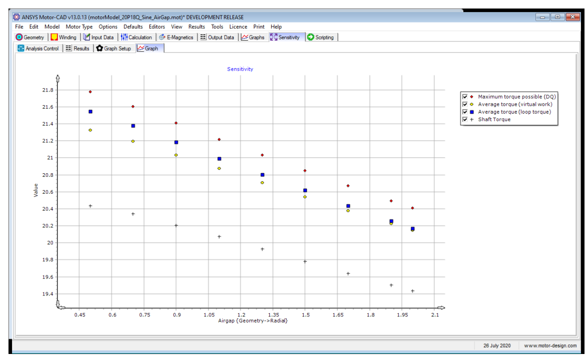

(d) Torque

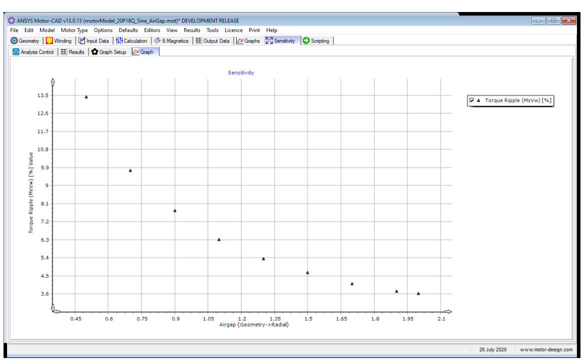

(e) Torque Ripple Percentage

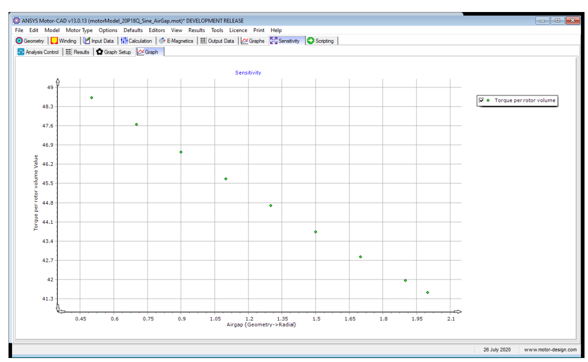

(f) Torque per Rotor Volume

Figure 4-2: Airgap:Sensitivity Analaysis

Armature Diameter

Resulting graphs from sensitivity analysis with respect to armature diameter are depicted in figure 4-3.

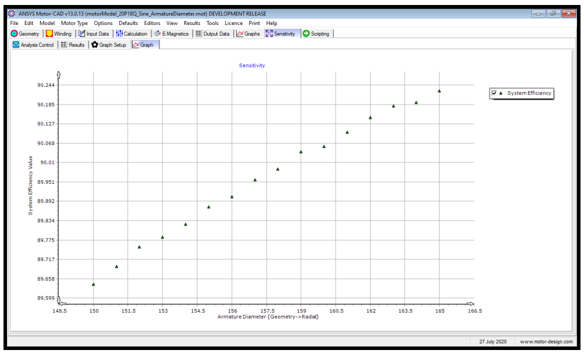

(a) Efficiency

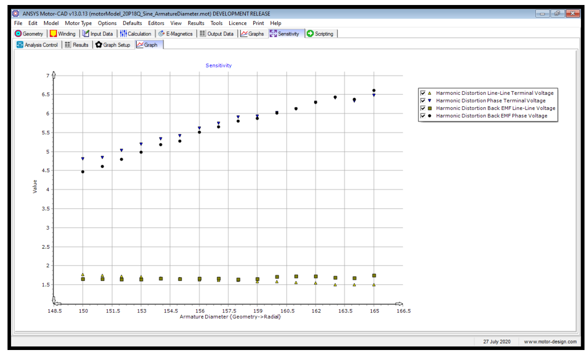

(b) Harmonic Distortion

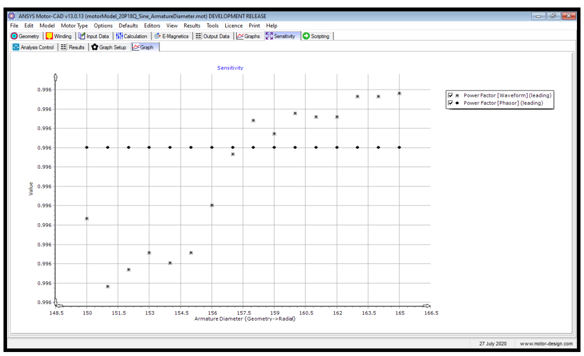

(c) Power Factor

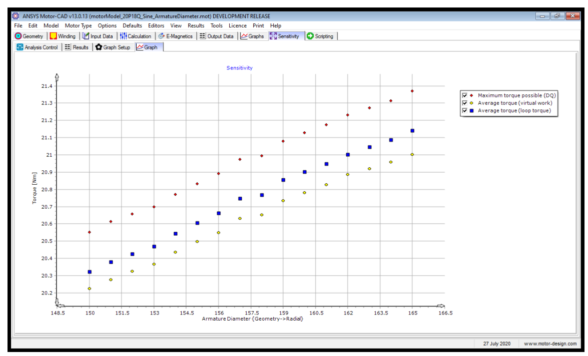

(d) Torque

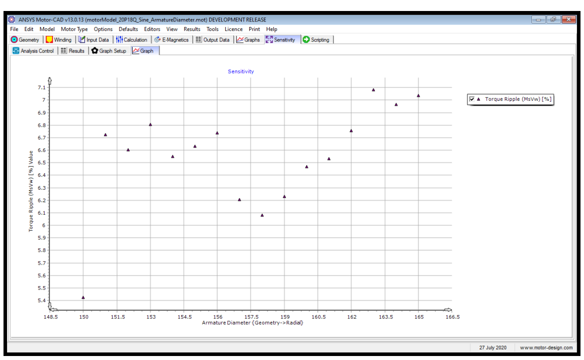

(e) Torque Ripple Percentage

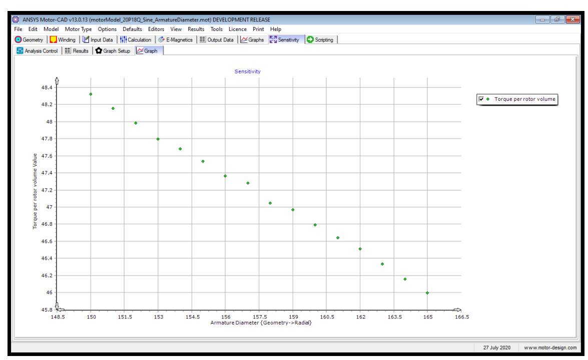

(f) Torque per Rotor Volume

Figure 4-3: Armature Diameter:Sensitivity Analysis

Magnet Arc

Resulting graphs from sensitivity analysis with respect to magnet arc are depicted in figure 4-4.

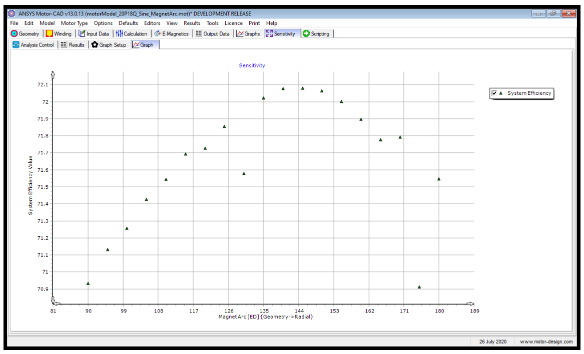

(a) Efficiency

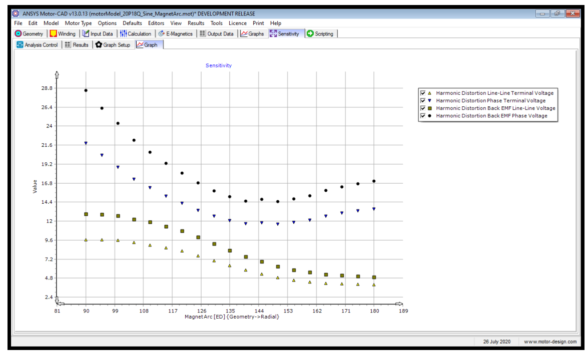

(b) Harmonic Distortion

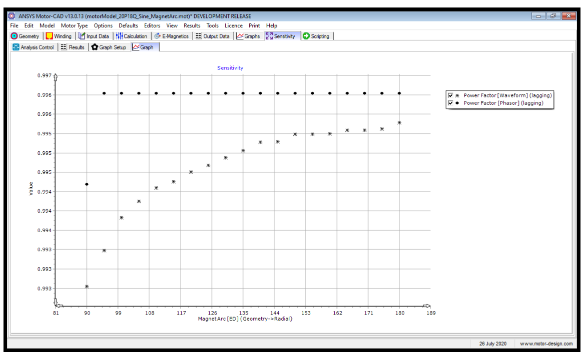

(c) Power Factor

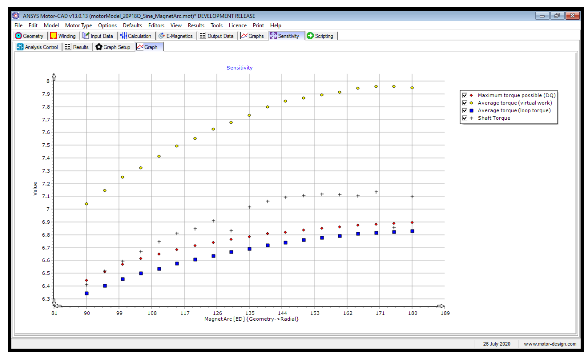

(d) Torque

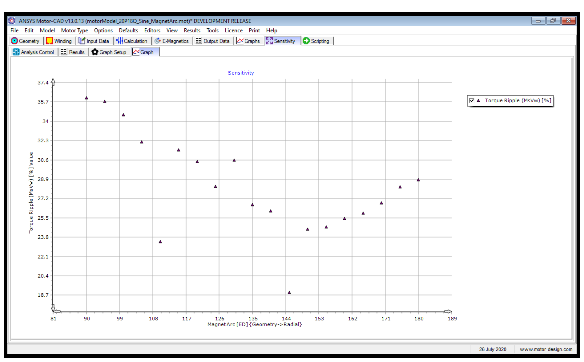

(e) Torque Ripple Percentage

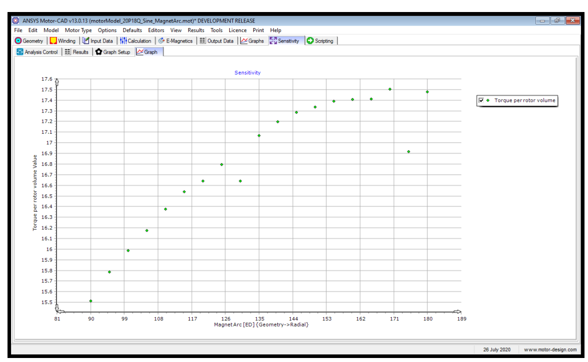

(f) Torque per Rotor Volume

Figure 4-4: Magnet Arc:Sensitivity Analysis

Slot Depth

Resulting graphs from sensitivity analysis with respect to slot depth are depicted in figure 4-5

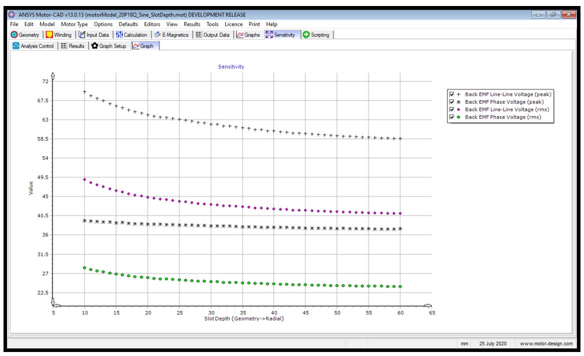

(a) Back EMF

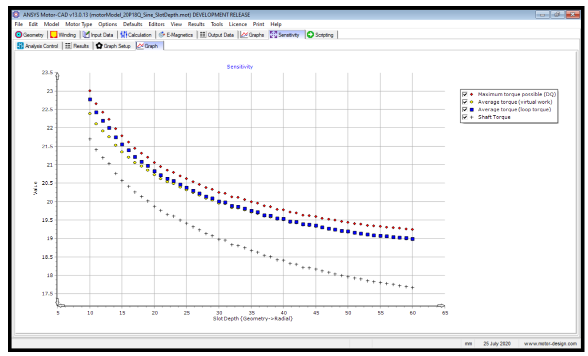

(b) Torque

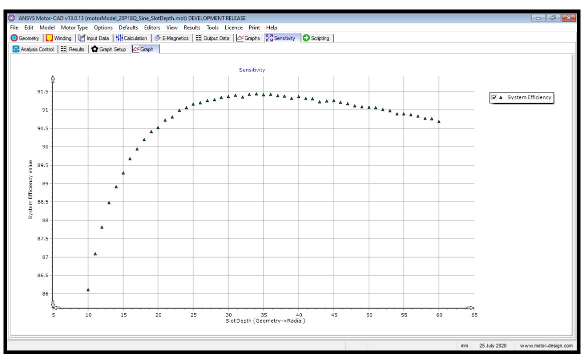

(c) Efficiency

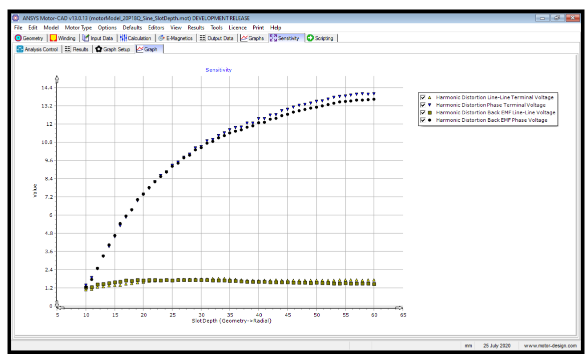

(d) Harmonic Distortion

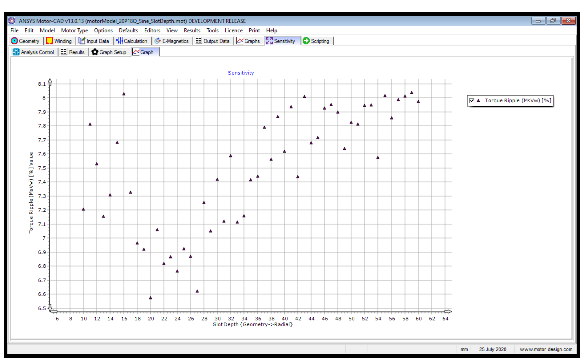

(e) Torque Ripple Percentage

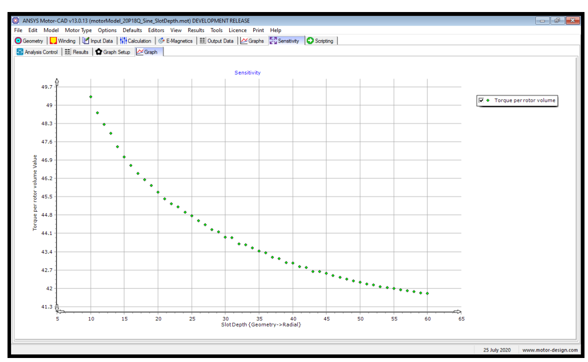

(f) Torque per Rotor Volume

Figure 4-5: Slot Depth:Sensitivity Analaysis

Slot Opening

Resulting graphs from sensitivity analysis with respect to slot opening are depicted in figure 4-6.

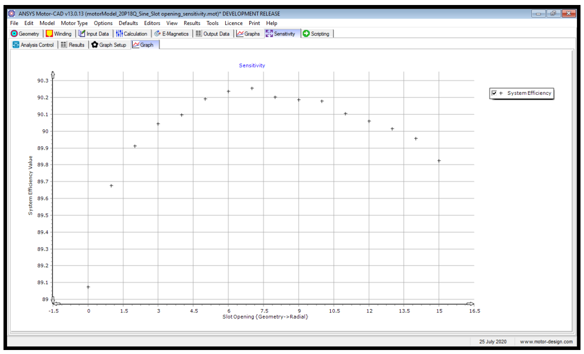

(a) Efficiency

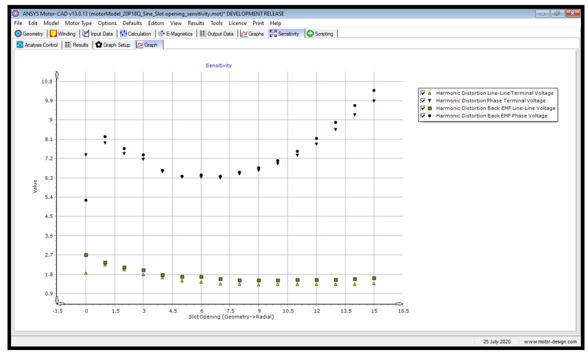

(b) Harmonic Distortion

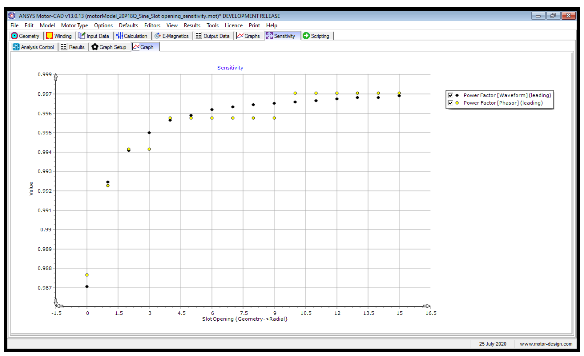

(c) Power Factor

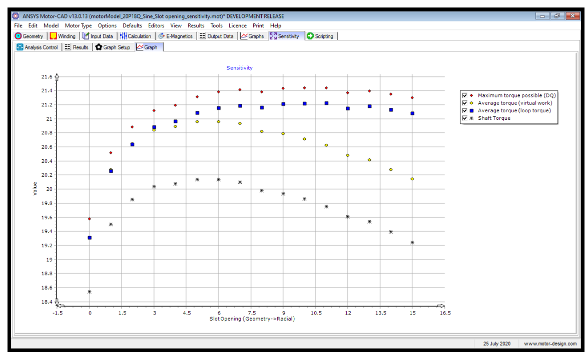

(d) Torque

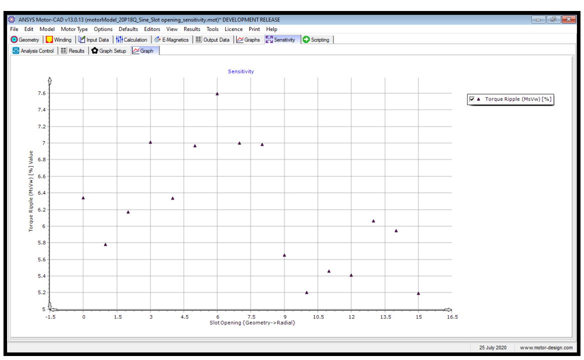

(e) Torque Ripple Percentage

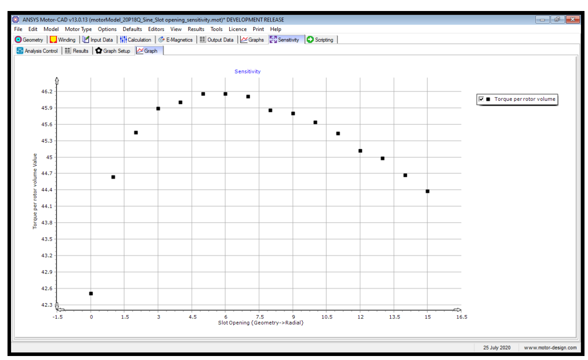

(f) Torque per Rotor Volume

Figure 4-6: Slot Opening:Sensitivity Analysis

Tooth Tip Angle

Resulting graphs from sensitivity analysis with respect to tooth tip angle are depicted in figure 4-7.

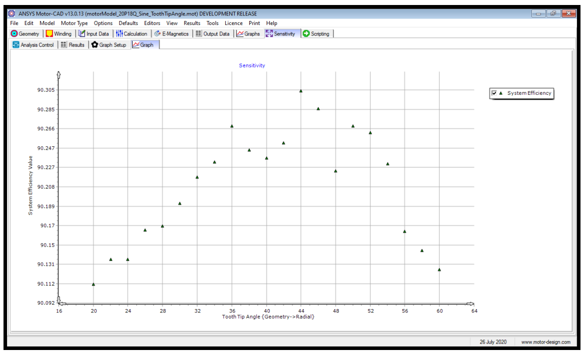

(a) Efficiency

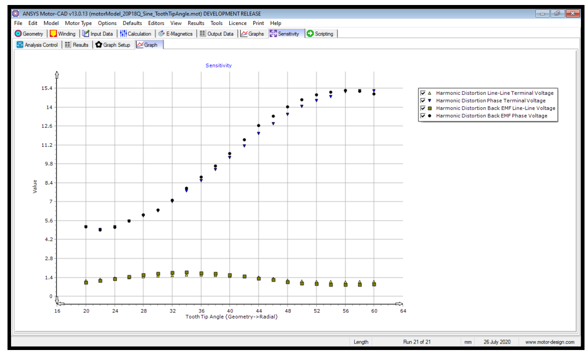

(b) Harmonic Distortion

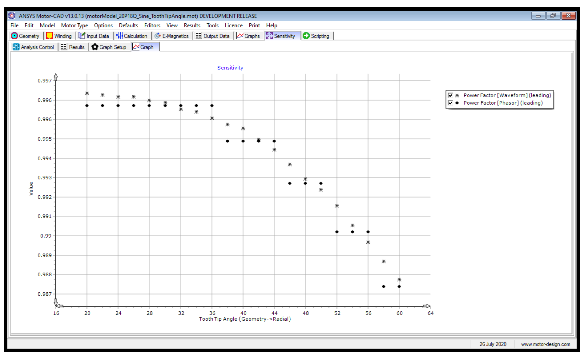

(c) Power Factor

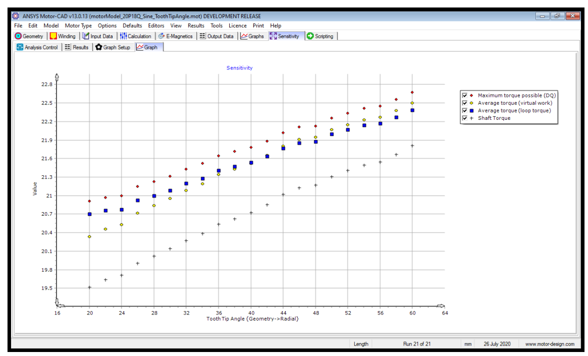

(d) Torque

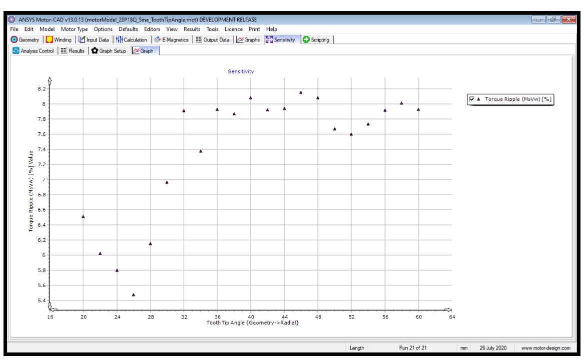

(e) Torque Ripple Percentage

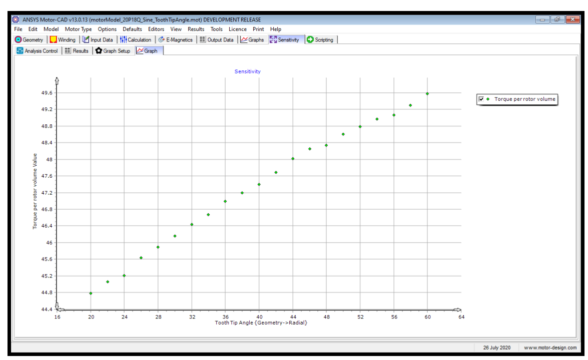

(f) Torque per Rotor Volume

Figure 4-7: Tooth Tip Angle:Sensitivity Analysis

Tooth Width

Resulting graphs from sensitivity analysis with respect to tooth width are depicted in figure 4-8.

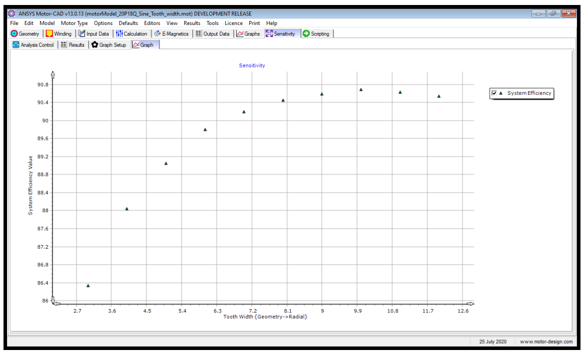

(a) Efficiency

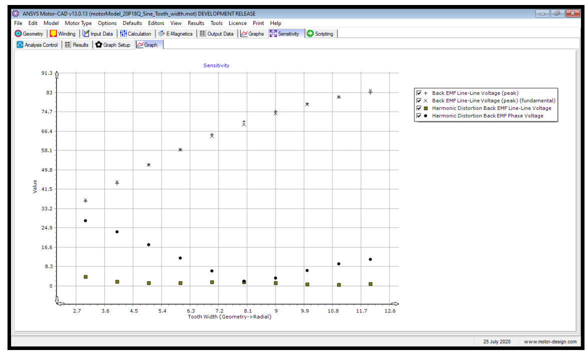

(b) Harmonic Distortion

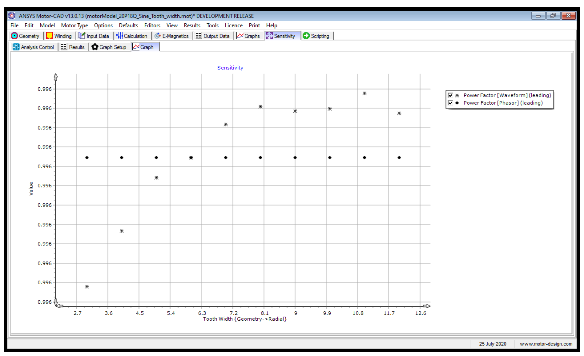

(c) Power Factor

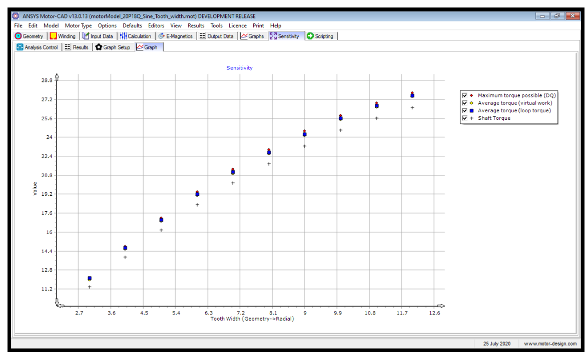

(d) Torque

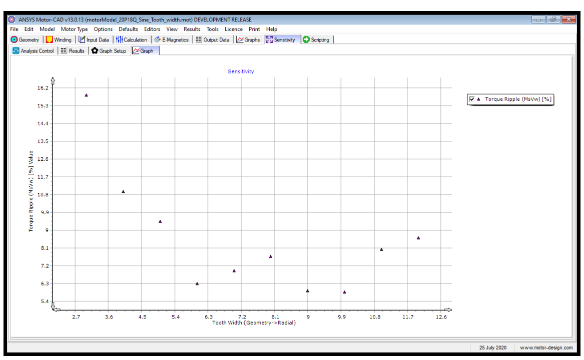

(e) Torque Ripple Percentage

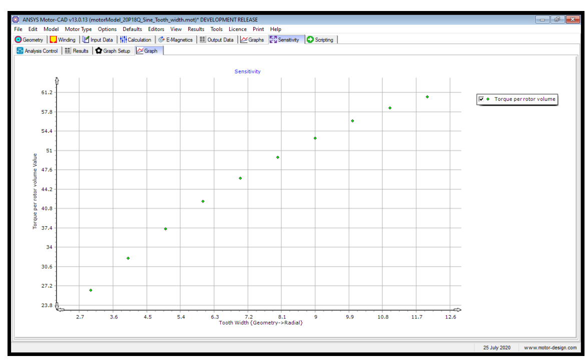

(f) Torque per Rotor Volume

Figure 4-8: Tooth Width:Sensitivity Analysis

Turns Number

Resulting graphs from sensitivity analysis with respect to turns number are depicted in figure 4-9

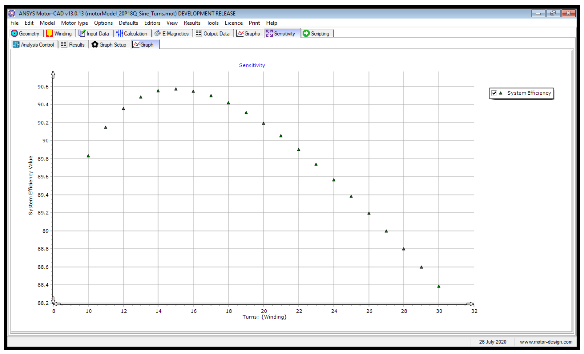

(a) Efficiency

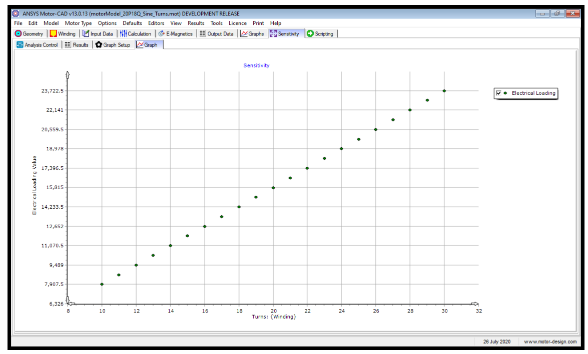

(b) Electrical Loading

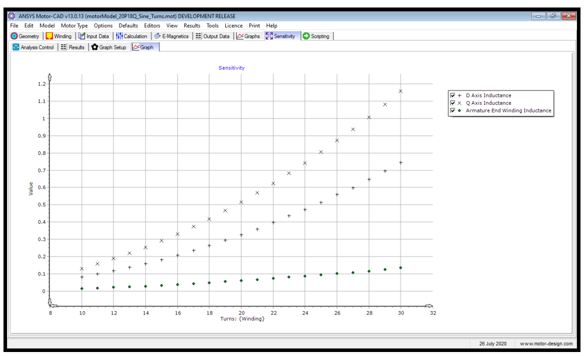

(c) DQ and End Winding Inductances

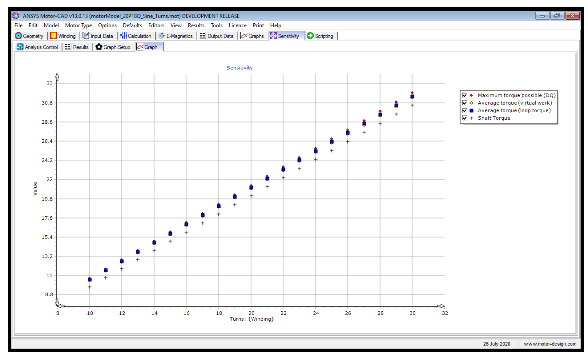

(d) Torque

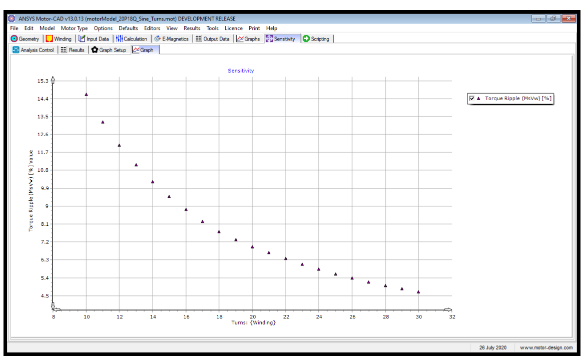

(e) Torque Ripple Percentage

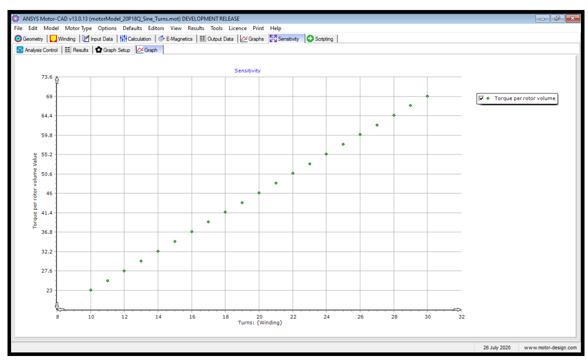

(f) Torque per Rotor Volume

Figure 4-9: Turns Number:Sensitivity Analysis

Copper Slot Fill

Resulting graphs from sensitivity analysis with respect to copper slot fill are depicted in figure 4-10.

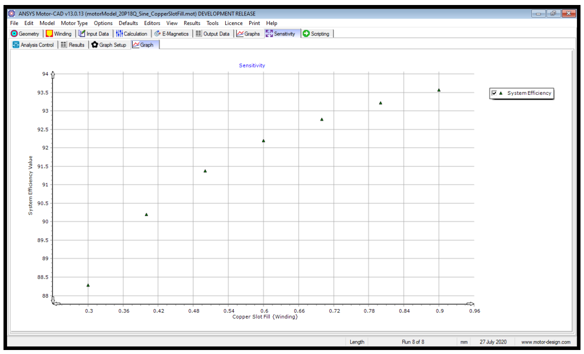

(a) Efficiency

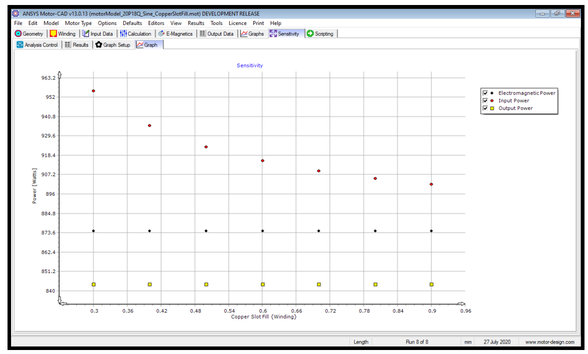

(b) Power

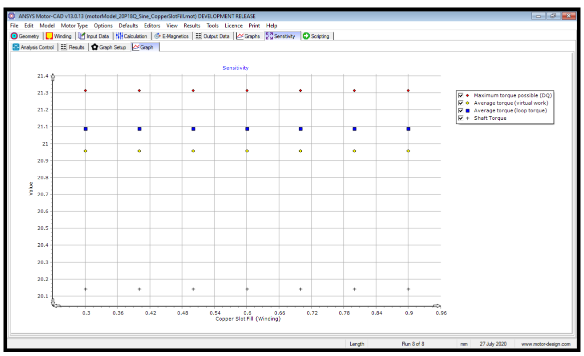

(c) Torque

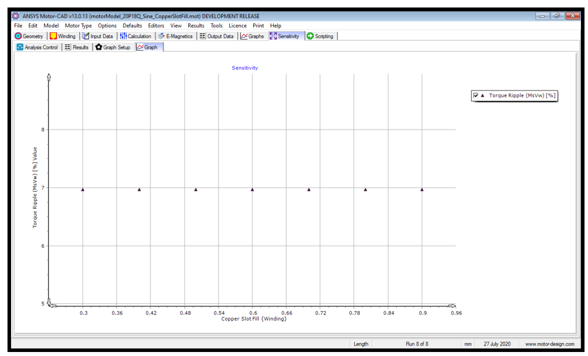

(d) Torque Ripple Percentage

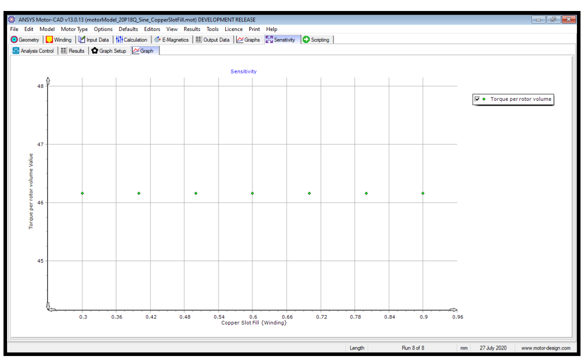

(e) Torque per Rotor Volume

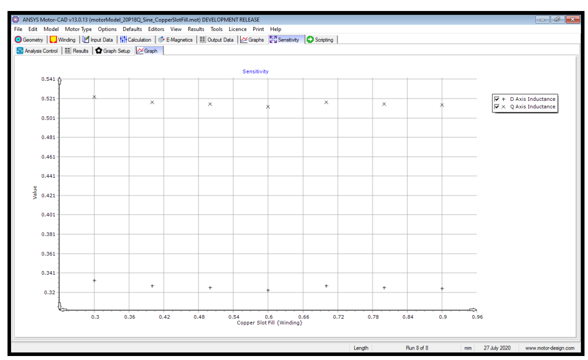

(f) DQ Inductances

Figure 4-10: Copper Slot Fill:Sensitivity Analysis

Peak Current

Resulting graphs from sensitivity analysis with respect to peak drive current are depicted in figure 4-11.

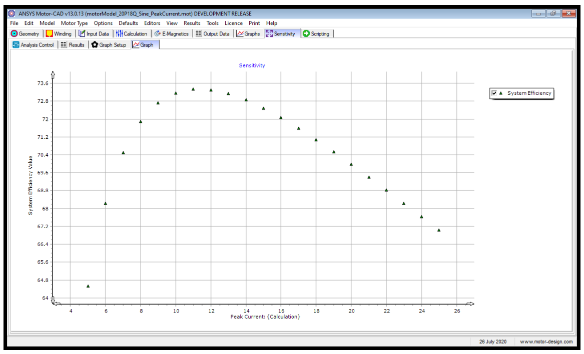

(a) Efficiency

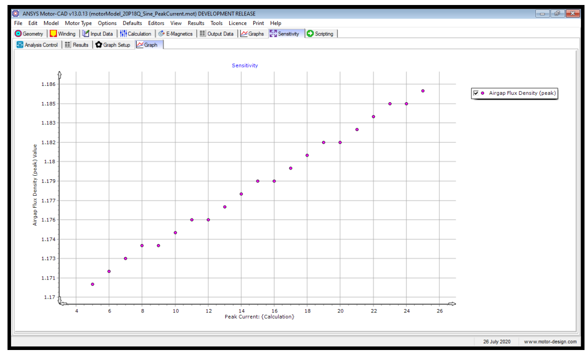

(b) Magnetic Flux Density

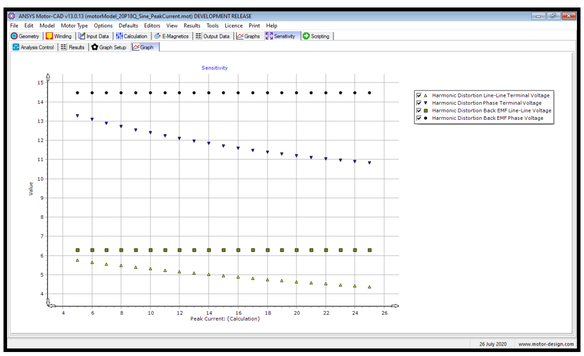

(c) Harmonic Distortion

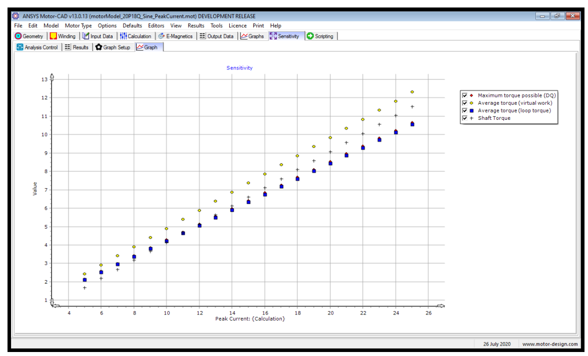

(d) Torque

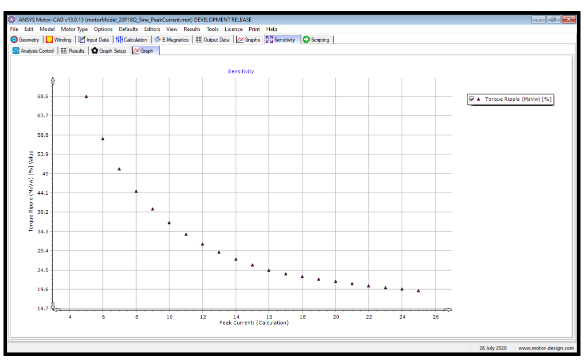

(e) Torque Ripple Percentage

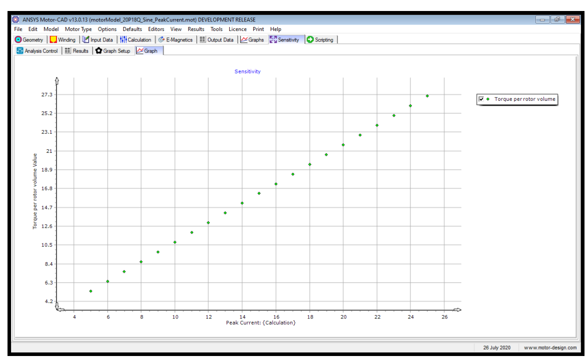

(f) Torque per Rotor Volume

Figure 4-11: Peak Current:Sensitivity Analysis

Thermal Sensitivity to variations in Ambient Temperature

Sensitivity analysis graphs with respect to ambient temperature affecting thermal performance of the motor are illustrated in 4-12.

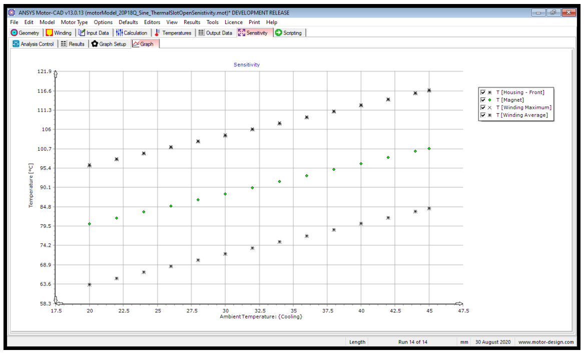

(a) Magnet and Winding temperatures

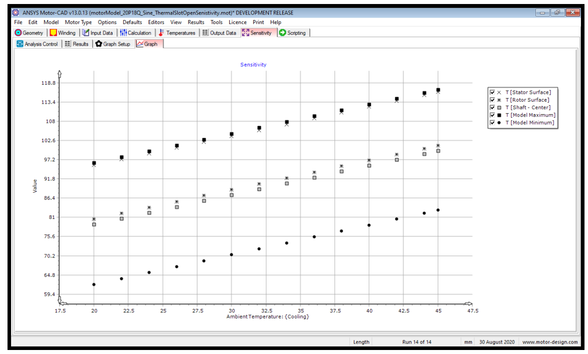

(b) Surface Temperatures

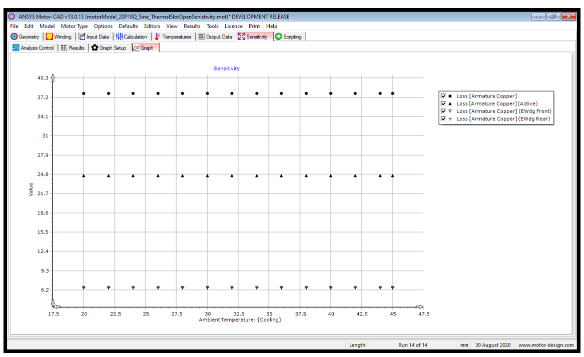

(c) Armature Losses

(d) Total Losses

Figure 4-12: Thermal Sensitivity : Ambient Temperature

4.1.2 Thermal Model Output Data

Thermal model output data of fractional slot motor fed by sinusoidal drive is tabulated in table 4.1.

4.2 Optimization of Motor Models

The optimization tool in MotorCAD allows to input a wide range of different design parameters including geometrical parameters, winding parameters, calculation

Temperature	Value	Temperature	Value	Temperature	value
T [Housing - Overhang (F)]	59.236	T [Housing - Active]	59.322	T [Housing - Overhang (R)]	59.23
T [Housing - Front]	59.137	T [Stator Lam (back iron)]	99.159	T [Housing - Rear]	59.13
T [Endcap - Front]	58.508	T [Stator Surface]	98.558	T [Endcap - Rear]	58.46
T [Bearing - Front]	77.311	T [Rotor Surface]	62.087	T [Bearing - Rear]	77.29
T [Axle Ohang - Front]	95.678	T [Magnet]	61.118	T [Axle Ohang - Rear]	95.68
T [Axle - Front]	95.68	T [Rotor Lamination]	59.621	T [Axle - Rear]	95.68
T [End Space (F)]	72.252	T [Axle - Center]	95.68	T [End Space (R)]	72.23
T [Rotor (F)]	59.672	T [Active Winding Maximum]	99.668	T [Rotor (R)]	59.67
T [EWdg (F) Maximum]	99.767	T [Active Winding Average]	99.623	T [EWdg (R) Maximum]	99.77
T [EWdg (F) Average]	99.614	T [Active Winding Minimum]	99.437	T [EWdg (R) Average]	99.61
T [EWdg (F) Minimum]	99.195	T [Winding Maximum]	99.767	T [EWdg (R) Minimum]	99.19
T [Winding Average]	99.619	T [End Winding Average]	99.614	T [Model Minimum]	58.462
T [Winding Minimum]	99.195	T [Model Maximum]	99.767		
Winding Temperatures	———	———	———	———	———
Temperature	Cuboid1 Value C^0	Cuboid2 C^0	Temperature	Cuboid1 Value C^0	Cuboid2 C^0
T [EWdg (F) Maximum]	99.767	99.767	T [Active Winding Minimum]	99.437	99.449
T [EWdg (F) Average]	99.651	99.578	T [EWdg (R) Maximum]	99.766	99.766
T [EWdg (F) Minimum]	99.423	99.195	T [EWdg (R) Average]	99.65	99.578
T [Active Winding Maximum]	99.668	99.634	T [EWdg (R) Minimum]	99.423	99.195
T [Active Winding Average]	99.638	99.608	T [Tooth]	99.39	99.024
Losses	———	———	———	———	———
Variable	Value	Unit	Variable	Value	Unit
Loss [Armature Copper]	41.64	Watts	Main Winding (Copper Loss Multiplier)	1	
Loss [Armature Copper] (Active)	24.55	Watts	Stall Operation (Copper Loss Multiplier)	1	
Loss [Armature Copper] (EWdg Front)	8.544	Watts	Fault Operation (Copper Loss Multiplier)	1	
Loss [Armature Copper] (EWdg Rear)	8.544	Watts	Loss[Stator Back Iron] Schematic Addition	0	Watts
Loss [Stator Back Iron]	2.578	Watts	Dissipation - Housing - Active [Con]	11.61	Watts
Loss [Stator Tooth]	25.16	Watts	Dissipation - Housing - Active [Rad]	7.128	Watts
Loss [Magnet]	1.778	Watts	Dissipation - Front Housing OH [Con]	0	Watts
Loss [Rotor Back Iron]	0.2564	Watts	Dissipation - Front Housing OH [Rad]	0	Watts
Loss [Airgap Banding]	0	Watts	Dissipation - Rear Housing OH [Con]	0	Watts
Loss [Winding Sleeve]	0	Watts	Dissipation - Rear Housing OH [Rad]	0	Watts
Loss [Windage]	0	Watts	Dissipation - Front Endcap [Con]	17.71	Watts
Loss [Windage] (Ext Fan)	0	Watts	Dissipation - Front Endcap [Rad]	8.319	Watts
Loss [Friction - F Bearing]	0	Watts	Dissipation - Rear Endcap [Con]	18.14	Watts
Loss [Friction - R Bearing]	0	Watts	Dissipation - Rear Endcap [Rad]	8.511	Watts
Loss [Total]	71.4097	Watts	Total Dissipation to model ambient node	71.4097	Watts

Table 4.1: Fractional Slot Motor Thermal Model Output Data

parameters and material as well. The optimization criteria are two-fold viz. error criteria and validity criteria.

Error Criteria: Error criteria usually work on outputs, for example flux densities. These are evaluated after an optimisation model is solved, and the error result is the sum of a multiple selection. The optimisation objective is to minimise the error sum, therefore lower values are considered as improvements.

Validity Criteria: Validity criteria work on inputs, for example geometry of the model, and they are Boolean expressions. If multiple validity criteria are selected and if at least one of the selected validity criteria is false the combined criteria will yield false.A false value is not considered a valid design to test. Therefore validity criteria are evaluated before an optimisation model is solved. MotorCAD default criteria are given below.

- Outer stator validity – a validity criterion

- Maximise Motor Constant – an error criterion
- Maximise Average Torque – an error criterion
- Maximise Load Point Torque – an error criterion

4.2.1 Electromagnetic Model Optimization

Initially the motor optimization was done solely considering the electromagnetic model without taking thermal aspects into account.The output data for the initial design and for an acceptable optimization solution are tabulated in table for comparison. 4.2.

4.2.2 Multi-Physics Model optimization

A suitable design solution was chosen after the initial optimization stage. Then the selected design was optimized considering both electromagnetic and thermal aspects.MotorCAD offers an iterative calculation option which takes electromagnetic and thermal coupling into account converging to a electromagnetic-thermal coupled solution. The final optimization results are tabulated in table 4.3.

According to the optimization results design 4 has the highest magnet weight reduction and highest torque per rotor volume(TRV). Design 6 has next best magnet weight reduction and TRV value. Design 6 also has a better efficiency and a lower torque ripple as well as lower magnet and armature winding temperatures. Considering these facts design 6 was chosen for the application.

Parameter (Initial Design)	**Value**	**Unit**	**Parameter (Optimized Design)**	**Value**	**Unit**
Maximum torque possible DQ (For Phase Advance of 2.033 EDeg)	19.678	Nm	Maximum torque possible DQ (For Phase Advance of 2.627 EDeg)	19.923	Nm
Average torque (virtual work)	19.535	Nm	Average torque (virtual work)	19.8	Nm
Average torque (loop torque)	19.454	Nm	Average torque (loop torque)	19.709	Nm
Torque Ripple (MsVw)	1.1199	Nm	Torque Ripple (MsVw)	1.3628	Nm
Torque Ripple (MsVw) [%]	5.7544	%	Torque Ripple (MsVw) [%]	6.917	%
(For Phase Advance of 0 EDeg)"	428.49	rpm	(For Phase Advance of 0 EDeg)"	460	rpm
No load speed	453.82	rpm	No load speed	475.09	rpm
—			—		
Electromagnetic Power	815.23	Watts	Electromagnetic Power	825.26	Watts
Input Power	877.01	Watts	Input Power	852.54	Watts
Output Power	786.61	Watts	Output Power	795.48	Watts
Total Losses (on load)	90.399	Watts	Total Losses (on load)	57.059	Watts
System Efficiency	89.692	%	System Efficiency	93.307	%
—			—		
Shaft Torque	18.779	Nm	Shaft Torque	18.991	Nm
—			—		
Power Factor [Waveform] (leading)	0.99639		Power Factor [Waveform] (leading)	0.99434	
Power Factor Angle [Waveform]	4.8696	EDeg	Power Factor Angle [Waveform]	6.0963	EDeg
Power Factor [Phasor] (leading)	0.99619		Power Factor [Phasor] (leading)	0.99452	
Power Factor Angle [Phasor]	5	EDeg	Power Factor Angle [Phasor]	6	EDeg
Load Angle [Phasor]	4.9836	EDeg	Load Angle [Phasor]	6.0563	EDeg
Phase Terminal Voltage (rms) [Phasor]	27.506	Volts	Phase Terminal Voltage (rms) [Phasor]	22.738	Volts
—			—		
Rotor Inertia	0.030365	kg.m	Rotor Inertia	0.021061	kg.m
Total Inertia	0.030365	kg.m	Total Inertia	0.021061	kg.m
Torque per rotor volume	43.021	kNm/m	Torque per rotor volume	59.219	kNm/m
Rotor peripheral velocity (on load)	3.4348	m/s	Rotor peripheral velocity (on load)	3.4111	m/s
Magnet Weight	1.762	kg	Magnet Weight	1.055	kg
—					
DC Supply Current (mean)	12.15	Amps	DC Supply Current (mean)	11.84	Amps
Line Current (peak)	15.2	Amps	Line Current (peak)	18	Amps
Line Current (rms)	10.75	Amps	Line Current (rms)	12.73	Amps
Phase Current (peak)	15.2	Amps	Phase Current (peak)	18	Amps
Phase Current (rms)	10.75	Amps	Phase Current (rms)	12.73	Amps
—					
DC Bus Voltage	72	Volts	DC Bus Voltage	72	Volts
Line-Line Supply Voltage (rms)	50.91	Volts	Line-Line Supply Voltage (rms)	50.91	Volts
Phase Supply Voltage (rms)	29.39	Volts	Phase Supply Voltage (rms)	29.39	Volts
Line-Line Terminal Voltage (peak)	67.84	Volts	Line-Line Terminal Voltage (peak)	55.78	Volts

Table 4.2: Comparison Output Data of the Initial Design and the Initial Optimized Design

Parameter	**Initial Value**	**Min**	**Max**	**Design 1**	**Design 2**	**Design 3**	**Design 4**	**Design 5**	**Design 6**	**Design 7**
Cup Radial Thickness(mm)	5	3	5	4.631239301	4.323260358	3.666975	4.359372	4.38799	4.957881	4.860439
Magnet Thickness(mm)	10	5	10	7.619230835	5.33763369	9.016304	6.412512	7.5926	6.163726	7.613213
Tooth Width(mm)	7	4	8	5.773974263	5.858767205	7.11223	7.96436	6.395715	6.610801	6.767478
Slot Depth(mm)	18	15	30	21.34443973	22.89401301	19.47368	15.7339	25.19741	27.2623	29.00687
Slot Opening(mm)	5	2	8	5.501536212	5.562118865	6.659138	6.741229	3.116827	4.74794	4.316576
Tooth Tip Angle(MDeg)	30	5	30	20.41676281	27.49306554	17.3236	20.65164	26.493	12.94273	26.9106
Armature Diameter(mm)	164	150	170	152.5414892	161.2547386	157.7696	152.3687	151.8595	162.8699	162.1341
Airgap(mm)	1	0.5	1	0.586364517	0.946017166	0.676639	0.637564	0.859044	0.982833	0.636688
Turns:	20	15	25	20	17	22	16	25	19	19
Copper Slot Fill	0.4	0.4	0.55	0.42376882	0.465240048	0.501002	0.52679	0.442017	0.526041	0.541373
Coil Divider(mm)	2	1	2	1.804407181	1.9901891	1.114667	1.547005	1.352052	1.193622	1.182279
Liner Thickness(mm)	0.25	0.25	1	0.443218018	0.695263786	0.810241	0.654167	0.823047	0.871555	0.791715
Total Weighted Error :				0.023328833	0.023328833	0.033855	0.033855	0.033855	0.028828	0.028828
Peak Current (A)	15.2	13	20	18	20	15	18	14	18	18
RMS Current(A)	10.75			12.73	14.4	10.61	12.73	9.89	12.73	12.73
RMS current Density(A/mm^2)	3.87			3.67	2.8	3.11	3.5	3.23	2.136	2.09
Torque(Nm)	18.78			18.46	17.33	19.07	18.09	18.54	18.518	19.42
Torque Ripple %	5.7			5.8	4.5	7.1	6.05	5.89	5.6	7.69
Output Power(W)	786.6			773.4	725	798.87	758.7	776.7	775.7	813.7
Efficiency(%)	89.69			88.9	90.77	90.8	90.9	90.09	92.36	92.12
Loss(W)	90.39			96	73.79	80.6	75.3	85.4	64.1	69.6
Magnet weight improvement %				-31.8181818	-48.8636364	-14.7727	-42.0455	-30.6818	-40.3409	-26.1364
TRV (kNm/m^3)	43.02			57.28	72.67	54.95	63.09	57.8	57.7	56.12
TRV Improvement				33.14737331	68.92143189	27.73129	46.65272	34.35611	34.12	30.45095
Armature Winding Temperature(C^0)	126.1	25	150	137.5	115.8	121.7	123.4	129.2	104.3	107.4
Magnet Temperature(C^0)	102.4	25	120	116.8	96.95	103.2	102.2	106.9	88.19	93.63
Shaft Temperature(C^0)	103.8	25	150	110.6	94.63	98.3	98.57	104.2	86.79	89.68

Table 4.3: Final Optimization Results

Chapter 5

Validation of the Motor Model by Finite Element Analysis

This chapter presents the MotorCAD simulation results of the selected design (Design 6 in the table 4.3). The results obtained by MotorCAD show that the designed motor meets the specified requirements of application. The simulation results closely comply with the analytical values.

5.1 Electromagnetic Validation (FEA of optimized design)

The flux density distribution and current density of radial cross -section of the optimized design is shown in figure 5-1. Some variables of the design were calculated analytically using the equations mentioned in chapter 3. Some of those analytical values and corresponding values yielded by simulations are tabulated in table 5.1. The output graphs corresponding to the optimized 20P18Q machine model are shown in figure 5-2. The torque- speed characteristic of the optimized 20P18Q motor is shown in figure 5-3.

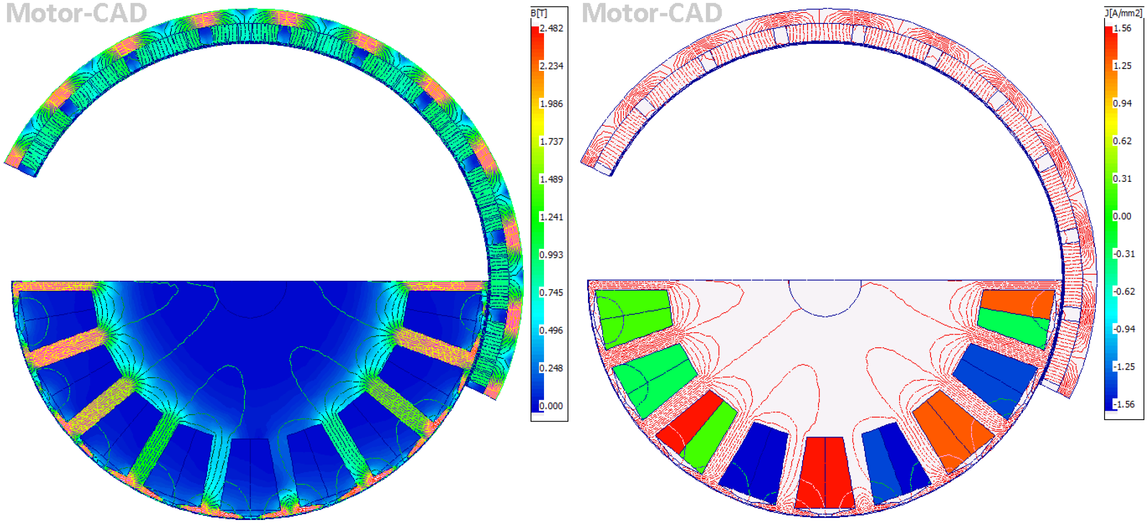

(a) Flux Density

(b) Current Density

Figure 5-1: Electromagnetic FEA Window :Optimized design

5.2 Lab Model

Motor-CAD Lab is a combined electromagnetic and thermal modelling toolbox.It can be used for calculations facilitating the modelling and optimisation of a motor design over its entire operating range.Motor-CAD Lab can be used create efficiency maps, plot torque/speed characteristics, study the continuous and peak thermally constrained operational envelope and analyse performance over driving cycles.However analysis of motor performance over a particular drive cycle is beyond the scope of this thesis.

The optimized 20P18Q was modelled in Motor-CAD Lab and the results maximum torque per ampere control strategy are provided in following sections.

Efficiency Map

The contour graph of efficiency and shaft torque versus speed of the final design is shown in 5-4. Torque, efficiency -speed curves are shown in figure 5-5.

Parameter	Analytical Value	Simulated Value	Units
Torque	19.1	18.52	Nm
Output Power	800	775.74	W
Phase Current	11.79	12.73	A
RMS Current Density	2	2.13	A/mm^2
Airgap Flux Density	1.52	1.03	T
Peak Current	16.67	18	A
Peak flux density in stator teeth	1.7	1.8	T
Losses	42	64	Watts
System Efficiency	95	92	%
Power Factor	0.998	0.993	
Torque per rotor volume	59.9	57	kNm/m^3
Electrical Loading	1.65E004	1.701E004	Amps/m

Table 5.1: Analytical and Simulated Values of Output variables

Operating Point under Maximum Torque per Amp Control Strategy

Operating point data under maximum torque per Ampere control strategy are tabulated in table 5.2.

5.3 Thermal Model Analysis and Validation (FEA of optimized design)

Schematic of thermal network steady state model of the optimized 20P18Q motor design is illustrated in 5-6. FEA evaluated temperature distribution of radial cross section is shown in 5-7. FEA evaluated temperature distributions of rotor and stator are shown in 5-8.

5.3.1 Thermal Validation

The temperatures and deviation from validation temperatures are shown in 5-9 and in 5-10. It can be seen that the simulated temperature values comply with the validation

Operating Point Parameter	Value	Unit	Operating Point Parameter	Value	Unit
Shaft Speed	400	rpm	Total Loss	66.05	Watts
Shaft Torque	19	Nm	Stator Copper Loss	37.7	Watts
Shaft Power	795.9	Watts	Iron Loss	28.2	Watts
Efficiency	92.34		Magnet Loss	0.1501	Watts
Stator Phase Current (peak)	18.31	Amps	Mechanical Loss	0	Watts
Stator Line Current (peak)	18.31	Amps	Electromagnetic Power	824.2	Watts
DC Terminal Current	11.97	Amps	Electromagnetic Torque	19.68	Nm
Phase Voltage (peak)	31.44	Volts	Magnet Torque	19.63	Nm
Line Voltage (peak)	54.46	Volts	Reluctance Torque	0.05154	Nm
Phase Advance	3.103	EDeg	Power Factor	0.998	
Flux Linkage D	71.27	mVs	Stator Winding Temperature (average)	113.5	C
Flux Linkage Q	8.637	mVs	Stator Winding Temperature (max)	113.8	C
Magnet Flux Linkage	71.55	mVs	Magnet Temperature	93.4	C
D axis Inductance	0.2827	mH	Q axis Inductance	0.4723	mH

Table 5.2: Operating Point Data Under Maximum Torque Per Ampere Control Strategy

temperatures. Temperature surface graphs of stator winding and magnets are shown in figure 5-11.

5.3.2 Mechanical model (FEA of optimized design)

Motor-CAD mechanical tool facilitates calculating the mechanical stresses using finite element analysis. The resulting mehanical stress distribution is shown in figure 5-12. It is suggested to fabricate a sample rotor cut and perform a spin test to evaluate the realistic centrifugal stresses and to validate the structural integrity,and durability of the rotor. It can be seen that the maximum stress on rotor cup (about 304kPa) is much less than typical yield stress 69MPa of aluminum.Also the stress on magnets is also at an acceptable level.

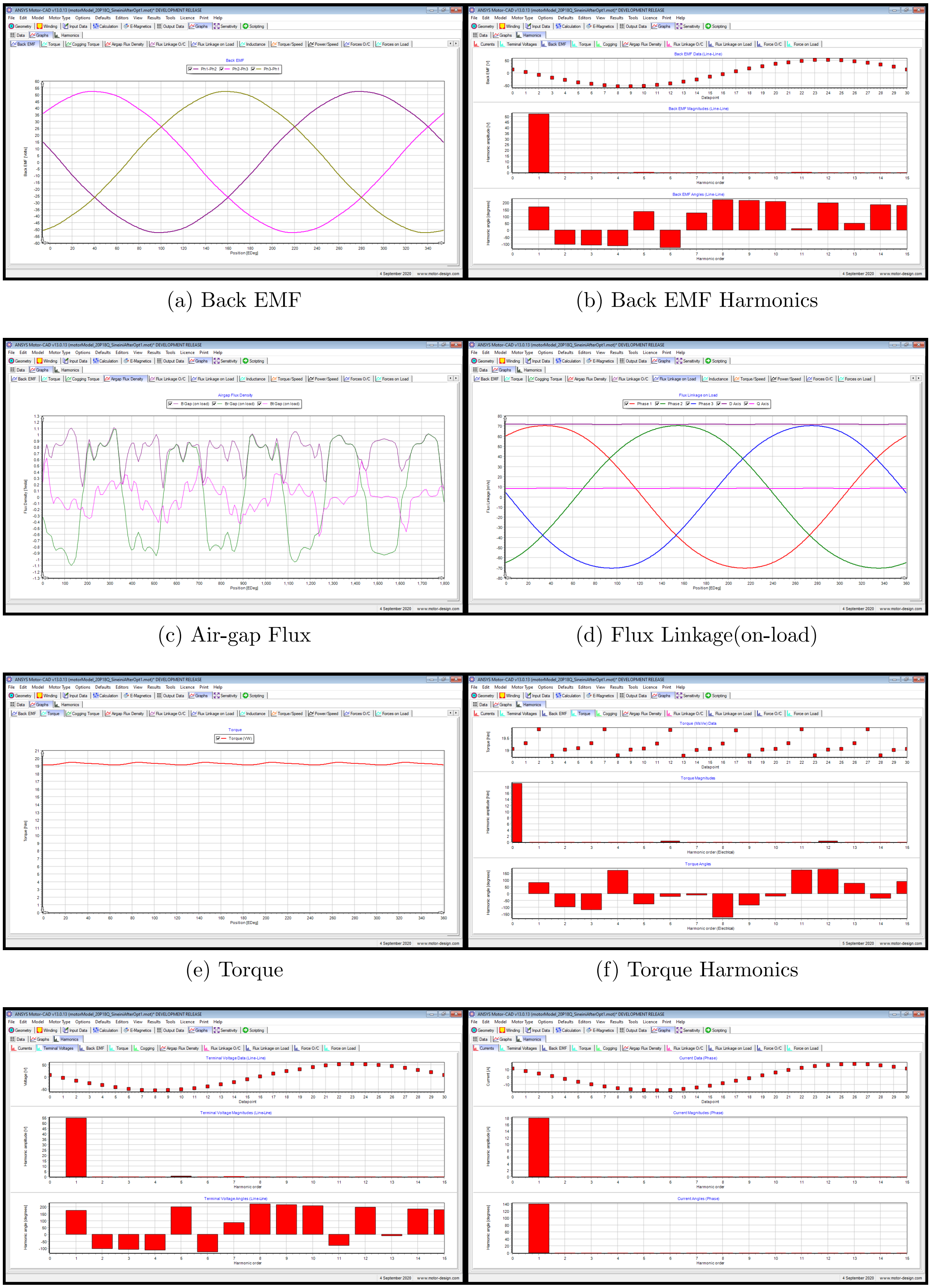

(a) Back EMF (b) Back EMF Harmonics

(c) Air-gap Flux (d) Flux Linkage(on-load)

(e) Torque (f) Torque Harmonics

(g) Terminal Voltage Harmonics (h) Current Harmonics

Figure 5-2: Output graphs of Optimized machine

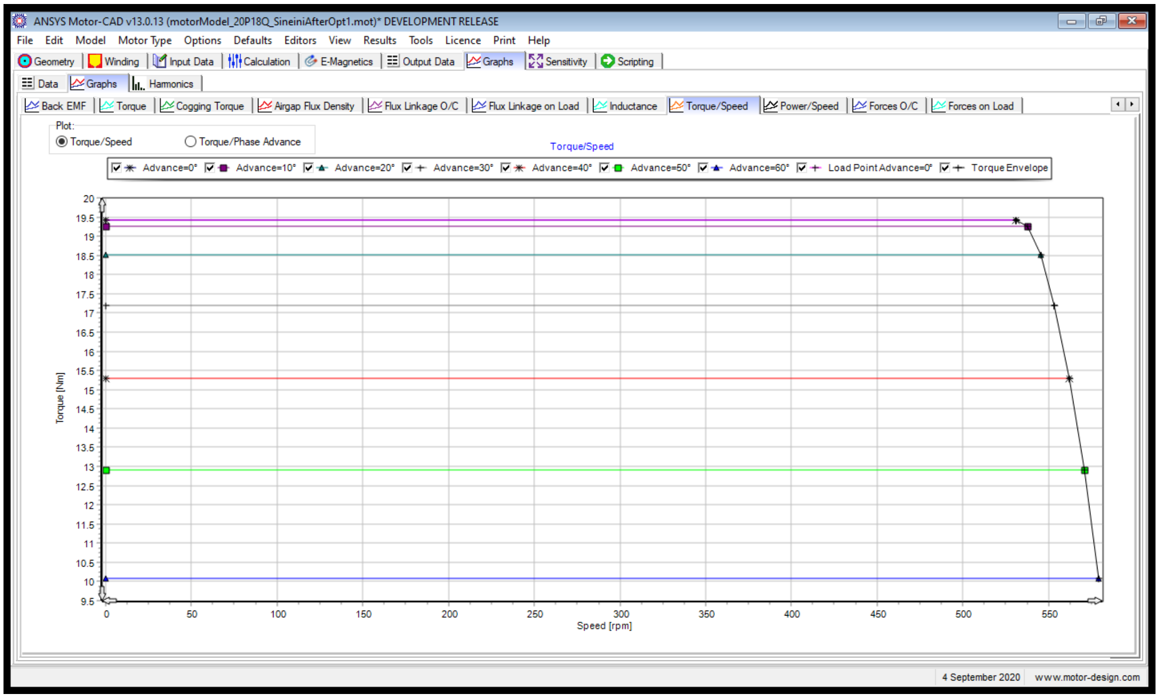

Figure 5-3: Torque-Speed Characteristic of the optimized 20P18Q Machine

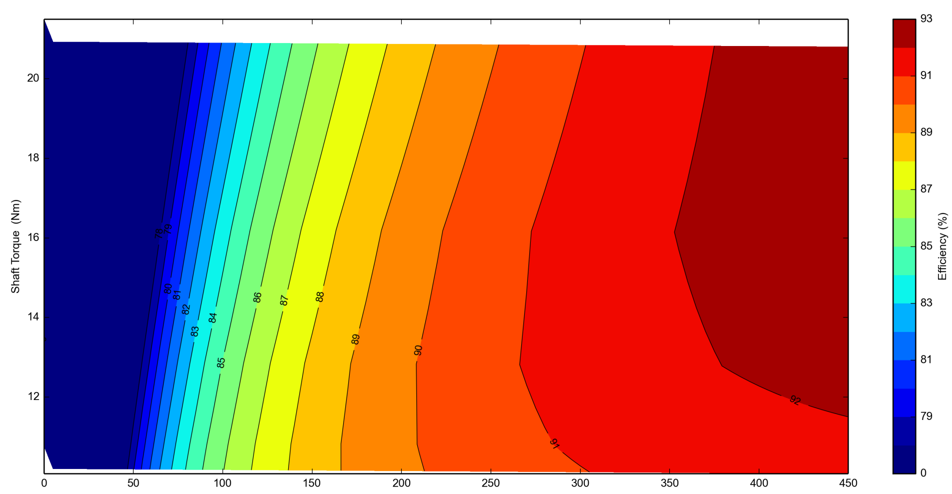

Figure 5-4: Contour graph of efficiency and shaft torque versus speed

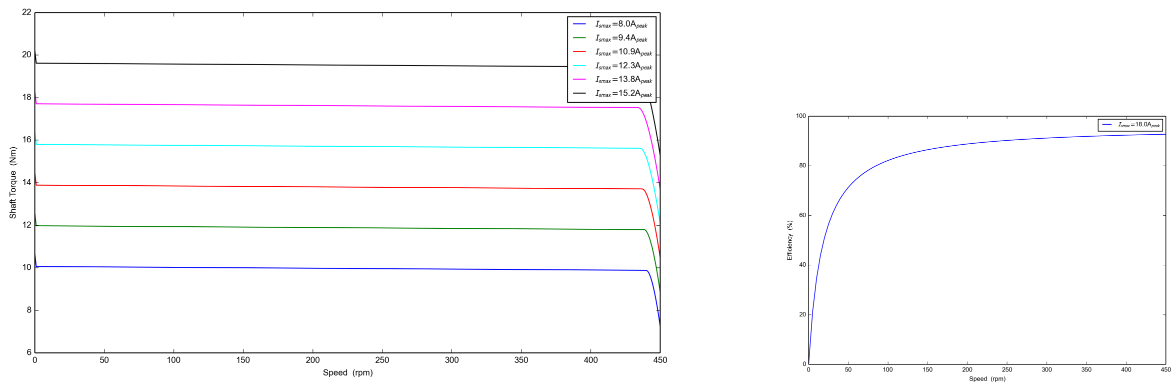

(a) Torque -Speed curves for different current levels (b) Efficiency Vs Speed

Figure 5-5: Torque, Efficiency - Speed curves

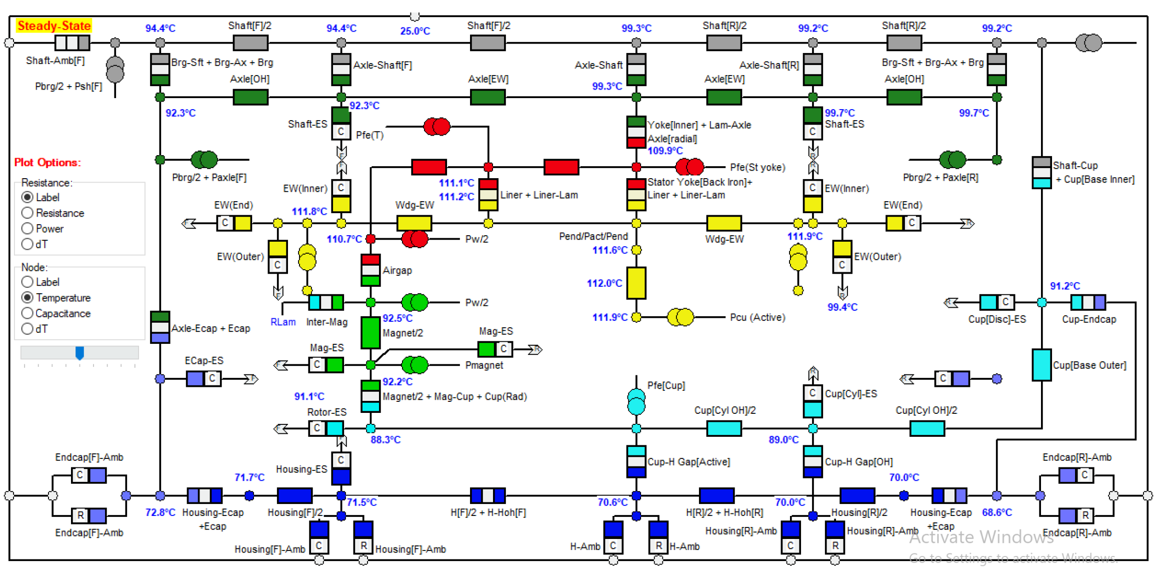

Figure 5-6: Schematic view of equivalent thermal network (steady state) model optimized 20P18Q motor

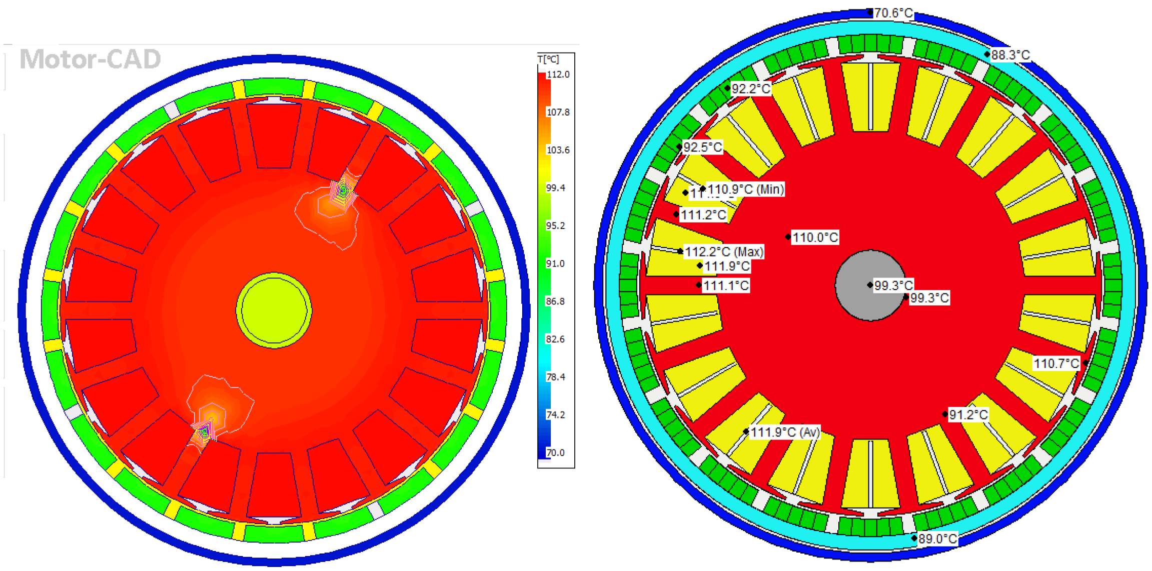

(a) Temperature distribution (FEA):Radial

(b) Temperatures:Radial cross section

Figure 5-7: Radial cross section FEA evaluated temperature distribution of Optimized 20P18Q motor

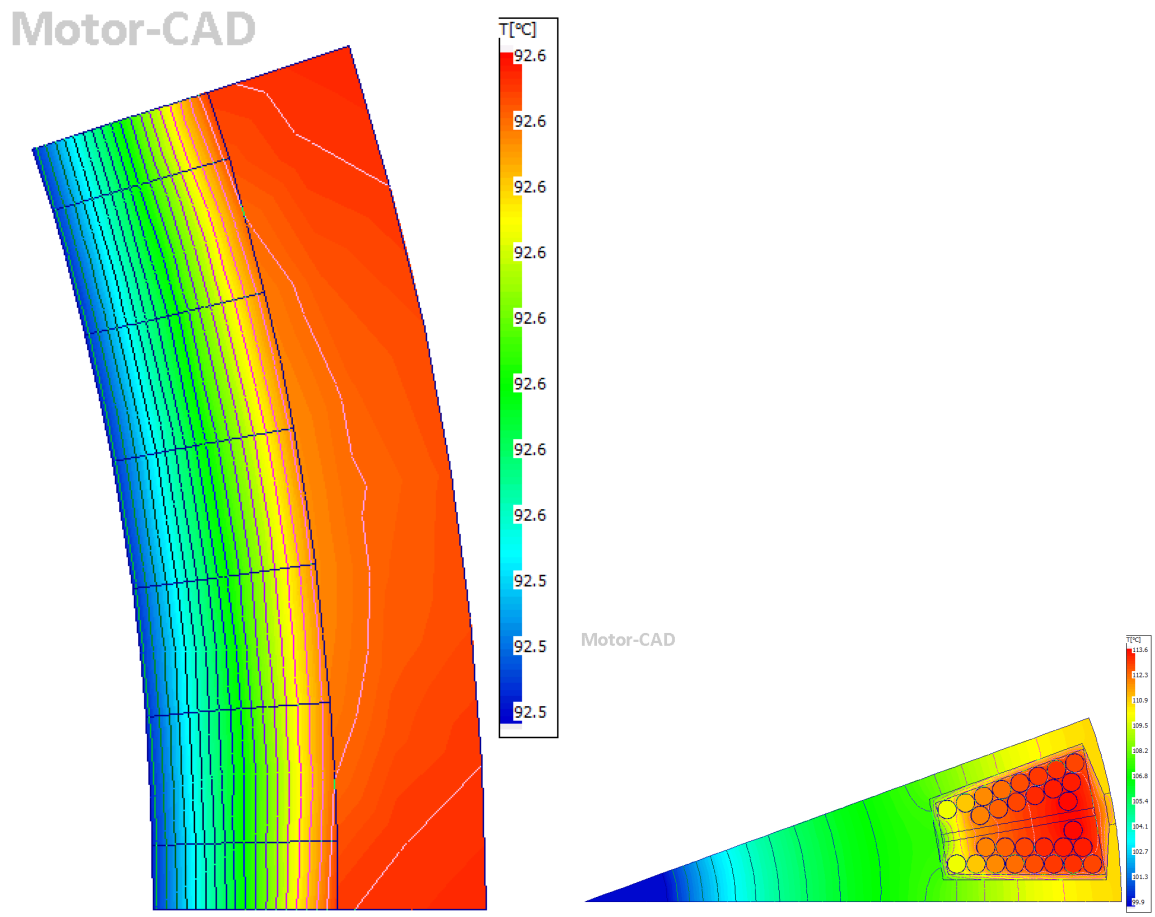

(a) Rotor Temperature Distribution (b) Stator Temperature Distribution

Figure 5-8: FEA evaluated temperature distribution of rotor and stator off optimized 20P18Q motor

Node	Legend	Compare	Optimisation Weighting	Motor-CAD Temperature	Validation Temperature	Difference	Percentage Difference
Units		☐		℃	℃	℃	%
Ambient	Ambient	☐		25	25	0	0.000
Housing [Active]	Housing [Active]	☑		70.577	75	-4.423	-5.897
Housing OH [Front]	Housing OH [Front]	☑		71.486	75	-3.514	-4.685
Housing [Front]	Housing [Front]	☑		71.653	75	-3.347	-4.463
Endcap [Front]	Endcap [Front]	☑		72.776	75	-2.224	-2.965
Housing OH [Rear]	Housing OH [Rear]	☑		70.034	75	-4.966	-6.621
Housing [Rear]	Housing [Rear]	☑		69.972	70	-0.028	-0.040
Endcap [Rear]	Endcap [Rear]	☑		68.59	70	-1.41	-2.014
Stator Back Iron	Stator Back Iron	☑		109.95	120	-10.05	-8.375
Stator Surface	Stator Surface	☑		110.66	120	-9.34	-7.783
Rotor Surface	Rotor Surface	☑		92.536	100	-7.464	-7.464
Magnet	Magnet	☑		92.213	100	-7.787	-7.787
Cup [Active]	Cup [Active]	☑		88.3	90	-1.7	-1.889
Shaft [Active]	Shaft [Active]	☑		99.319	100	-0.681	-0.681
Shaft OHang [F]	Shaft OHang [F]	☑		94.378	100	-5.622	-5.622
Shaft OHang [R]	Shaft OHang [R]	☑		99.205	100	-0.795	-0.795
End Space [F]	End Space [F]	☑		91.098	100	-8.902	-8.902
End Space [R]	End Space [R]	☑		99.432	100	-0.568	-0.568
Axle [Active]	Axle [Active]	☑		99.319	100	-0.681	-0.681
Axle OHang [F]	Axle OHang [F]	☑		92.32	100	-7.68	-7.680
Axle OHang [R]	Axle OHang [R]	☑		99.747	100	-0.253	-0.253
Cup Overhang	Cup Overhang	☑		89.01	90	-0.99	-1.100
Cup Base	Cup Base	☑		91.191	100	-8.809	-8.809
Rotor Lam [F]	Rotor Lam [F]	☑		88.583	90	-1.417	-1.574
Rotor Lam [R]	Rotor Lam [R]	☑		88.948	90	-1.052	-1.169

Figure 5-9: Thermal validation Data of the Optimized 20P18Q Machine

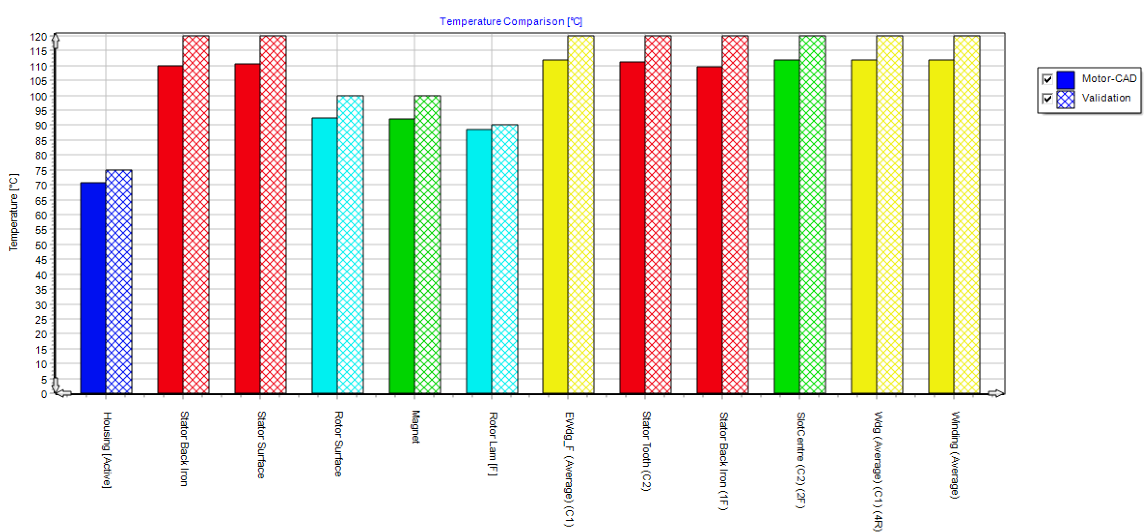

Figure 5-10: Thermal validation Graph

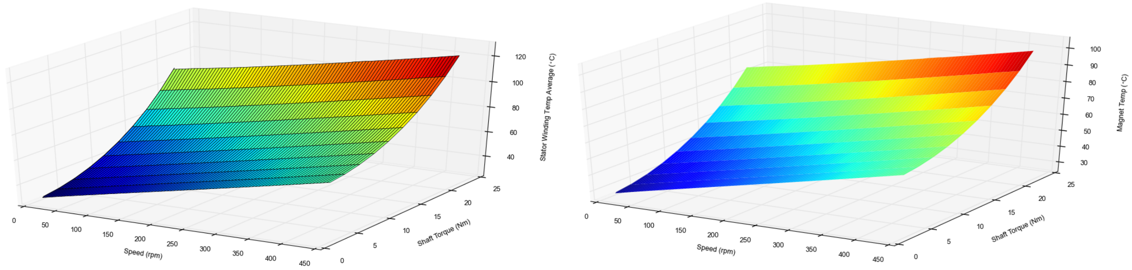

(a) Stator winding temperature (b) Magnet temperature

Figure 5-11: Temperature surface graphs of the optimized 20P18Q machine

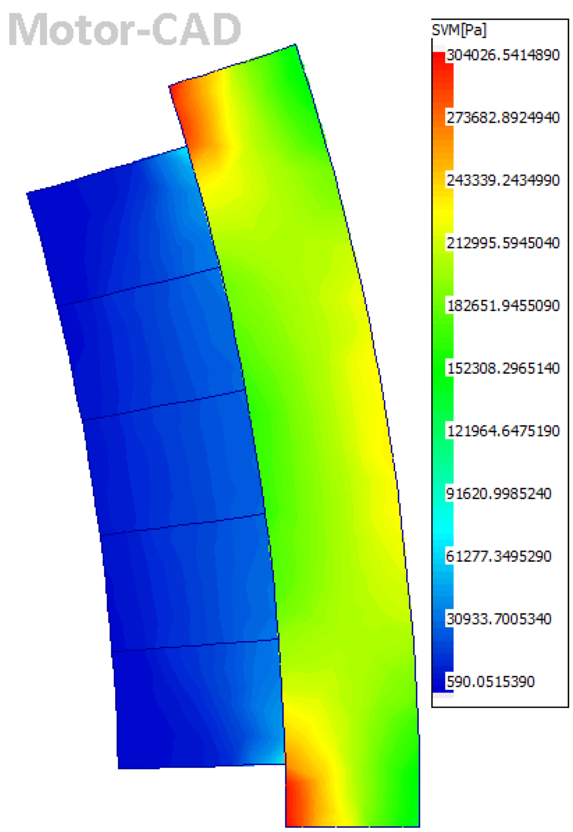

Figure 5-12: mechanical stress distribution on rotor

Chapter 6

Conclusion

6.1 Conclusion

In this project, a permanent magnet synchronous motor was designed for a two wheeler application. A review on available motor types/topologies was performed and based on that study two main permanent magnet synchronous motor(surface mounted) designs (A motor with Square-Wave shaped Back EMF waveform and a motor with Sinusoidal shaped back EMF waveform) were chosen for modelling in MotorCAD software. Several possible winding configurations were considered and fractional- slot double layer winding and a integer slot double layer winding were used in initial simulations.Initial design calculations were performed using analytical equations and design algorithms which are published by different authors [1, 2]. Performance evaluation of two main motor designs was carried out using MotorCAD software.The torque density of square-wave motor was higher than that of sinusoidal -wave motor for a given peak drive current. However Considering the favorable performance(in terms of torque ripple and efficency) of the motor with sinusoidal back EMF waveform fed by a sinusoidal-wave drive was chosen for further analysis and optimization. A sensitivity analysis was performed using tools available in MotorCAD focusing on main design parameters affecting the electromagnetic and thermal performance of the machine.

After that,in order to improve the performance and cost effectiveness of the motor a general optimization was performed using the optimization tool provided by MotorCAD. The final design was validated with respect to electromagnetic performance using MotorCAD.Further thermal performance validation was done using MotorCAD thermal model analysis to ensure the temperature levels of the motor are satisfactory. According to simulation results it can be concluded that the designed motor meets the requirements specified in the application in terms of electromagnetic and thermal performance.

6.2 Future Work

The performance of proposed motor design with respect to electromagnetic and thermal aspects was validated using MotorCAD. However the mechanical losses of the machine were not considered in simulations.In the calculations mechanical losses were neglected.Therefore modelling the design taking into mechanical losses is suggested as a future work. Moreover the author suggests to fabricate a sample stator and rotor cuts and to conduct spin tests to evaluate the realistic mechanical stresses and performance of the machine.

Even though the designed motor exhibits good performance and meets the basic requirements of the application there's still some room for further improvement of the design. Particularly, the proposed design uses stranded windings in the stator where it's practically very difficult have a higher copper slot fill.Therefore the author suggests to investigate the possibility using hairpin type windings (which allows to achieve a higher copper slot fill factor) in any future attempt to improve the performance of the motor.Also the investigation of suitability of the motor for a particular driving cycle is yet to be done as a future work. Moreover , the scope of this project was limited to the design of the motor and hence the aspects related to motor drive and control wasn't considered. The circular tracking sine drive modulation method which is the default option in MotorCAD was used in simulations.Therefore, it is suggested to investigate the appropriate motor drive technologies as a future work.

Appendix A

Tables

Table A.1: Initial Design Calculations 20P18Q Machine with Sinusoidal Excitation

Parameter	**Design 1**	**Design 2**	**Design 3**	**Design 4**	**Design 5**	**Design 6**
L_stk	0.05	0.05	0.05	0.05	0.05	0.05
g Air gap	0.001	0.001	0.001	0.001	0.001	0.001
m	3	3	3	3	3	3
q	1/4	2/5	1/3	2/7	2/7	0.5
Kc Carter Coefficient	1.085	1.085	1.085	1.085	1.085	1.085
n_l Number of layers	2	2	2	2	2	2
Br T	1.45	1.45	1.45	1.45	1.45	1.45
lm/g	10	10	10	10	10	10
Bfe_peak	1.7	1.7	1.7	1.7	1.7	1.7
kjo (W/mˆ2)_target	700	700	700	700	700	700
Sigma_0_target (N/mˆ2)	7000	7000	7000	7000	7000	7000
km	5/6	5/6	5/6	5/6	5/6	0.83
Design of Elementary Block						
kb	1.23	1.23	1.23	1.23	1.23	1.23
B (T)	1.61	1.61	1.61	1.61	1.61	1.61

A (A/m)	4351.23	4351.23	4351.23	4351.23	4351.23	4351.23
Area	0.08	0.08	0.08	0.08	0.06	0.08
Loss	58.69	58.69	58.69	58.69	40.08	58.69
Kcu Fill factor	0.4	0.4	0.4	0.4	0.4	0.4
Temperature C	40	40	40	40	40	40
Rho_Cu	1.8E-08	1.8E-08	1.8E-08	1.8E-08	1.8E-08	1.8E-08
kw Winding factor	0.95	0.95	0.95	0.95	0.95	0.87
kt	0.5	0.5	0.5	0.5	0.5	0.5
k_end	0.3	0.3	0.3	0.3	0.3	0.3
l_t (m)	0.009	0.009	0.009	0.009	0.009	0.009
lt/g	9	9	9	9	9	9
kj	120.33	121.41	121.41	121.41	121.41	144.63
Q0	10	10	10	9	9	6
a/g |L_min	11.42	18.27	16.61	13.64	13.64	22.21
L_pole,pu_min	15.15	9.56	10.51	12.68	12.68	8.86
n_s (turns per slot per phase)	20	20	20	20	20	20
N (turns per pole per phase)	5	8	7	6	6	10
L_base H	4.6E-06	4.5E-06	4.5E-06	4.5E-06	4.5E-06	3.8E-06
L_pole_min	6.9E-05	4.3E-05	4.7E-05	5.7E-05	5.7E-05	3.4E-05
Tan_Phi	0.04	0.04	0.04	0.04	0.04	0.04
Phi	0.04	0.04	0.04	0.04	0.04	0.04
PF	1.00	1.00	1.00	1.00	1.00	1.00
Power W	800	800	800	800	500	800
T_target Nm	19.10	19.10	19.10	19.10	11.94	19.10
Speed RPM	400	400	400	400	400	400

r^2L_stk	0.000	0.000	0.000	0.000	0.000	0.000
r	0.093	0.093	0.093	0.093	0.074	0.093
D_rotor (Outer)	0.186	0.186	0.186	0.186	0.147	0.186
Stator Diameter	0.164	0.164	0.164	0.164	0.125	0.164
TRV kN/m^3	14	14	14	14	14	14
a |L_min	0.01	0.02	0.02	0.01	0.01	0.02
p Pole pairs	25.64	16.03	17.63	21.47	16.97	13.18
2p Approximated	26	16	20	20	20	8
Slots Z	24	18	18	18	18	12
q_calculated	0.31	0.38	0.30	0.30	0.30	0.50
Pole pitch (a)	0.02	0.04	0.03	0.03	0.02	0.07
n (turns per pole per phase)	6.15	7.50	6.00	6.00	6.00	10.00
DC bus Voltage V	72	72	72	72	72	72
Phase Supply voltage V	29.39	29.39	29.39	29.39	29.39	29.39
Efficiency	0.9	0.9	0.9	0.9	0.9	0.9
Iq Current	11.18	14.97	14.97	14.97	11.84	24.52
I_dc DC mean current	12.35	12.35	12.35	12.35	7.72	12.35
LCM(2p,Z)	312	144	180	180	180	24
Cogging torque Periodicity n	13	8	10	10	10	2
Is (Slot current)	335.43	449.25	449.25	449.25	355.16	735.49
Iph	7.91	10.59	10.59	10.59	8.37	17.34
Ipk	11.18	14.97	14.97	14.97	11.84	24.52
t periodicity	1	2	2	2	2	4
q_ph= Z/mt (an integer)	8	3	3	3	3	1
Alpha_ph	0.26	0.70	0.70	0.70	0.70	2.09
Kd if q_ph is even	0.96	0.97	0.97	0.97	0.97	1.15
Kd if q_ph is odd	0.96	0.96	0.96	0.96	0.96	1.00

y_q Slot pitch_max	1	1	1	1	1	1
Epsilon (remainder)	0.92	0.13	0.90	0.90	0.90	0.50
Cph coils per phase	8.00	6.00	6.00	6.00	6.00	4.00
HCF(Cph,p) number of sections	1.00	2.00	2.00	2.00	2.00	4.00
Nss Slots per Section	24.00	9.00	9.00	9.00	9.00	3.00
Sf progressive ,epsilon=0.5	2.00	2.00	2.00	2.00	2.00	2.00
Sf retrogressive ,epsilon0.5	23.00	8.00	8.00	8.00	8.00	2.00
Sigma_w Coil span Angle	3.40	2.79	3.49	3.49	3.49	2.09
Kp Pitch factor	0.99	0.98	0.98	0.98	0.98	0.87
K_p	0.99	0.98	0.98	0.98	0.98	0.87
Kw winding factor calculated	0.95	0.95	0.95	0.95	0.95	0.87
Q0_new	10	10	10	9	9	9
kjo_Recalculated	477.07	477.07	477.07	477.07	698.69	477.07
k_end_Recalculated	1.19	1.18	1.18	1.18	1.73	0.99
L_slot_pu	7.58	4.78	5.26	6.34	6.34	4.64
L_g_pu	1.45	1.91	2.17	1.78	1.78	1.90
L_pole_pu_new	12.31	10.19	12.74	12.68	12.68	9.07
L_base_new	0.00	0.00	0.00	0.00	0.00	0.00
L_pole_new H	0.00	0.00	0.00	0.00	0.00	0.00
tan Phi_new	0.02	0.01	0.02	0.02	0.02	0.01
Phi_new	0.02	0.01	0.02	0.02	0.02	0.01
PF_new	1.00	1.00	1.00	1.00	1.00	1.00
minimum Wt Tooth width	0.00	0.01	0.01	0.01	0.01	0.01
Back iron thickness	0.00	0.01	0.01	0.00	0.00	0.01
Rotor Back iron	0.01	0.01	0.01	0.01	0.01	0.01
Stator diameter Ds	0.16	0.16	0.16	0.16	0.13	0.16

n_p	13	8	10	10	10	2
Magnet arc	150	150	150	150	150	150
Throw	1	1	1	1	1	1

Table A.2: Integer - Slot Motors Initial Designs.

Parameter	**Design 1**	**Design 2**	**Design 3**	**Design 4**	**Design 5**
L_stk	0.05	0.05	0.05	0.05	0.05
g Air gap	0.001	0.001	0.001	0.001	0.001
m	3	3	3	3	3
q	1	2	3	1	1
Kc Carter Coefficient	1.05	1.05	1.05	1.05	1.05
n_l Number of layers	2	2	2	2	2
Br T	1.45	1.45	1.45	1.45	1.45
lm/g	10	10	10	10	10
Bfe_peak	1.7	1.7	1.7	1.7	1.7
kjo (W/m^2)_*target*	450	450	450	450	450
Sigma_0_target (N/m^2)	7000	7000	7000	7000	7000
km	5/6	1	1	1	2/3
Design of Elementary Block					
kb	1.23	1.27	1.27	1.27	1.102658
B (T)	1.61	1.67	1.67	1.67	1.446927
A (A/m)	4337.489326	4189.693	4189.693	4189.693	4837.841
Kcu Fill factor	0.4	0.4	0.4	0.4	0.4
Temperature C	40	40	40	40	40
Rho_Cu	1.81104E-08	1.81E-08	1.81E-08	1.81E-08	1.81E-08
kw Winding factor	0.866025404	0.933013	0.945214	0.866025	0.866025
kt	0.5	0.5	0.5	0.5	0.5
k_end	0.3	0.3	0.3	0.3	0.3

Continued on next page

Table A.2 – continued from previous page

Parameter	Design 1	Design 2	Design 3	Design 4	Design 5
l_t (m)	0.009	0.009	0.009	0.009	0.009
lt/g	9	9	9	9	9
kj	144.1285948	119.6717	116.6022	138.901	163.9755
a/g —L_min	23.77700327	24.16523	24.16523	24.16523	22.73832
L_pole,pu_min	9.48	8.30	8.09	9.64	9.067403
n_s (turms per slot per phase)	20	20	20	20	20
L_base H	3.81972E-06	4.43E-06	4.55E-06	3.82E-06	3.82E-06
L_pole_min	3.6217E-05	3.68E-05	3.68E-05	3.68E-05	3.46E-05
Tan_Phi	0.041569569	0.038785	0.038785	0.038785	0.051713
Phi	0.04154565	0.038766	0.038766	0.038766	0.051667
PF	0.999137104	0.999249	0.999249	0.999249	0.998666
Power W	800	800	800	800	800
T_target Nm	19.09859317	19.09859	19.09859	19.09859	19.09859
Speed RPM	400	400	400	400	400
Efficiency	0.9	0.9	0.9	0.9	0.9
DC bus Voltage V_DC V	72	72	72	72	72
Supply Voltage v_s V	29.39387691	29.39388	29.39388	29.39388	29.39388
Phase Current I_ph A	10.08891039	10.08778	10.08778	10.08778	10.09367
Peak Current I_peak	12.35634125	12.35496	12.35496	12.35496	12.36218
Slot Current Is A	244.3898373	109.557	72.09519	236.0625	272.5814
$r^2 L\_stk$	0.000434234	0.000434	0.000434	0.000434	0.000434
r	0.093191592	0.093192	0.093192	0.093192	0.093192
D_rotor	0.186383185	0.186383	0.186383	0.186383	0.186383
a —L_min	0.023777003	0.024165	0.024165	0.024165	0.022738
p Pole pairs	12.31315901	12.11534	12.11534	12.11534	12.87562
2p Approximated	12	12	12	12	12

Continued on next page

Table A.2 – continued from previous page

Parameter	Design 1	Design 2	Design 3	Design 4	Design 5
Slots	36.00	72.00	108.00	36.00	36
q_calculated	1	2	3	1	1
Z/2p	3	6	9	3	3
t periodicity	6	6	6	6	6
q_ph= Z/mt	2	4	6	2	2
Alpha_ph	1.047197551	0.523599	0.349066	1.047198	1.047198
Kd even q_ph	1	0.965926	0.959795	1	1
Kd odd q_ph	0.965925826	0.957662	0.956143	0.965926	0.965926
y_q Slot pitch	2	5	8	2	2
Sigma_w Coil span Angle	2.09	2.62	2.79	2.09	2.09
Kp	0.866025404	0.965926	0.984808	0.866025	0.866025
Kw calculated	0.866025404	0.933013	0.945214	0.866025	0.866025
kjo_Recalculated	477.0741353	477.0741	477.0741	477.0741	477.0741
k_end_Recalculated	0.993017664	1.195957	1.227441	1.03039	0.872827
L_slot_pu	4.740800325	4.15118	4.044704	4.818207	4.533702
L_g_pu	4.71934874	4.132397	4.026402	4.796405	4.513187
L_pole_pu_new	9.48160065	8.302361	8.089408	9.636414	9.067403
L_base_new	1.90986E-07	2.22E-07	2.28E-07	1.91E-07	1.91E-07
L_pole_new H	1.81085E-06	1.84E-06	1.84E-06	1.84E-06	1.73E-06
tan Phi_new	0.013627615	0.011133	0.010848	0.012922	0.016212
Phi_new	0.013626772	0.011133	0.010847	0.012922	0.016211
PF_new	0.999907157	0.999938	0.999941	0.999917	0.999869
minimum Wt Tooth width	0.002866889	0.001508	0.001005	0.003016	0.002458
Back iron thickness	0.007184854	0.00756	0.00756	0.00756	0.00616
Rotor Back iron	0.005	0.005	0.005	0.005	0.005
Stator diameter Ds	0.164383185	0.164383	0.164383	0.164383	0.164383

Continued on next page

Table A.2 – continued from previous page

Parameter	**Design 1**	**Design 2**	**Design 3**	**Design 4**	**Design 5**
n_p	1	1	1	1	1
Magnet arc	150	180	180	180	120
Throw	2	5	8	2	2

Parameter	Sinusoidally fed 20P18Q	20P18QMotor fed by Square wave drive	12P36Q Motor_ 150Deg MagnetArc fed by Sq-Wave Drive	12P36Q_ 120Deg MagnetArc
pole number	20	20	12	12
slots	18	18	36	36
Winding factor Kw	0.945	0.945	0.866	0.866
Current desisty J A/mmˆ2	4.2	2.77	6	5.99
Tooth width (mm)	7	7	6	5
Amature dia (mm)	164	164	164	164
stack lenghth (mm)	50	50	50	50
Turns	20	20	20	20
Throw	1	1	2	2
Average Torque (Nm)	20.8	11.83	20.4	20.39
Shaft Torque Nm	20.04	11.08	19.93	19.9
Torque ripple	7%	25%	121%	139%
Input Power W	932.27	521	960.5	971.59
EM power W	869.57	493.8	853.95	852.35
Output Power W	839.44	464.2	834.8	833.78
total Loss (on load) W	92.83	56.8	125.7	137.8
Efficiency	90.04%	89.10%	86.90%	85.81%
Power factor	0.99	0.91	0.94	0.95
PF angle Edeg	5.49	-23.5	-19.8	-17.44
torque per Volume kNm/m3	45.88	26.06	45.06	44.98
Torque const Kt Nm/A	1.29	0.736	1.27	1.27
BEMF const Ke Vs/Rad	1.54	0.92	1.71	1.52
BEMF const fundamental Ke_fund Vs/Rad	1.518	0.87	1.65	1.45
Motor Const Km Nm/Wˆ0.5	2.62	2.26	1.97	1.86
Cogging Period Mdeg	2	2	10	10
Cogging Frequency Hz	1200	1200	240	240
Fundamental Freq Hz	66.67	66.67	40	40
Mechanical freq Hz	6.67	6.67	6.67	6.67
Drive peak Line current A	16	16	16	16
peak phase current A	16	12.47	10.72	10.67
RMS Line current A	11.31	12.72	11.47	7.49

Table A.3: Performance Comparison of Initial Designs

Appendix B

Figures

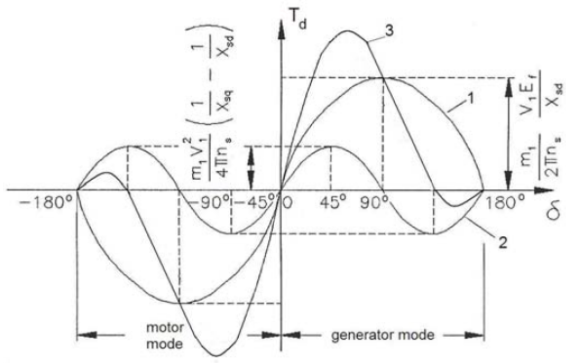

Figure B-1: Torque-angle characteristics of a salient-pole synchronous machine with X_{sd} ¿ X_{sq}: 1 — synchronous torque T_{dsyn}, 2 — reluctance torque T_{drel}, 3 — resultant torque T_d [15]

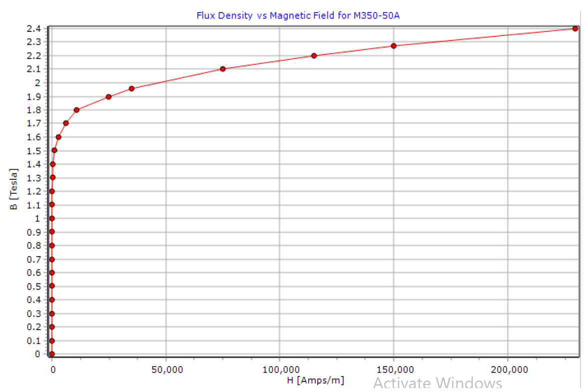

Figure B-2: Flux Density Vs Magnetic Field for M350 50A Electrical steel

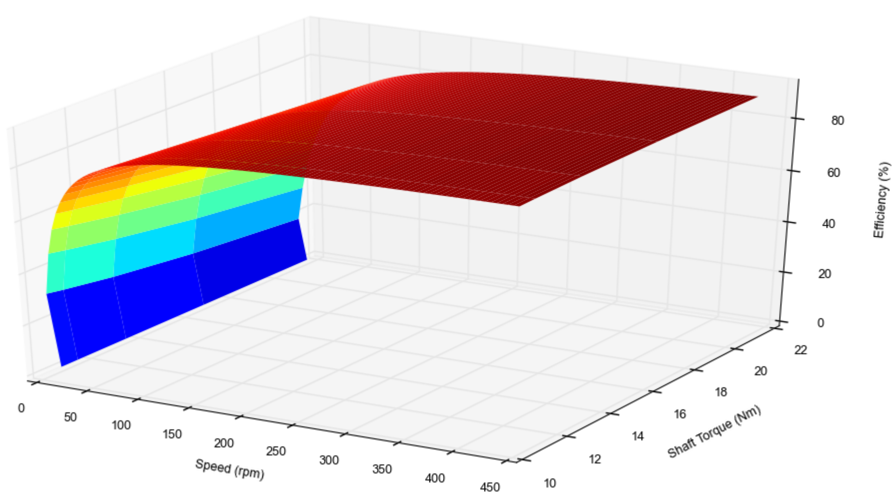

Figure B-3: Torque, speed and efficiency surface graph of optimized 20P18Q Machine

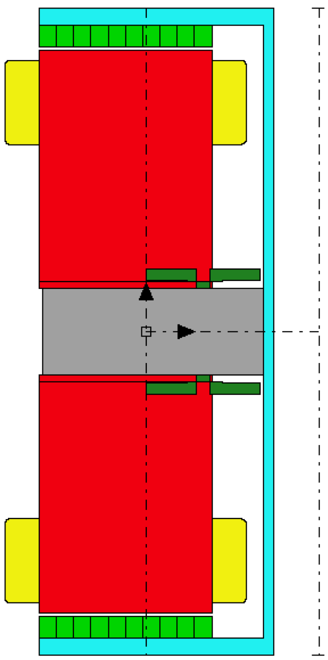

(a) Axial Section of 20P18Q Machine

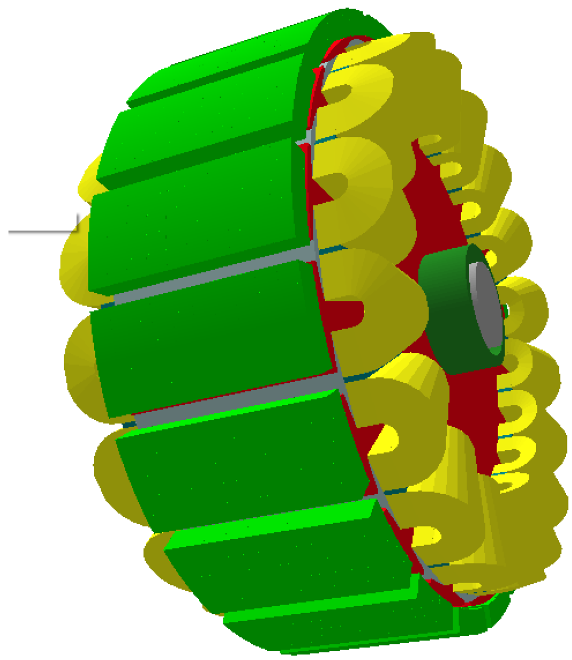

(b) 3D Model without Rotor Cup 20P18Q Machine

Figure B-4: Axial cross Section and Motor CAD 3D Model

Bibliography

[1] B. Boazzo, G. Pellegrino, and A. Vagati, "Multipolar SPM machines for direct-drive application: A general design approach," *IEEE Transactions on Industry Applications*, vol. 50, no. 1, pp. 327–337, 2014.

[2] P. Salminen, *Fractional Slot Permanent Magnet Synchronous*, 2004.

[3] A. E. Machines, "ADVANCED ELECTRICAL MACHINES."

[4] N. Bianchi and G. Berardi, "Analytical Approach to Design Hairpin Windings in High Performance Electric Vehicle Motors," *2018 IEEE Energy Conversion Congress and Exposition, ECCE 2018*, pp. 4398–4405, 2018.

[5] "Homepage - Magnequench." [Online]. Available: https://mqitechnology.com/

[6] "Permanent Magnet Division — Arnold Magnetic Technologies." [Online]. Available: https://www.arnoldmagnetics.com/permanent-magnets/

[7] J. Pyrhonen, T. Jokinen, and V. Hrabovcova, *Design of Rotating Electrical Machines- Wiley 2009,0470695161.pdf*, 2008. [Online]. Available: www.wiley.com

[8] K. Wang and Z. Q. Zhu, *Third harmonic utilization in permanent magnet machines*, 2018.

[9] A. Mebarki, D. Gerada, and N. L. Brown, "Analysis of an axial PM flux machine with field weakening capability for engine integration," *7th IET International Conference on Power Electronics, Machines and Drives, PEMD 2014*, 2014.

[10] J. R. Hendershot, T. J. E. Miller, D. C. Hanselman, B. Boukais, H. Zeroug, A. N. Patel, Y. Kim, C. Lee, and A. N. Patel, *Design of Brushless PM motors*, 2016, vol. 46, no. 11.

[11] T. Reichert, T. Nussbaumer, and J. Kolar, "Torque scaling laws for interior and exterior rotor permanent magnet machines," *Aa*, vol. 1, pp. 1–4, 2009. [Online]. Available: http://www.pes.ee.ethz.ch/uploads/tx_ethpublications/Reichert_Transmag09_TorqueScaling_Final.pdf

[12] A. M. EL-Refaie, Z. Q. Zhu, T. M. Jahns, and D. Howe, "Winding inductances of fractional slot surface-mounted permanent magnet brushless machines," *COMPEL - The International Journal for Computation and Mathematics in Electrical and Electronic Engineering*, vol. 28, no. 6, pp. 1590–1606, 2009.

[13] F. Parasiliti, M. Villani, and M. Castello, "PM Brushless DC Motor with exterior rotor for high efficiency household appliances," *Proceedings - 2014 International Conference on Electrical Machines, ICEM 2014*, pp. 623–628, 2014.

[14] F. Libert, *Design, optimization and comparison of permanent magnet motors for a low-speed direct-driven mixer*, 2004. [Online]. Available: http://faculty.mu.edu.sa/public/uploads/1338064112.6994pmsg.pdf

[15] J. F. Gieras, *Permanent magnet motor technology : design and applications*, 3rd ed. Boca Raton, Fla.: CRC Press, 2010.

[16] Y. B. Apatya, A. Subiantoro, and F. Yusivar, "Design and prototyping of 3-phase BLDC motor," *QiR 2017 - 2017 15th International Conference on Quality in Research (QiR): International Symposium on Electrical and Computer Engineering*, vol. 2017-Decem, pp. 209–214, 2017.

[17] F. Meier, *Permanent-Magnet Synchronous Machines with Non-Overlapping Concentrated Windings for*, 2008. [Online]. Available: http://www.ee.kth.se/php/modules/publications/reports/2008/TRITA-EE_2008_041.pdf

[18] A. Vagati, G. Pellegrino, and P. Guglielmi, "Comparison between SPM and IPM motor drives for EV application," *19th International Conference on Electrical Machines, ICEM 2010*, 2010.

[19] K. T. Chau, C. C. Chan, and C. Liu, "Overview of permanent-magnet brushless drives for electric and hybrid electric vehicles," *IEEE Transactions on Industrial Electronics*, vol. 55, no. 6, pp. 2246–2257, 2008.

[20] J. B. Bartolo, H. Zhang, D. Gerada, L. De Lillo, and C. Gerada, "High speed electrical generators, application, materials and design," *Proceedings - 2013 IEEE Workshop on Electrical Machines Design, Control and Diagnosis, WEMDCD 2013*, pp. 47–59, 2013.

[21] Y. Jeong, K. Kim, Y. Kim, B. Park, and S. Jung, "Design Characteristics of PMa-SynRM and Numerical Analysis," pp. 164–170, 2012.

[22] A. El-Refaie, "Motors / Generators for Traction / Propulsion Applications," *IEEE Vehicular Technology Magazine*, no. march, pp. 90–99, 2013.

[23] R. Cao, C. Mi, and M. Cheng, "Quantitative comparison of flux-switching permanent-magnet motors with interior permanent magnet motor for EV, HEV, and PHEV applications," *IEEE Transactions on Magnetics*, vol. 48, no. 8, pp. 2374–2384, 2012.

[24] A. M. El-Refaie, J. P. Alexander, S. Galioto, P. B. Reddy, K. K. Huh, P. De Bock, and X. Shen, "Advanced high-power-density interior permanent magnet motor for traction applications," *IEEE Transactions on Industry Applications*, vol. 50, no. 5, pp. 3235–3248, 2014.

[25] J. K. Tangudu and T. M. Jahns, "Comparison of interior PM machines with concentrated and distributed stator windings for traction applications," *2011 IEEE Vehicle Power and Propulsion Conference, VPPC 2011*, 2011.

[26] M. Norhisam, A. Nazifah, I. Aris, H. Wakiwaka, and M. Nirei, "Effect of magnet size on torque characteristic of three phase permanent magnet brushless DC motor," *Proceeding, 2010 IEEE Student Conference on Research and Development - Engineering: Innovation and Beyond, SCOReD 2010*, no. SCOReD, pp. 293–296, 2010.

[27] M. Jalalifar, A. F. Payam, B. Mirzaeian, and S. M. Nezhad, "Dynamic modeling and simulation of an induction motor with adaptive backstepping design of an input-output feedback linearization controller in series hybrid electric vehicle," *2006 International Conference on Power Electronics, Drives and Energy Systems, PEDES '06*, 2006.

[28] W. Xu, J. Zhu, Y. Guo, S. Wang, Y. Wang, and Z. Shi, "Survey on electrical machines in electrical vehicles," *2009 International Conference on Applied Superconductivity and Electromagnetic Devices, ASEMD 2009*, no. c, pp. 167–170, 2009.

[29] D. Gerada, D. Borg-Bartolo, A. Mebarki, C. Micallef, N. L. Brown, and C. Gerada, "Electrical machines for high speed applications with a wide constant-power region requirement," *2011 International Conference on Electrical Machines and Systems, ICEMS 2011*, pp. 3–8, 2011.

[30] K. Nakamura, K. Murota, and O. Ichinokura, "Characteristics of a novel switched reluctance motor having permanent magnets between the stator pole-tips," *2007 European Conference on Power Electronics and Applications, EPE*, pp. 10–14, 2007.

[31] J. B. Bartolo and C. Gerada, "The electromagnetic design of a high speed, 45kW, switched reluctance machine having a novel rotor geometry for aerospace application," *Proceedings - 2014 International Conference on Electrical Machines, ICEM 2014*, pp. 2513–2519, 2014.

[32] K. Watanabe, S. Aida, A. Komatsuzaki, and I. Miki, "Driving force characteristics of 40kW switched reluctance motor for electric vehicle," *Proceeding of International Conference on Electrical Machines and Systems, ICEMS 2007*, pp. 1894–1898, 2007.

[33] B. Bilgin, A. Emadi, S. Member, and M. Krishnamurthy, "Comprehensive Evaluation of the Dynamic Performance of a 6 / 10 SRM for Traction Application in PHEVs," vol. 60, no. 7, pp. 2564–2575, 2013.

[34] W. Wang and B. Fahimi, "Comparative study of electric drives for EV/HEV propulsion system," *Electrical Systems for Aircraft, Railway and Ship Propulsion, ESARS*, 2012.

[35] P. Giangrande, D. Ronchetto, G. Pellegrino, F. Cupertino, C. Gerada, and M. Sumner, "Hybrid sensorless control of axial flux permanent magnet motor drives, including zero speed," *Proceedings of the 2011 14th European Conference on Power Electronics and Applications, EPE 2011*, pp. 1–8, 2011.

[36] C. Versèle, Z. De Grève, F. Vallée, R. Hanuise, O. Deblecker, M. Delhaye, and J. Lobry, "Analytical design of an axial flux permanent magnet in-wheel synchronous motor for electric vehicle," *2009 13th European Conference on Power Electronics and Applications, EPE '09*, no. Im, 2009.

[37] T. Arakawa, M. Takemoto, S. Ogasawara, K. Inoue, O. Ozaki, H. Hojo, and H. Mitani, "Examination of an interior permanent magnet type axial gap motor for the hybrid electric vehicle," *IEEE Transactions on Magnetics*, vol. 47, no. 10, pp. 3602–3605, 2011.

[38] K. Lu and E. Ritchie, "Preliminary comparison study of drive motor for electric vehicle application," *ICEMS 2001 - Proceedings of the 5th International Conference on Electrical Machines and Systems*, vol. 2, pp. 995–998, 2001.

[39] M. Gärtner, P. Seibold, and N. Parspour, "Laminated circumferential transverse flux machines - Lamination concept and applicability to electrical vehicles," *2011 IEEE International Electric Machines and Drives Conference, IEMDC 2011*, pp. 831–837, 2011.

[40] E. Padurariu, L. E. Somesan, I. A. Viorel, and L. Szabo, "Large power permanent magnet transverse flux motor, steady-state and dynamic behavior," *Proceedings of 9th International Conference, ELEKTRO 2012*, pp. 221–224, 2012.

[41] F.-s. P.-m. Machine, T. Raminosoa, C. Gerada, and M. Galea, "Design Considerations for a Fault-Tolerant," *Design*, vol. 58, no. 7, pp. 2818–2825, 2011.

[42] W. Hua, M. Cheng, and G. Zhang, "A novel hybrid excitation flux-switching motor for hybrid vehicles," *IEEE Transactions on Magnetics*, vol. 45, no. 10, pp. 4728–4731, 2009.

[43] R. Cao, C. Mi, and M. Cheng, "Quantitative comparison of flux-switching permanent-magnet motors with interior permanent magnet motor for EV, HEV, and PHEV applications," *IEEE Transactions on Magnetics*, vol. 48, no. 8, pp. 2374–2384, 2012.

[44] T. Raminosoa, A. M. EL-Refaie, D. Pan, K. K. Huh, J. P. Alexander, K. Grace, S. Grubic, S. Galioto, P. B. Reddy, and X. Shen, "Reduced Rare-Earth Flux-Switching Machines for Traction Applications," *IEEE Transactions on Industry Applications*, vol. 51, no. 4, pp. 2959–2971, 2015.

[45] F. N. Jurca and C. Martis, "Analysis of outer rotor synchronous reluctance motor for low-speed applications," *International Conference on Electical Drives and Power Electronics*, vol. 2017-Octob, pp. 242–247, 2017.

[46] M. Obata, S. Morimoto, M. Sanada, and Y. Inoue, "Characteristic of PMASynRM with ferrite magnets for EV/HEV applications," *ICEMS 2012 - Proceedings: 15th International Conference on Electrical Machines and Systems*, 2012.

[47] J. Malan, M. J. Kamper, and P. N. Williams, "Reluctance synchronous machine drive for hybrid electric vehicle," *IEEE International Symposium on Industrial Electronics*, vol. 2, pp. 367–372, 1998.

[48] M. M. Ansari, W. A. Cronje, and A. Meyer, "Evaluation of a reluctance synchronous motor: For use in an Electric Mine Shuttle Vehicle (EMSV)," *2012 IEEE International Electric Vehicle Conference, IEVC 2012*, 2012.

[49] F. Cupertino, G. M. Pellegrino, E. Armando, and C. Gerada, "A SyR and IPM machine design methodology assisted by optimization algorithms," *2012 IEEE Energy Conversion Congress and Exposition, ECCE 2012*, pp. 3686–3691, 2012.

[50] G. Pellegrino, F. Cupertino, and C. Gerada, "Automatic Design of Synchronous Reluctance Motors Focusing on Barrier Shape Optimization," *IEEE Transactions on Industry Applications*, vol. 51, no. 2, pp. 1465–1474, 2015.

[51] "External rotor motor basics: Design and applications." [Online]. Available: https://www.motioncontroltips.com/external-rotor-motor-basics-design-applications/

[52] T. Y. Lee, M. K. Seo, Y. J. Kim, and S. Y. Jung, "Motor Design and Characteristics Comparison of Outer-Rotor-Type BLDC Motor and BLAC Motor Based on Numerical Analysis," *IEEE Transactions on Applied Superconductivity*, vol. 26, no. 4, pp. 5–10, 2016.

[53] P. D. I. Milano, "DESIGN AND OPTIMIZATION OF AN OUTER ROTOR PERMANENT MAGNETS BRUSHLESS MOTOR DESIGN AND OPTIMIZATION OF AN OUTER ROTOR PERMANENT," 2018.

[54] A. M. EL-Refaie, "Fractional-slot concentrated-windings synchronous permanent magnet machines: Opportunities and challenges," *IEEE Transactions on Industrial Electronics*, vol. 57, no. 1, pp. 107–121, 2010.

[55] A. M. El-Refaie, T. M. Jahns, and D. W. Novotny, "Analysis of surface permanent magnet machines with fractional-slot concentrated windings," *IEEE Transactions on Energy Conversion*, vol. 21, no. 1, pp. 34–43, 2006.

[56] J. Cros and P. Viarouge, "Synthesis of high performance PM motors with concentrated windings," *IEEE International Electric Machines and Drives Conference, IEMDC 1999 - Proceedings*, vol. 17, no. 2, pp. 725–727, 1999.

[57] F. Magnussen and C. Sadarangani, "Winding Factors and," 2006.

[58] S. Skaar, O. Krovel, and R. Nilssen, "Distribution, coil-span and winding factors for PM machines with concentrated windings," *XVII International Conference on Electrical Machines, ICEM 2006*, p. 346, 2006. [Online]. Available: http://www.elkraft.ntnu.no/eno/Papers2006/icem-skaar-krovel-nilssen06.pdf

[59] A. D. Gerlando, G. M. Foglia, R. Perini, M. Ubaldini, E. Politecnico, D. O. Ayer, and C. O. W. Indings, "Synchronous Machines with Concentrated Armature Windings," *Leonardo*, pp. 1165–1172, 2005.

[60] J. Cros, P. Viarouge, and C. Gelinas, "Design of PM brushless motors using iron-resin composites for automotive applications," *Conference Record - IAS Annual Meeting (IEEE Industry Applications Society)*, vol. 1, pp. 5–11, 1998.

[61] A. G. Jack, B. C. Mecrow, P. G. Dickinson, D. Stephenson, J. S. Burdess, N. Fawcett, and J. T. Evans, "Permanent-magnet machines with powdered iron cores and prepressed windings," *IEEE Transactions on Industry Applications*, vol. 36, no. 4, pp. 1077–1084, 2000.

[62] N. Bianchi and S. Bolognani, "Design techniques for reducing the cogging torque in surface-mounted PM motors," *IEEE Transactions on Industry Applications*, vol. 38, no. 5, pp. 1259–1265, 2002.

[63] A. G. Jack, B. C. Mecrow, and J. A. Haylock, "A comparative study of permanent magnet and switched reluctance motors for high-performance fault-tolerant applications," *IEEE Transactions on Industry Applications*, vol. 32, no. 4, pp. 889–895, 1996.

[64] N. Bianchi, M. D. Pré, G. Grezzani, and S. Bolognani, "Design considerations on fractional - Slot fault - Tolerant synchronous motors," *2005 IEEE International Conference on Electric Machines and Drives*, pp. 902–909, 2005.

[65] S. O. Kwon, S. I. Kim, P. Zhang, and J. P. Hong, "Performance comparison of IPMSM with distributed and concentrated windings," *Conference Record - IAS Annual Meeting (IEEE Industry Applications Society)*, vol. 4, no. c, pp. 1984–1988, 2006.

[66] J. Goss, D. Staton, R. Wrobel, and P. Mellor, "Brushless AC interior-permanent magnet motor design: Comparison of slot/pole combinations and distributed vs.

concentrated windings," *2013 IEEE Energy Conversion Congress and Exposition, ECCE 2013*, pp. 1213–1219, 2013.

[67] L. Chong, R. Dutta, and M. F. Rahman, "Performance comparison between concentrated and distributed wound IPM machines used for field weakening applications," *International Aegean Conference on Electrical Machines and Power Electronics, ACEMP 2011 and Electromotion 2011 Joint Conference*, no. September, pp. 616–619, 2011.

[68] M. Galea, C. Gerada, T. Raminosoa, and P. Wheeler, "A thermal improvement technique for the phase windings of electrical machines," *IEEE Transactions on Industry Applications*, vol. 48, no. 1, pp. 79–87, 2012.

[69] D. C. Hanselman, *Brushless Motor Design*, 1994.

[70] N. Bianchi, H. Mahmoud, and S. Bolognani, "Fast synthesis of permanent magnet assisted synchronous reluctance motors," vol. 10, pp. 312–318, 2016.

[71] C. López-Torres, A. Garcia-Espinosa, and J.-R. Riba, "Reliable Design of PMaSynRM," *New Trends in Electrical Vehicle Powertrains*, 2019.

[72] M. G. M. G. Say, *The performance and design of alternating current machines : transformers, three-phase induction motors and synchronous machines*, 3rd ed. London: Pitman Paperbacks, 1968.

[73] J. H. J. H. Walker, *Large synchronous machines : design, manufacture, and operation*, ser. Monographs in electrical and electronic engineering ; [14]. Oxford: Clarendon Press, 1981.

[74] R. A. Inte, F. N. Jurca, and C. Martis, "Design And Analysis Of Outer Rotor Permanent Magnet Assisted Synchronous Reluctance Machine With Concentrated Winding For Small Electric Propulsion," pp. 14–19, 2019.

[75] P.-m. Motors, Y. Kano, and N. Matsui, "A Design Approach for Direct-Drive," vol. 44, no. 2, pp. 543–554, 2008.

[76] F. Libert and J. Soulard, "Investigation on pole-slot combinations for permanent-magnet machines with concentrated windings," *International Conference on Electrical Machines (. . .*, no. June, pp. 5–8, 2004. [Online]. Available: http://www.ee.kth.se/php/modules/publications/reports/2004/IR-EE-EME_2004_005.pdf

[77] N. Bianchi and M. Dai Pré, "Use of the star of slots in designing fractional-slot single-layer synchronous motors," *IEE Proceedings: Electric Power Applications*, vol. 153, no. 3, pp. 459–466, 2006.

[78] K. F. Rasmussen, J. H. Davies, T. J. Miller, M. L. McGilp, and M. Olaru, "Analytical and numerical computation of air-gap magnetic fields in brushless motors with surface permanent magnets," *IEEE Transactions on Industry Applications*, vol. 36, no. 6, pp. 1547–1554, 11 2000.